Parameterized Analysis of Optical Inter-satellite Links for High Resolution Satellite Communication

by

James Bernard Glettler

B. S. Electrical Engineering, University of Michigan, 2003

Submitted to the Department of Electrical Engineering and Computer Science
in partial fulfillment of the requirements for the degree of

Master of Science in Electrical Engineering

at the

MASSACHUSETTS INSTITUTE OF TECHNOLOGY

June 2009

Author ....
Department of Electrical Engineering and Computer Science
22 May 2009

Certified by ....
Vincent W. S. Chan
Joan and Irwin Jacobs Professor of Electrical Engineering &
Computer Science and Aeronautics & Astronautics
Claude E. Shannon Communication and Network Group
Thesis Supervisor

Accepted by ....
Arthur C. Smith
Chairman, Department Committee on Graduate Theses

THIS PAGE INTENTIONALLY LEFT BLANK

Parameterized Analysis of Optical Inter-satellite Links for High Resolution Satellite Communication

by

James Bernard Glettler

Submitted to the Department of Electrical Engineering and Computer Science
on 22 May 2009, in partial fulfillment of the
requirements for the degree of
Master of Science in Electrical Engineering

Abstract

The use of antenna arrays to exploit spatial information in single and multi-user RF communication receivers is well established for reducing interference and enabling frequency reuse. Antenna arrays have been deployed in single satellite applications but arrays have not been exploited in multi-satellite constellations where increased array size enables high spatial selectivity between ground transmitters. One requirement for these array systems is sufficient fidelity in transporting the received RF signals at each antenna to the array processor. Optical inter-satellite link architectures for signal transport are investigated and parameterized models to compare the performance of each are synthesized. Both analog and digital modulation schemes for the link are considered. A two-channel receiver with both low and high interference is analyzed. It is shown that high resolution satellite array receivers are practical with low required optical power. The optimum selection of transport architecture is shown by selecting for lowest error probability or minimum required optical power. A satellite-to-satellite distance threshold is found for selecting the optimum inter-satellite link architecture for a given application.

Thesis Supervisor: Vincent W. S. Chan
Title: Joan and Irwin Jacobs Professor of Electrical Engineering & Computer Science and Aeronautics & Astronautics
Claude E. Shannon Communication and Network Group

THIS PAGE INTENTIONALLY LEFT BLANK

Acknowledgments

I would like to deeply thank my thesis advisor, Professor Vincent Chan. His broad knowledge and experience, deep insight and strong commitment to academic rigor have been invaluable both for the completion of this thesis as well as strengthening my own thought process. I am grateful for his time and patience in guiding me through my return to academia. I would also like to thank Dr. John Chapin, Visiting Scientist at MIT, for his direction and clear reasoning in helping define and complete this work.

I cannot overstate my thanks to Larry Candell and Dr. Pablo Hopman. From the moment I joined MIT Lincoln Laboratory, these two have been not only inspirational mentors, but also friends. They have encouraged me to grow, pursue high goals and work on the most interesting things. I would also like to thank the rest of my friends and colleagues in Group 99 of whom I have seen so little of over the past two years. I am indebted to the Lincoln Scholars Committee for supporting this academic endeavor.

For the good company and conversation, I thank my officemates, Andrew, Anurupa, Etty, Guy, Lei, Lillian, and Mia. For helping me to smoothly navigate this experience, I want to express my gratitude to the staff including Kathy, Liz, Lynne, Pardis, Sue, and Trish.

I am also indebted to the educators that have guided me in my career. Jim Koepsel and Gary VanVels, at KC/TC, gave me an inestimable head start to becoming a successful engineer. I had a tremendous experience working with Professor England and Dr. Roger De Roo at the University of Michigan.

I must thank Jean Kung, my girlfriend, for her unwavering love and support throughout this journey. She is the joy in my life.

I would not be here if it were not for the love and sacrifice of my parents, Robert and Elise Glettler. I would not be the person I am without my wonderful brother, Brian Glettler. It is to my family that I dedicate this thesis.

THIS PAGE INTENTIONALLY LEFT BLANK

Contents

List of Figures

THIS PAGE INTENTIONALLY LEFT BLANK

List of Tables

THIS PAGE INTENTIONALLY LEFT BLANK

Chapter 1

Introduction

1.1 Introduction & Motivation

Allocated spectrum for radio frequency (RF) communication systems is always a precious resource. Simultaneous independent transmitters on the same frequency interfere with the communication receiver's ability to extract the information from a specific transmitter. If the transmitters are spatially distinct, the communication receiver can take advantage of this to separate the signals from each transmitter. This frequency reuse enables multi-access communication systems but requires spatial selectivity in the RF receiver.

We are interested in high resolution satellite communication receiver systems. High resolution is defined in this thesis to mean ground spatial selectivity in the range of meters to kilometers when the receiver is on a satellite platform, nominally a geosynchronous orbit. High resolution is necessary to support applications such as high bandwidth data or sensor terminals deployed to a geographically small area (e.g. within a city). It also is necessary to mitigate the effects intentional or unintentional RF interference sources. The applications of such high resolution techniques are useful for both commercial and military users.

One interesting example application is covert frequency reuse where a user transmits a low power RF signal on the same frequency as a nearby higher power transmitter. Ground based radio detection equipment would have a low probability of detection or intercept but a high resolution satellite receiver would be able to extract the signal from the user.

The fine grain spatial selectivity required by these applications is unavailable in current satellite communications systems. To see why, we review the physical and practical limitations for current communication satellites. The simplest communication receiver has a single antenna of some size. The diffraction limited antenna pattern of a reflector antenna with diameter D has a first null at approximately $\frac{\lambda}{D}Z$ where λ is the operational wavelength and Z is the distance from the antenna.[43] This is a reasonable estimate of the minimum supportable stand-off distance. To achieve the diffraction limit the shape of the antenna must be controlled to within a fraction of a wavelength.[21] This constraint is challenging to meet as the antenna must survive launch induced stresses and be meet size and weight restrictions. At lower frequencies, large segmented antennas can be deployed after launch. The ETS-8/KIKU-8 satellite launched in 2006 is an example, deploying a 19 meter reflector antenna for operation at 2.3 GHz (130 mm).[25] This would support a stand-off distance of approximately 250 km. However, at higher frequencies the shape requirement becomes much more stringent and deployable segmented reflectors are inadequate. A monolithic reflector can be used but it must fit within the launch vehicle. For instance the Delta IV rocket has a fairing diameter of up to 5 meters.[6] At 20 GHz (requiring better than 1 mm antenna precision) and assuming a 5 meter antenna, this would support a 110 km stand-off distance.

If an antenna array is used (Figure 1-2a) instead of a single antenna the stand-off distance can be improved. If the maximum separation between elements in the array is d, the stand-off distance is approximately $\frac{\lambda}{4d}Z$. This metric is based on the complete nulling with two antennas as discussed in Section 3.4.1. Antenna arrays are used but the capabilities are limited due to the limits on d. The MILSTAR series of satellites is approximately 16 meters long and utilize a number of smaller array and multi-beam antennas.[27] If the full length was used for an array with $d = 16$ meters the best case stand-off distance would be 73 km and 8 km for 2.3 GHz and 20 GHz respectively.

It is apparent that using arrays of antennas can overcome the physical limitations of single antennas and increasing the size of the array significantly improves the minimum stand-off distance. As the size of a single satellite is limited, a constellation of satellites as in Figure 1-1 is proposed. Each satellite in the constellation makes one or more observations of the radio signal and relays the observations to an array processor via a free-space optical (FSO) inter-satellite links (ISL). An inter-satellite distance in the range of 10^0 to 10^2 kilometers would reduce the stand-off distance to less than 100 meters (depending on frequency). Roughly two orders of magnitude improvement is possible over the single satellite case.

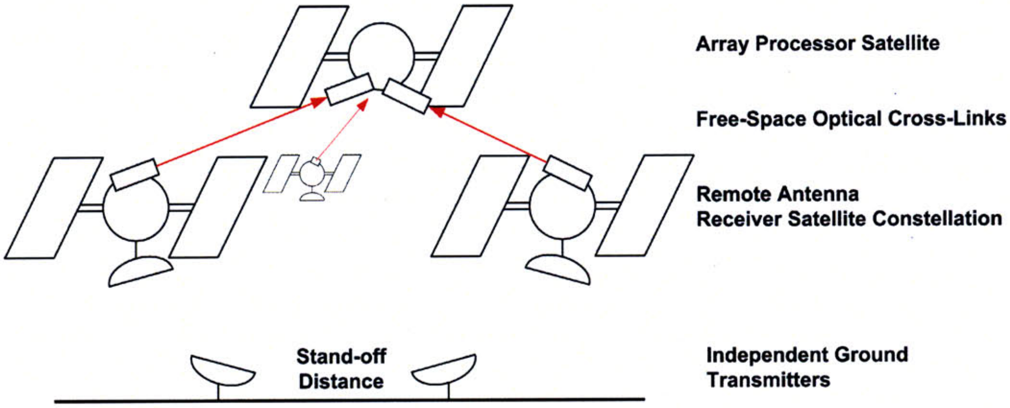

Figure 1-1: General block diagram of satellite array concept.

Optical versus RF inter-satellite links are preferred for a variety of reasons. The shorter wavelengths of optical ISLs results in much narrower beams for equivalent aperture size which reduces the required prime power and mass required for the ISL subsystem.[12, 42, 9] Optical links offer very high bandwidths and are resistant to both eavesdropping and jamming due to the narrow beams. Table 1.1 shows a quick comparison of characteristics in RF and optical systems adapted from Table 3 of [9]. Thus, RF inter-satellite links are precluded from further consideration.

Parameter	RF	Optical
Wavelength (frequency)	1 cm (30 GHz)	1.5 μm (200 THz)
Receiver noise limit	Thermal ($k_B T = -174 \frac{\text{dBm}}{\text{Hz}}$)	Shot ($h\nu = -159 \frac{\text{dBm}}{\text{Hz}}$)
Bandwidth limitation	Regulated	Unregulated
	$\ll$30 GHz	$\ll$200 THz
Free space diffraction angle	$10^{-2}/D$	$10^{-6}/D$
State-of-the-art amplifiers		
Gain	10 dB	50 dB
Bandwidth	~50 GHz	~50 THz
Average efficiency	~5%–46%	~5%–21%

Table 1.1: Comparison of RF and optical characteristics and technical limitations, adapted from [9].

1.2 Architectures for Analysis

A simple array receiver with three antennas is shown in Figure 1-2a. The proposed satellite constellation places some or all of those antennas on remote satellites as in Figure 1-2b. The free-space optical inter-satellite link is shown in two parts, the electrical-to-optical conversion (E/O) and the optical-to-electrical conversion (O/E). In some cases, the O/E process may even be after the array processor. Antenna observations from local antennas will not suffer degradation from the ISL. For the purposes of this thesis, focus will be restricted to symmetric systems where all antennas are remote.

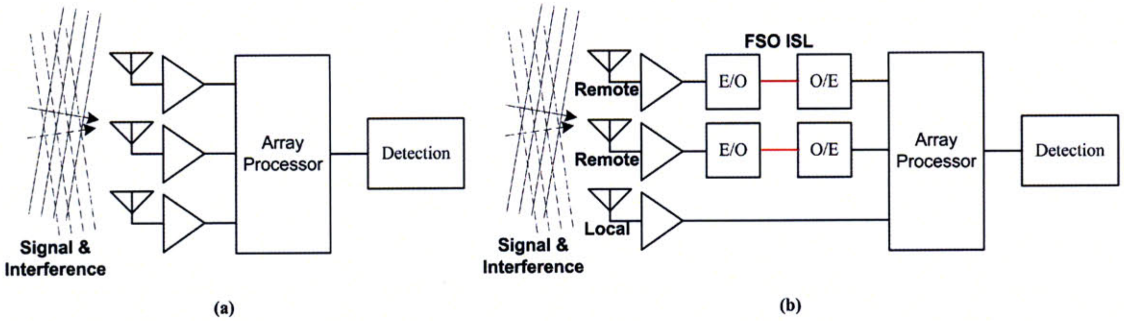

Figure 1-2: General block diagram of array receiver (a), with remote antennas (b) (see text).

The architecture and analysis of the inter-satellite link and array processor is the focus of this thesis. There is a range of choices that affect architecture as shown in Figure 1-3. The array processing can be performed in the digital domain or analog domain. Analog processing may be implemented electronically or optically. For electronic and optical processing, digitization must be after processing. However, digital processing requires digitization first and there is an option to digitize at the remote antenna before transport or at the array processor after transport. Digitizing at the antenna obviously means the optical transport system uses digital modulation. Digitizing at the array processor after transport requires analog modulation and opens a range of possible modulation and detection schemes. Two analog schemes focused on herein are intensity modulation with direct detection (IM–DD) and frequency modulation with coherent detection (FM–CD). Phase modulation with coherent detection (PM–CD) is an extension of FM–CD. We will compare the architectures that use digital array processing as a common element (drawn in solid lines). Digital processing is also more readily scalable for supporting multiple simultaneous communication users.

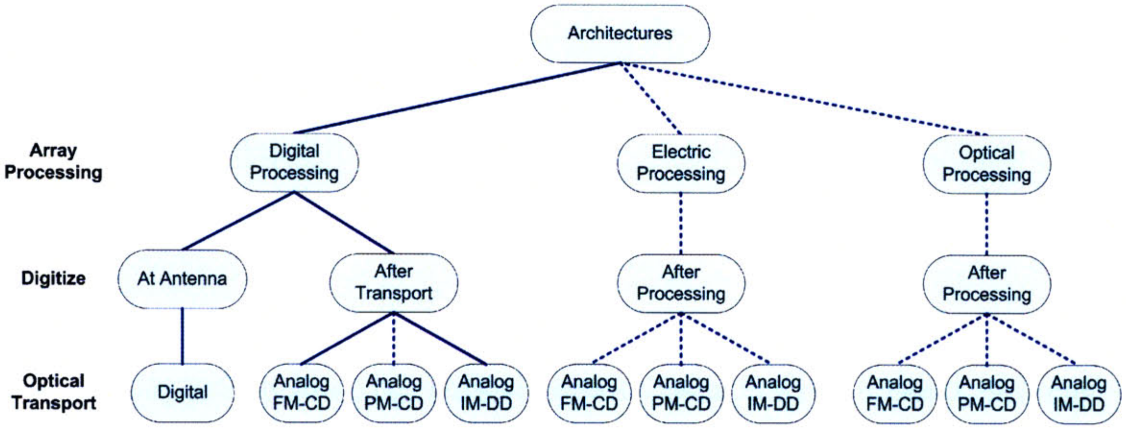

Figure 1-3: Tree diagram of possible system architectures (see text).

Architectures using high-fidelity analog transport have some interesting capabilities not generally available with digital transport. In array systems that are limited by current analog to digital converter technology, the array performance can be upgraded by replacing just the array processor satellite increasing the utility and lifetime of the remaining satellite assets.[14] It shall be demonstrated that coherent detection enables significant performance gains over more traditional direct detection schemes. The gain comes from the ability to reach the shot noise limit, use angle modulation techniques and have highly frequency selective filters for only modest increases in system complexity.[38]

The evaluation criteria must be selected for the appropriate audience. Possible audiences would be the system end-user, the system owner or funder, and the system engineer. The end-user is concerned with the performance and reliability of the communication system once deployed. The owner is concerned with the cost of development, deployment and ongoing operating costs. As the engineer must design a system satisfying the needs and constraints of the other two audiences, it is for the system engineer that we tailor our evaluation criteria.

The analysis of each candidate architecture must be parameterized to include the antenna/satellite configuration including the inter-satellite link distance, the standoff distance between ground users and the signal to interference power ratio. Other parameters are constraints seen in any satellite system such as prime power, mass and volume. As these constraints are often difficult to quantify in a high level analysis, the transport laser power will be used as a reasonable surrogate. It is also necessary to be cognizant of the practical limitations in current technologies when considering any system for deployment (see [28]).

1.3 Prior Work

The groundwork for this thesis has been laid by a great number of contributors. The concept for distributed antenna communication with digital and analog transport over a multiplexed optical backbone was proposed by Chan in 2003.[14].

There is certainly a great body of work on the detection and processing of signals in the presence of Gaussian noise. Wozencraft and Jacob's book on communication is a great reference.[51] Detection has been extended to array processing and interference cancellation for both radar and communication systems. Harry Van Tree's Detection, Estimation and Modulation Theory series is a comprehensive guide.[45, 44, 46]

In 1985, Kaufmann and Hutchinson demonstrated the use of K-band inter-satellite and satellite-to-ground communication for transmitter localization.[24]. Observations at each satellite were digitized and relayed to ground for off-line processing, but this demonstrated the capability of distributed antennas for high resolution radio systems. The report was recently declassified and the work was based on post deployment enhancements to the LES-8 and LES-9 satellites by Lincoln Laboratory.

In 1988, Kaufmann and Chan proved that coherently detected optical inter-satellite links were feasible for high-rate digital communication. They showed these links had significant performance advantages over both direct detected optical and extremely high frequency (EHF) radio links.[23] Recent advances in avalanche photodiodes and turbo coding have enabled photon counting receivers to operate at single bit-per-photon levels.[19] Caplan's extended work on laser communication in 2007 is an excellent reference on digital laser communication theory and practical limitations.[9]

Analog modulated optical links, primarily over a fiber medium, have been well studied, both using direct detection and coherent detection. Bo Cai and Alwyn Seeds in 1994 and 1997 proved and then demonstrated the advantages of FM–CD links over IM–DD.[8, 7]

Nick Andrikogiannopoulous extended the work of Cai & Seeds in his 2006 Masters thesis under professor Chan.[4] Andrikogiannopoulous looked at using FM–CD for antenna nulling applications, finding the optimal bandwidth expansion in the FM case, and possible implementations of analog array processing.[4] His analyses only accounted for un-whitened noise from optical detection.

Although optical processing is not discussed further, there has been progress in both the theory and experimental implementation of optical array processing system. Kriehn et al. demonstrated an optical interference nulling system in 2000.[26] Saengudomlert and Chan also showed methods for implementing hybrid optical array processing for wide-band RF arrays.[36]

1.4 Thesis Outline

Chapter 2 – Signal Transport A parameterized performance analysis of the signal transport subsystems including both analog and digital optical modulation schemes and the noise processes that affect each. The RF front-end electronics that prepare the received RF signals for transport are also discussed including necessary bandwidths, frequency translation and gain. The optical power loss due to free space propagation is analyzed.

Chapter 3 – Array Processing and Detection An analysis of the necessary array processing to combine the remote antenna signals, mitigate interference, and recover the information in the communication signal. Multi-channel communication receivers and the probability of a bit error are reviewed. The receiver is extended to deal with colored noise using a whitening filter. The antenna geometry is formulated and array combining using complex weights is discussed in terms of a narrow-band approximation. The weighting for complete nulling of an interference source is derived.

The focus is on two-antenna systems.

Chapter 4 – Example Parameterized Analysis Two sets of parameters are enumerated to specify the communication system and the antenna geometry. Reasonable performance goals are set. Using these parameters, the performance of each signal transport architecture under various operating conditions is compared. The performance after incorporating the antenna geometry for a two channel system in geosynchronous orbit with weak and strong interference sources is compared. The threshold inter-satellite distance to determine the optimum architecture for minimum error probability is discussed.

Chapter 5 – Results and Conclusions Conclusions based on the results of Chapter 4 are explained. The limitations of the analytical techniques and results in this thesis are discussed. Finally, a number of extensions to the work are proposed.

1.5 Contributions

The fundamental contribution of this research is to parameterize the conditions for the optimal selection of digital or analog transport in high resolution satellite communication arrays. A method to directly evaluate and compare candidate transport architectures in terms of link performance is provided herein. Both the raw probability of error for a simple uncoded RF modulation scheme and minimum optical power to support an error rate goal as a surrogate for a coded RF system are evaluated. It is shown that low power free space optical inter-satellite links can support satellite communication arrays and provide high (meter-class) spatial resolution for interference suppression and frequency reuse. A distance dependent threshold where the analog FM–CD transport architecture outperforms the digital modulation architecture is also shown. This work is necessary for any system engineer considering communication constellations.

THIS PAGE INTENTIONALLY LEFT BLANK

Chapter 2

Signal Transport

2.1 Introduction

Chapter 1 introduced the concept of a distributed antenna array using optical intersatellite links. A number of architectures were presented that varied in the use of analog or digital optical modulation schemes and placement of the digitizers in the signal chain. In this chapter, we analyze the behavior of the signal transport subsystems used to carry observations from the remote antennas to the array processor. The performance of each component is parameterized as it affects the signal chain.

The chapter begins in Section 2.2 by discussing the fundamental sources of noise present in the RF and optical communication subsystems. This covers thermal and shot noise sources as well as relative intensity noise in transmitting lasers.

Section 2.3 covers the properties of analog modulated optical transport. Two modulation and detection methods are included. First in Section 2.3.1 we review the classical analysis of intensity modulation with direct detection. Then in Section 2.3.2 we investigate frequency modulation with coherent optical detection and an electrical FM discriminator. The effects of bandwidth expansion and FM weak noise suppression are discussed. Post analog transport digitization is covered in the next section.

Digital transport is covered in Section 2.4. The effect of amplitude quantization and an estimate for the power spectrum of the resulting quantization is reviewed in

Section 2.4.1. The result is useful for the analog transport case with post transport digitization. Then the bit error rate of an uncoded digital optical inter-satellite is approximated. Finally, the two are combined to approximate the end-to-end performance of a quantization system with degradation due to the cross-link.

Section 2.5 discusses the RF front-end electronics. The high center frequency for of a band pass RF signal adds some complexity to the transport system. This section has a qualitative discussion of various signal chains focusing on quadrature heterodyning to preserve phase information. As both analog and digital modulation schemes can behave non-linearly due to signal amplitude (over-modulation and clipping respectively), the RF front end must appropriately scale the RF received signals before transport. Required gains are analyzed.

Section 2.6 presents a simple analysis on the free space optical loss due to finite aperture size and inter-satellite distance based on the Friis transmission formula.

2.2 Noise Mechanisms

Any electrical circuit is subject to the degradation caused by noise. Here we review the relevant noise mechanisms and their parameters. We primarily are concerned with the noise generated in the optical detector, usually a photodiode.

In general, we can consider the noise mechanisms to be zero mean Gaussian processes. A noise signal x would take on values with the following probability distribution.

$$\begin{aligned} \mathrm{p}_X(x) &= \mathcal{N}(0, \tfrac{N_0}{2}) \\ &= \frac{1}{\sqrt{\pi} N_0} \exp\left(-\frac{x^2}{N_0}\right) \end{aligned} \tag{2.1}$$

where the term N_0 is the noise power per mode. If the receiver has an additive white Gaussian noise process the complete power spectral density of the noise can be written as follows in Joules (or Watts/Hertz).

$$S_n(f) = \frac{N_0}{2} \tag{2.2}$$

If a white Gaussian noise process is passed through a frequency selective filter, the output is no longer truly white. A useful filter in this thesis is a "brick-wall" filter, which has unity gain over the passband and perfectly suppresses energy outside the passband. White noise passed through a brick wall filter is obviously no longer white but for convenience is often referred to as band-limited white noise. If the frequency selective filter is more complex than a "brick-wall" then the noise is known as colored noise.

Under all circumstances, we consider the noise processes to be independent from each other and from the operational signals.

Thermal (Johnson/Nyquist) Noise The thermally induced motion of charge carriers within a conductor results in a net potential at any given instant. The "statistical fluctuation" of these carriers is the cause of thermal noise in any conductor with non-zero resistance and non-zero temperature.[22] The thermal noise power is proportional to the device temperature, T, and the Boltzmann constant, k_B. When using the current output of a photodiode the load resistor, R_L must be taken into account. The thermal noise density is $N_{0_{\text{Therm}}}$.

$$N_{0_{\text{Therm}}} = \frac{4k_BT}{R_L} \tag{2.3}$$

Shot Noise Current in a conductor is not a continuous process due to the quantized nature of charge carriers. This is true for electrons in a conductor and photo-generated carriers in a photo detector. The charge carrier arrivals have a Poisson distribution. The central limit theorem allows the behavior to be modeled as a Gaussian process. The shot noise density depends only on the average current passing through the conductor or photo-detector, $\overline{I}$, and the basic electric charge, q. In a photo-detector

$\overline{I}$ is the sum of the mean photo-generated current, I_0, and the dark current I_{dk}.[8, 40, 2, 34] In most cases we can assume that the device has sufficiently small dark current to ignore the I_{dk} term.

$$\begin{aligned} N_{0_{\text{Shot}}} &= 2q\overline{I} \\ &= 2q(I_0 + I_{dk}) \end{aligned} \tag{2.4}$$

Relative Laser Intensity Noise The output of a laser with constant drive unfortunately is perturbed with random fluctuations in intensity.[2] High quality laser diodes are less affected but not immune from these fluctuations.[34] This instability is known as relative intensity noise (RIN) and to first order is proportional to the square of the mean photocurrent.

$$N_{0_{\text{RIN}}} = I_0^2 \, RIN \tag{2.5}$$

The relative intensity noise is quantum limited by RIN $\geq \frac{2q}{I_0}$, which is approachable in solid-state lasers.[3] There are also known techniques to mitigate RIN.[18] In coherent detection, balanced mixer techniques can be used to cancel RIN.[1, 52] Therefore, relative intensity noise will be ignored in this thesis.

Quantization Noise The noise generated by amplitude quantization is not a fundamental physical property but is actually dependent on the signal. It will be discussed later in Section 2.4.1.

2.3 Analog Transport

2.3.1 Review of Intensity Modulation with Direct Detection

The classical analog modulated optical link is intensity modulated (IM) and detected using direct detection (DD). In this section, we review the properties of an IM–DD optical link.

Intensity Modulation

The electric field, $E_s(t)$, of an intensity modulated signal is given in equation (2.6). ω_s radians/s is the carrier frequency and $\kappa \in (0,1]$ is the modulation index. The modulating signal, $g(t)$, has a one-sided bandwidth of B.

$$E_s(t) = |E_s|\sqrt{1+\kappa g(t)}\exp\left(j\omega_s t + j\phi_s(t)\right) \tag{2.6}$$

The un-modulated carrier amplitude is $|E_s|$ resulting in a modulated signal power of $|E_s|^2 = P_s$. Assume the phase noise $\phi_s(t)$ is negligible or mitigated by some means. The resulting modulated signal now has a single sided pass-band bandwidth of W centered at ω_s where $W = B$.

Figure 2-1 shows a simple signal chain with intensity modulation and direct detection. The baseband signals are shown in blue, the pass band modulated signal in red and the added noise from the detection process shown in green.

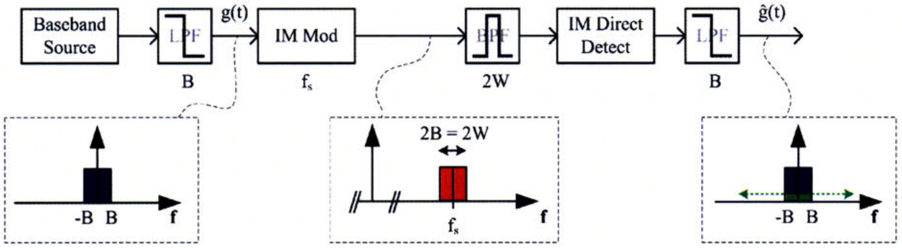

Figure 2-1: Classical IM signal chain with signal and noise spectrums (see text).

For linear operation of the intensity modulator, not only must $\kappa \leq 1$ but $|g(t)| \leq 1$. If $g(t)$ goes below -1 the intensity modulator output becomes ambiguous and we say signal is over modulated. An example of this can be seen in Figure 2-2. A sinusoidal $g(t)$ modulates the carrier and the signal power is shown for various amplitudes of $g(t)$. The envelope of the intensity has an obvious error in the third graph. A further consequence of overmodulation is the average signal power is increased and spurious frequencies are generated from the non-linear effects.

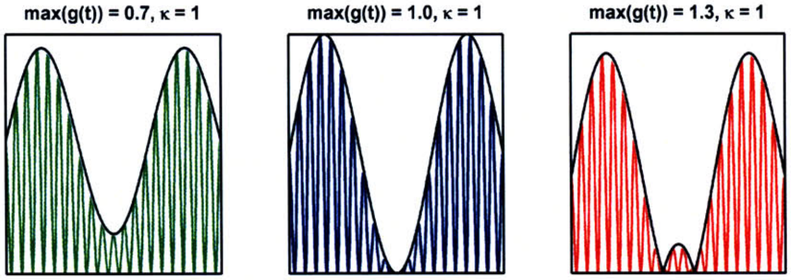

Figure 2-2: Modulation depth in Intensity Modulation (see text).

Direct Detection

In direct detection the received optical field is applied directly to a square-law detector, most commonly a photo-diode. Due to propagation losses, the received optical signal, $E_u(t)$ will be weaker than the original transmitted signal, $E_s(T)$. The power ratio is denoted as G_{optical} such that the received optical power is $P_u = P_s G_{\text{optical}}$.

The photocurrent induced in the photo-diode, I_{PD}, is proportional to the optical power and the responsivity, R, of the photo-diode plus a noise term. The responsivity, expressed in terms of amps per watt, is based on the physical properties of the detector and the optical signal.[2]

$$R = \frac{\eta q}{h\nu} = \frac{\eta q \lambda}{hc} \tag{2.7}$$

Here, η is the quantum efficiency of the detector, q is the charge of an electron and $h\nu$ is the energy of a photon. The energy of a photon is expressed in terms of Planck's constant, h, and its frequency, ν. The photo-detector current is then $I_{PD}(t)$.

$$
\begin{aligned}
I_{PD}(t) =&R\,E_u(t)E_u^*(t) + I_N(t) \\
=&R\,P_u(1+\kappa g(t)) + I_N(t) \\
=&R\,G_{\text{optical}}|E_s|^2(1+\kappa g(t)) + I_N(t) \\
=&R\,G_{\text{optical}}P_s + R\,G_{\text{optical}}P_s\kappa g(t) + I_N(t) \\
=&I_0 + I_s(t) + I_N(t)
\end{aligned}
\tag{2.8}
$$

The photocurrent is split into two additional terms. I_0 represents the average current due to DC component of the IM signal. $I_s(t)$ represents the information content of the photocurrent. By ignoring I_0 and normalizing the gain we can recover an estimate of the source signal, $\hat{g}(t)$, corrupted by the noise term.

$$
\begin{aligned}
\hat{g}(t) &= \frac{I_s(t) + I_N(t)}{RP_u\kappa} \\
&= g(t) + \frac{I_N(t)}{RP_u\kappa}
\end{aligned}
\tag{2.9}
$$

Direct Detection Noise Density

The noise term $I_N(t)$ is a Gaussian random process because of thermal and shot noise with a noise spectral density of $N_{0_{DD}}$. The normalization applied to recover $\hat{g}(t)$ is frequency agnostic so the power spectral density of noise with IM–DD is

$$
S_{n_{\text{IMDD}}}(f) = \frac{N_{0_{DD}}}{2}\frac{1}{R^2P_u^2\kappa^2}
\tag{2.10}
$$

Next, substitute the expression for shot and thermal noise.

$$
S_{n_{\text{IMDD}}}(f) = \frac{2k_bT/R_L + qRP_u}{P_u^2R^2\kappa^2}
\tag{2.11}
$$

If the received optical power, P_u, is high enough we might consider shot noise to dominate. The shot noise limit may also be achieved by using an optical pre-amplifier prior to direct detection.

$$S_{n_{\mathrm{IMDD}}}(f) = \frac{h\nu}{\eta P_u \kappa^2} \tag{2.12}$$

2.3.2 Frequency Modulation with Coherent Detection

Optical Frequency Modulation

The frequency modulation of a signal $g(t)$ onto an optical carrier for transport with center frequency ω_s results in the electric field $E_s(t)$.

$$E_s(t) = |E_s| \exp\left(j\omega_s t + j2\pi f_\Delta \int^t g(t)\mathrm{d}t + \phi_s(t) \right) \tag{2.13}$$

Consider that $g(t)$ has been normalized to $[-1, 1]$ and f_Δ is the maximum instantaneous frequency deviation when $|g(t)| = 1$. The modulation index is then $\beta = \frac{f_\Delta}{B}$. Assume that the phase noise of the transmitter $\phi_s(t)$ is negligible or can be mitigated.[52] The power of the modulated carrier is the square of the electric field amplitude, $|E_s|$ so $P_s = |E_s|^2$.

It is important to consider the bandwidth expansion effect of frequency modulation as it significantly differs from intensity modulation. Determining the bandwidth of $E_s(t)$ analytically is complex for any non-trivial $g(t)$ including a steady state sinusoid. The absolute bandwidth technically is unbounded, however the power spectral density drops off quickly outside of a central range. In general the one-sided bandwidth required for an FM signal is considered to be W with [51]

$$\begin{aligned} W =& f_\Delta + 2B \\ =& (\beta + 2)B \end{aligned} \tag{2.14}$$

Carson's rule is a similar bandwidth estimator although it is not discussed further in this paper.[10] Carson pointed out that even for $\beta < 1$ the bandwidth of a frequency modulated channel will always be greater than B. Therefore only $\beta \geq 1$ is of interest.

The classical discussion of frequency modulation assumes the modulating signal bandwidth, B, is baseband not pass band. This causes some confusion as to the implementation and meaning of bandwidth. These issues will be separated and dealt with in Section 2.5.1. For now, consider the classical heterodyne frequency modulated communications channel as depicted in Figure 2-3 where $g(t)$ is a baseband signal shown in blue with one-sided bandwidth of B. After frequency modulation at a center frequency of f_s the pass-band width has expanded, as shown in red, from B to W. The modulated signal is mixed with a local oscillator at frequency f_{LO} and filtered before passing through the FM discriminator. The post-discriminator noise, in green, will be discussed in Section 2.3.2.

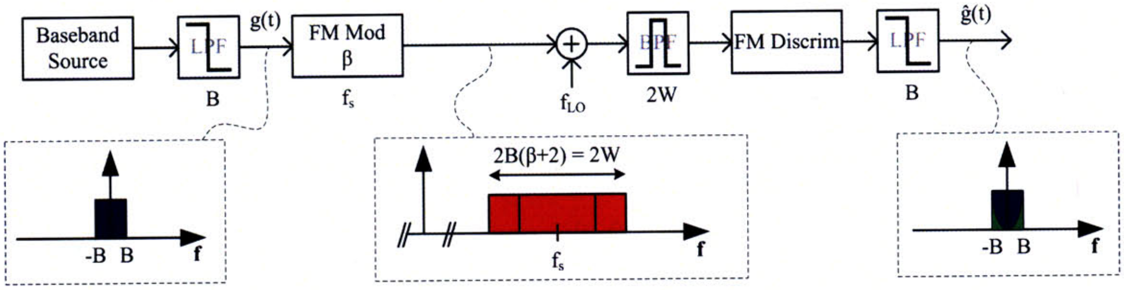

Figure 2-3: Classical heterodyne FM signal chain with signal and noise spectrums (see text).

A variation on this signal chain is homodyne detection where $f_{LO} = f_s$. The band pass filter before the FM discriminator is replaced with a low pass filter of width W. Synchronization of the local oscillator with the source must be considered, but the homodyne case reduces the total noise seen by the FM discriminator by a factor of two.

In the event that $|g(t)| > 1$ the instantaneous frequency deviation will be greater than f_Δ. Even if the modulator remains linear the optical bandwidth will be greater than W and therefore the pre-discriminator filter will cut off part of the signal. When this event occurs, the discriminator will only see the detector noise causing a discontinuity in the phase extraction. It is by this mechanism that overmodulation in an FM system leads to non-linear behavior.

Coherent Detection

For coherent detection, the modulated signal field is added to a local oscillator field and detected by a square-law detector. The local oscillator (LO) provides a reference to compare the modulated signal's phase. The LO has frequency ω_{LO} and amplitude $|E_{LO}|$. The electric field of the LO is

$$E_{LO}(t) = |E_{LO}| \exp\left(j\omega_{LO}t + j\phi_{LO}(t)\right) \tag{2.15}$$

Assume that the LO phase noise is slow enough compared to the signal modulation that the phase noise can be tracked out. The mixing of the received signal results in an intermediate frequency component, $\omega_{IF} = \omega_s - \omega_{LO}$ (see equation (2.16)) The frequency response of practical photo-detectors is limited to hundreds of gigahertz or less so the intermediate frequency must be chosen to be much less than ω_s. In the homodyne case $\omega_s = \omega_{LO}$ so $\omega_{IF} = 0$ although this requires active phase synchronization of the LO. The electric field at the detector, $E_{PD}(t)$, after accounting for the propagation gain, G_{optical}, is then:

$$\begin{aligned}
E_{PD}(t) &= E_u(t) + E_{LO}(t) \\
&= \sqrt{G_{\text{optical}}} E_s(t) + E_{LO}(t) \\
&= \sqrt{G_{\text{optical}}} |E_s| \exp\left(j\omega_s t + j2\pi f_\Delta \int^t g(t)\mathrm{d}t\right) + |E_{LO}| \exp\left(j\omega_{LO}t + j\phi_{LO}(t)\right) \\
&= \left[\sqrt{G_{\text{optical}}} |E_s| \exp\left(j2\pi f_\Delta \int^t g(t)\mathrm{d}t\right) + |E_{LO}| \exp\left(-j\omega_{IF}t\right)\right] \exp\left(j\omega_s t\right)
\end{aligned} \tag{2.16}$$

As before, the output of the photo-detector is proportional to the square of the electric field and its responsivity. See equation (2.7) for the definition of R. The output also includes a noise term, $I_N(t)$. The final expression is given in terms of the optical power received, P_u.

$$
\begin{aligned}
I_{PD}(t) =& R\, E_{PD}(t)E^*_{PD}(t) + I_N(t) \\
=& R\left[\sqrt{G_{\text{optical}}}|E_s|\exp\left(j2\pi f_\Delta \int^t g(t)\mathrm{d}t\right) + |E_{LO}|\exp\left(-j\omega_{IF}t\right)\right]\exp\left(j\omega_s t\right) \\
&+ \left[\sqrt{G_{\text{optical}}}|E_s|\exp\left(-j2\pi f_\Delta \int^t g(t)\mathrm{d}t\right) + |E_{LO}|\exp\left(j\omega_{IF}t\right)\right]\exp\left(-j\omega_s t\right) \\
&+ I_N(t) \\
=& R\,\sqrt{G_{\text{optical}}}|E_s|^2 + R\,|E_{LO}|^2 \\
&+ R\,\sqrt{G_{\text{optical}}}|E_s||E_{LO}|\cos\left(2\pi f_\Delta \int^t g(t)\mathrm{d}t - \omega_{IF}t\right) + I_N(t) \\
=& R(G_{\text{optical}}P_s + P_{LO}) + 2R\sqrt{G_{\text{optical}}P_s P_{LO}}\cos\left(2\pi f_\Delta \int^t g(t)\mathrm{d}t - \omega_{IF}t\right) \\
&+ I_N(t) \\
=& R(P_u + P_{LO}) + 2R\sqrt{P_u P_{LO}}\cos\left(2\pi f_\Delta \int^t g(t)\mathrm{d}t - \omega_{IF}t\right) + I_N(t) \qquad (2.17) \\
=& I_0 + I_s(t) + I_N(t)
\end{aligned}
$$

The photocurrent is split into two additional terms as in the direct detection analysis. I_0 is the average current due to the received FM signal and the LO. $I_s(t)$ is the information content of the photocurrent. Notice that the information content sees an amplification due to the LO power.

To verify, average detector current is:

$$
\begin{aligned}
I_0 =& \mathsf{E}\left[R(P_u + P_{LO}) + 2R\sqrt{P_u P_{LO}}\cos\left(2\pi f_\Delta \int^t g(t)\mathrm{d}t - \omega_{IF}t\right) + I_N(t)\right] \\
=& R(P_u + P_{LO}) + 2R\sqrt{P_u P_{LO}}\,\mathsf{E}\left[\cos\left(2\pi f_\Delta \int^t g(t)\mathrm{d}t - \omega_{IF}t\right)\right] + 0 \\
=& R(P_u + P_{LO}) \qquad (2.18)
\end{aligned}
$$

The detector noise, $I_N(t)$, is effectively an additive white Gaussian process, as in the direct detection case. Here we specify the noise spectral density for coherent detection as $N_{0_{CD}}$. Since the FM signal has a one-sided bandwidth of W the total noise power reaching the discriminator must be accounted for over this entire range. The noise power for heterodyne detection where $\omega_{IF} \neq 0$ must account for both band-pass regions (positive and negative frequency).

$$\mathsf{E}\left[I_N(t)I_N^*(t)\right] = 2N_{0_{CD}}W \quad : \text{Heterodyne CD} \tag{2.19}$$

In the homodyne detection case where $\omega_{IF} = 0$ the signal is at baseband so only half of the noise is captured. The remaining analysis will assume homodyne detection.

$$\mathsf{E}\left[I_N(t)I_N^*(t)\right] = N_{0_{CD}}W \quad : \text{Homodyne CD} \tag{2.20}$$

Carrier to Noise Ratio

An important parameter in the performance analysis of frequency modulation is the carrier to noise ratio (CNR). To calculate the CNR we must determine the total carrier power and the total noise power over the FM bandwidth.

The total carrier power calculation is contained in the sinusoidal component of $I_s(t)$ as there is no information in I_O.

$$\begin{aligned}\mathsf{E}\left[I_s(t)I_s^*(t)\right] &= 4R^2(P_uP_{LO})\,\mathsf{E}\left[\cos^2\left(2\pi f_\Delta \int^t g(t)\mathrm{d}t - \omega_{IF}t\right)\right] \\ &= 4R^2(P_uP_{LO})\frac{1}{2} \\ &= \frac{I_s^2}{2}\end{aligned} \tag{2.21}$$

The noise power determined in the previous section as proportional to the coherent detection noise spectral density $N_{0_{CD}}$. Thus the carrier to noise ratio at the FM discriminator is

$$\begin{aligned}\text{CNR} &= \frac{I_s^2}{2N_{0_{CD}}W} \\ &= \frac{I_s^2}{2N_{0_{CD}}(\beta+2)B}\end{aligned} \tag{2.22}$$

Shot Noise Limit

As Seeds pointed out, coherent detection allows for shot noise limited performance.[38] This result comes from the fact that both shot noise power and carrier power are proportional to the optical power at the photo-detector and we can increase the optical power by increasing the strength of the local oscillator.

To investigate the shot noise limit, first expand $N_{0_{CD}}$.[3] Here we ignore relative intensity noise for reasons discussed previously.

$$\begin{aligned} N_{0_{CD}} =& N_{0D_{\text{Therm}}} + N_{0D_{\text{Shot}}} \\ =& \frac{4kT}{R_L} + 2q\left(I_0 + I_{dk}\right) \end{aligned} \tag{2.23}$$

Now substitute this into the CNR in (2.22) and combine with (2.18), (2.21), and (2.23). The shot noise limit is found by taking the limit as the local oscillator power approaches infinity.

$$\begin{aligned} \text{CNR} &= \lim_{P_{LO}\to\infty} \frac{I_s^2}{2N_{0D}W} \\ &= \lim_{P_{LO}\to\infty} \frac{2R^2P_uP_{LO}}{\left(\frac{4kT}{R_L} + 2q\left(I_0 + I_{dk}\right)\right)W} \\ &= \lim_{P_{LO}\to\infty} \frac{2R^2P_uP_{LO}}{\left(\frac{4kT}{R_L} + 2q\left(R(P_u + P_{LO}) + I_{dk}\right)\right)W} \\ &= \lim_{P_{LO}\to\infty} \frac{R^2P_uP_{LO}}{qR(P_u + P_{LO})W} \\ &= \frac{RP_u}{qW} = \frac{\eta P_u}{h\nu W} \\ &= \frac{\eta P_u}{h\nu B(\beta + 2)} \end{aligned} \tag{2.24}$$

The key result is that carrier to noise ratio is directly proportional to the received laser power at the photo-detector and inversely proportional to the full optical signal bandwidth.

FM Discriminator and Noise

The FM discriminator recovers an estimate, $\hat{g}(t)$, of the modulating signal $g(t)$. It first extracts the phase component of the input, $I_{PD}(t)$. If the photo-detector was noiseless the phase component is $\left(2\pi f_\Delta \int^t g(t)\mathrm{d}t - \omega_{IF}t\right)$. In the homodyne case the intermediate frequency ω_{IF} is zero. The phase is differentiated and then filtered by the post-demodulation filter, $H_D(f)$. As bandwidth of the modulating signal is B we may consider the post-demodulation filter to have a matching bandwidth. By normalizing the output with an amplitude gain of $A_D = 1/(2\pi f_\Delta)$ this method recovers the original signal.

$$\frac{\partial}{\partial t}\left[2\pi f_\Delta \int^t g(t)\mathrm{d}t\right] A_D = \hat{g}(t) \tag{2.25}$$

However, the detector noise in $I_{PD}(t)$ must be accounted for and corrupts the phase extraction. With the phase corrupted, the recovered signal, $\hat{g}(t)$, is also be corrupted by noise. Therefore, we must analyze the post discriminator noise. Wozencraft and Jacobs perform a classical analysis FM demodulation where the noise is Gaussian, which will be used here.[51] The analysis involves treating the noise in terms of independent in-phase, n_c, and quadrature, n_s, components and assuming the time rate of change of $g(t)$ is low relative to the bandwidth of the modulated signal (where $\beta \gg 1$).

Consider the phasor representation of the signal and noise as we did in the previous section. Figure 2-4 depicts the phasor domain of a signal corrupted by noise. The phasor in blue is circling the origin with a fixed length (given a fixed power level). The noise component in red is broken into an in-phase, n_c, and quadrature, n_s, component. The sum of signal and noise, shown in violet, is used by the phase extractor to measure ϕ. From inspection, we can see that the in-phase noise component should not materially affect the phase extraction.

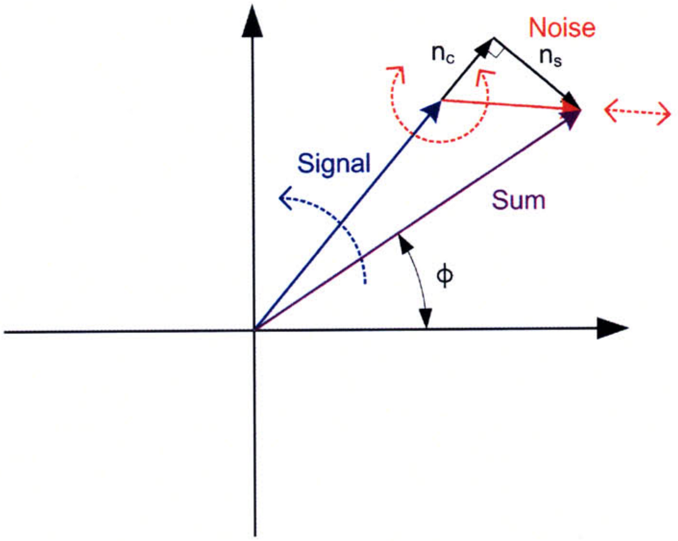

Figure 2-4: Phasor representation of signal and noise (see text).

In general, the power spectral density of the noise of each component can be written as

$$S_{n_s}(f) = S_{n_c}(f) = \begin{cases} \frac{N_{0_{CD}}}{2} & |f| < W \\ 0 & \text{else} \end{cases} \tag{2.26}$$

Consider in the following analysis that $g(t)$ is a constant so the received signal denoted $I_{PD}(t)$ is a sinusoid with constant frequency ω. This constrained signal will be referred to as $\tilde{I}_{PD}(t)$. We use a rectangular to polar transformation on the quadrature noise components in equation (2.28). This method is based on assuming the signal power from equation (2.21) is significantly greater than the total noise power across the entire bandwidth. We can take the shot noise limit using the results of equation (2.24) to simplify the expression. The condition necessary for the weak noise assumption is shown in Equation (2.27).

$$\begin{aligned}
2N_{0_{CD}}W &\ll \frac{I_s^2}{2} \\
1 &\ll \frac{4R^2 P_u P_{LO}}{4(2q\,R(P_u + P_{LO}))W} \\
1 &\ll \frac{1}{2}\frac{\eta}{h\nu W}\frac{P_u P_{LO}}{P_u + P_{LO}} \\
1 &\ll \tfrac{1}{2}\mathrm{CNR} \qquad (2.27) \\
1 &\ll \frac{\eta P_u}{2h\nu(\beta + 2)B}
\end{aligned}$$

$$\begin{aligned}
\tilde{I}_{PD}(t) =& [I_s + \sqrt{2}n_c(t)]\cos(\omega t) + \sqrt{2}n_s(t)\sin(\omega t) \\
=& \sqrt{(I_s + \sqrt{2}n_c(t))^2 + n_s^2(t)}\cos\left(\omega t + \tan^{-1}\left(\frac{-n_s(t)\sqrt{2}}{I_s + n_c(t)}\right)\right) \\
\approx& \sqrt{(I_s + \sqrt{2}n_c(t))^2 + n_s^2(t)}\cos\left(\omega t + \tan^{-1}\left(\frac{-n_s(t)\sqrt{2}}{I_s}\right)\right) \\
\approx& \sqrt{(I_s + \sqrt{2}n_c(t))^2 + n_s^2(t)}\cos\left(\omega t - \frac{n_s(t)\sqrt{2}}{I_s}\right) \\
=& \sqrt{(I_s + \sqrt{2}n_c(t))^2 + n_s^2(t)}\cos\left(\omega t + \phi_{n_s}(t)\right) \qquad (2.28)
\end{aligned}$$

The phase of the signal $\tilde{I}_{PD}(t)$ is corrupted by a Gaussian noise term. Denote this phase noise component as $\phi_{n_s}(t)$. The amplitude of the signal is also corrupted but amplitude variations are ignored in general with an FM discriminator.

To calculate the power spectral density of the post-discriminator noise, we pass $\phi_{n_s}(t)$ through the discriminator process. The differentiator has the transfer function $H'(f) = j2\pi f$. Assume the final filter, $H_D(f)$, is a unit gain "brick-wall" filter with a cutoff of B.

$$\begin{aligned}S_{n_D}(f) =&A_D^2\left(\frac{\sqrt{2}}{I_s}\right)^2 S_{n_s}(f)\left|H'(f)\right|^2\left|H_D(f)\right|^2\\=&\left(\frac{1}{2\pi f_\Delta}\right)^2\frac{1}{2R^2P_uP_{LO}}\frac{N_{0_{CD}}}{2}\left(2\pi f\right)^2(1)^2, \quad |f|<B\\=&\frac{1}{4R^2P_uP_{LO}}N_{0_{CD}}\frac{f^2}{f_\Delta^2}, \quad |f|<B\\=&\frac{1}{4R^2P_uP_{LO}}\left(\frac{4kT}{R_L}+2q\left(I_0+I_{dk}\right)\right)\frac{f^2}{f_\Delta^2}, \quad |f|<B\end{aligned} \tag{2.29}$$

As in the CNR analysis, we can take the shot noise limit to find the general FM–CD noise power spectral density.

$$\begin{aligned}S_{n_{\text{FMCD}}}(f) =& \lim_{P_{LO}\to\infty} S_{n_D}(f)\\=& \lim_{P_{LO}\to\infty}\frac{\frac{4kT}{R_L}+2q\left(R(P_u+P_{LO})+I_{dk}\right)}{4R^2P_uP_{LO}}\frac{f^2}{f_\Delta^2}, \quad |f|<B\\=&\frac{2qR}{4R^2P_u}\left(\frac{f}{f_\Delta}\right)^2, \quad |f|<B\\=&\begin{cases}\frac{h\nu}{2\eta P_u}\left(\frac{f}{f_\Delta}\right)^2 & |f|<B\\ 0 & \text{else}\end{cases}\\=&\begin{cases}\frac{h\nu}{2\eta P_u B^2\beta^2}f^2 & |f|<B\\ 0 & \text{else}\end{cases}\end{aligned} \tag{2.30}$$

The result is that the noise spectrum after FM demodulation is no longer flat but is quadratic. This noise component is shown in Figure 2-3 in green overlaid on the received signal in blue. One processing approach is preemphasis where high frequencies are amplified prior to modulation. This can be accomplished by moving $H'(f)$ in front of the FM modulator, which results in a phase modulation and a flat noise spectrum. Alternately, the post-detection signal can be passed through a whitening filter to flatten the noise. The implementation and effects of whitening the noise is discussed in Section 3.2.4.

An important observation from (2.30) is that the noise decreases with received optical power and with the square of β. Thus, frequency modulation with coherent detection offers bandwidth expansion as an additional parameter to increase performance without increasing the optical power. However we shall see that there is a competing mechanism that prevents us from setting β to an arbitrarily large value.

FM Anomaly

The noise analysis in the previous section assumes that the weak noise assumption holds in equation (2.27). Wozencraft and Jacobs also bound the probability of an anomaly where the phase extraction fails. As the noise process is Gaussian, the path of the noise phasor will cause on occasion the sum phasor to encircle the origin. A very clear graphical example of this behavior is shown on page 160 of *Detection, Estimation and Modulation Theory, Part II.*[44] Thus, the phase extraction will no longer be correct, but off by a full cycle. In terms of practical FM discriminators, this event is analogous to a phase locked loop (PLL) losing lock. Thus, when this anomaly occurs, the output of the discriminator is essentially unknown and may require some time to recover.

Without reproducing their work, the probability of an anomaly, $\mathcal{A}$, can be upper bounded.[51]

$$\begin{aligned} Pr\{\mathcal{A}\} \leq& \frac{1}{\sqrt{3}}\frac{W}{B}Q\left(\frac{I_s}{\sqrt{2WN_{0D}}}\right) \\ =& \frac{\beta+2}{\sqrt{3}}Q\left(\sqrt{\text{CNR}}\right) \\ =& \frac{\beta+2}{\sqrt{3}}Q\left(\sqrt{\frac{\eta P_u}{h\nu B(\beta+2)}}\right) \end{aligned} \tag{2.31}$$

Increasing β or B certainly increases the probability of an anomaly while increased received power counteracts that. It is important to note that the upper bound is not well behaved. For larger β or small P_u it will take on values greater than 1. Thus when evaluating the probability of anomaly we limit the value to 1.

The FM detection anomaly causes the FM threshold effect. In (2.30) we saw that increasing β decreased noise, but the probability of the anomaly grows with β as well.

At some point, the degradation due to the anomaly overwhelms the system regardless of decreased noise; this is the FM threshold. Thus for an FM–CD link given a fixed received optical power there is an optimal modulation index, β, that maximizes the performance of the link. For an analysis of the signal to noise ratio of an FM–CD link including the FM threshold effect refer to Appendix A

2.4 Digital Transport

2.4.1 Quantization

An analog to digital converter (ADC) performs two functions on a continuous time, continuous amplitude signal. It samples the signal discretely in time and then quantizes the amplitude of each sample out of a fixed set of values. Depending on the architecture, the ADC may be placed before or after the optical transport link. However, the analysis of the degradation due to sampling is the same.

Sampling

To prevent aliasing of a baseband signal in the frequency domain the sample rate f_{samp} must be at least twice the highest signal frequency. Thus for a baseband signal with single sided bandwidth B, $f_{\mathrm{samp}} \geq 2B$.[33] We focus here on uniformly distributed samples.

Sampling can be extended to the pass band as long as the signal remains band-limited. Here the sampling function acts similarly to a heterodyne mixer followed by baseband sampling. An equivalent rule applies where the sample rate must be at least twice the bandwidth of the pass band signal. An in depth analysis of pass band sampling can be found in [47].

If the sample rate is set much higher than the minimum required, digital noise shaping techniques can be used to shift the amplitude quantization noise (discussed next) out of the frequency band of interest.[33] Although these techniques exist, we will ignore them for now as they do not decrease the required bit rate. Thus assuming the band-limiting filter prior to the ADC (anti-aliasing filter) has a sharp cutoff at B, we set the sample rate to

$$f_{\text{samp}} = 2B \tag{2.32}$$

The samples in this communication system will be passed into an array processor where the phase of the RF signal must be preserved. As heterodyning or band pass sampling may be used, we must consider quadrature sampling techniques to keep the phase information. These are discussed in Section 2.5.1.

Amplitude Quantization

The quantization of continuous amplitude to discrete amplitude generates distortion. Obviously, the number of finite levels is directly related to the precision of the quantized signal. Reducing the levels increases the coarseness of the quantizer. Although one may choose to construct a quantizer with any number of levels, we shall restrict our analysis to quantizers with $L = 2^b$ levels where b is an integer number of binary bits. The output of the quantizer is encoded into a binary word b-bits long.

Figure 2-5 depicts the transfer function for a 3-bit quantizer. The quantizer here has a full-scale range between $[-1, 1]$. The spacing between levels is noted as Δ. The far right has two columns that show example binary encodings of each level. It also shows the quantizer response to a full-scale sine wave.

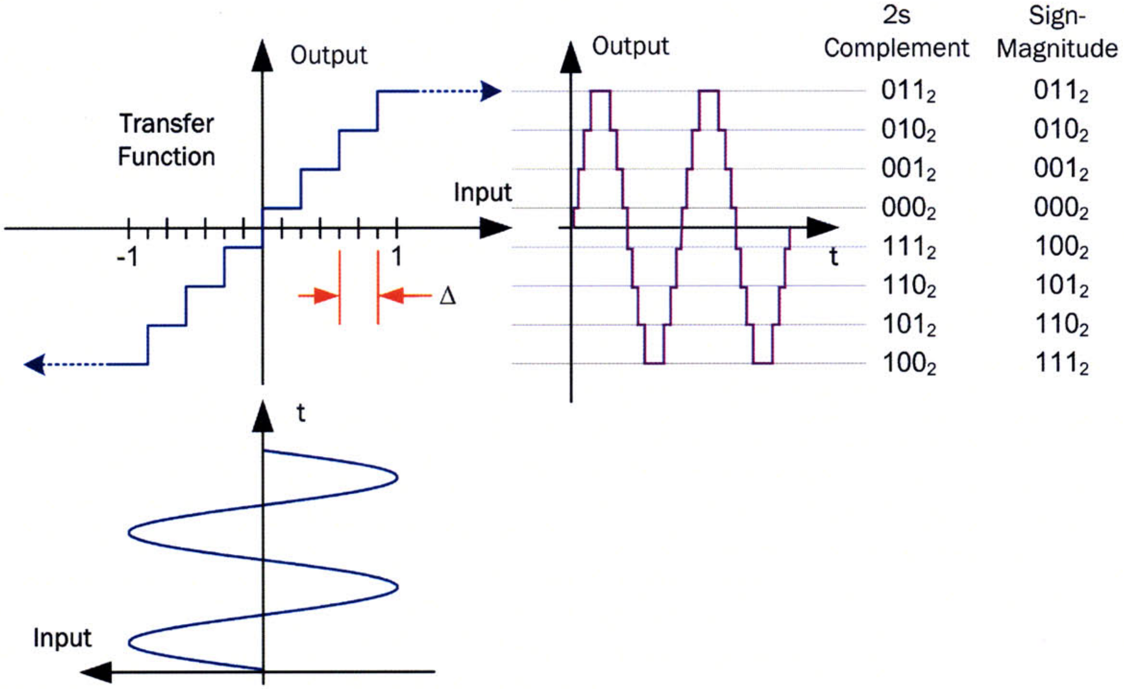

Figure 2-5: Transfer function of 3-bit uniform amplitude quantizer, example output shown with binary coding (see text.

To fully specify the quantizer transfer function that maps a signal $x \mapsto y$ the range of x must be partitioned and the output levels of y must be specified. The set boundaries of each partition are noted $\{x_i : i = 1, \ldots, L+1\}$ where $x_1 = -\infty$, $x_{L/2} = 0$, and $x_{L+1} = \infty$. The set of output levels are $\{y_i : i = 1, \ldots, L\}$. Thus quantizer maps x to $\{y_i : x_i \leq x < x_{i+1}\}$. The difference between the input and output is distortion, which we would like to minimize for any choice of b and signal input.

The most common distortion measure is mean square error (MSE) denoted by ξ_q in (2.33). To calculate the MSE we must know the probability distribution function of the input signal, $\mathrm{p}_X(x)$.

$$\begin{aligned}\xi_q &= \mathsf{E}\left[(x-y)^2\right] \\ &= \sum_{i=1}^{L} \int_{x_i}^{x_{i+1}} (y_i - x)^2 \mathrm{p}_X(x) \mathrm{d}x \qquad (2.33)\end{aligned}$$

We can find the optimum values for x_i and y_i by differentiating ξ_q and setting the derivatives to zero. This method is used by Max.[30]

$$\frac{\partial \xi_q}{\partial x_i} = (x_i - y_{i-1})^2 \mathrm{p}_X(x_i) - (x_i - y_i)^2 \mathrm{p}_X(x_i) = 0 \quad i = 2, \dots, L \tag{2.34}$$

$$\frac{\partial \xi_q}{\partial y_i} = \int_{x_i}^{x_{i+1}} (2x - 2y_i) \mathrm{p}_X(x) \mathrm{d}x = 0, \quad i = 1, \dots, L \tag{2.35}$$

For a signal with a non-uniform $\mathrm{p}_X(x)$, this method will return a non-uniform quantizer transfer function. Practical quantizers however use equally spaced quantization steps where with fixed spacing, Δ. Thus,

$$\Delta = y_{i+1} - y_i \quad \forall i \in [1, \dots, L-1] \tag{2.36}$$

These methods lend themselves to numerical computation. Table 2 of [30] has computed the optimum ξ and Δ over $L = 2, \dots, 36$ for an equally spaced quantizer given a standard normal distribution.

We make the following simplification to approximate the PDF of the quantization error. If Δ is made small enough, the probability over each interval $[x_i, x_{i+1}]$ (excluding the first and last) is approximately uniform.[50, 29] The distortion is evenly distributed between $[-\frac{\Delta}{2}, \frac{\Delta}{2}]$, as shown in blue in Figure 2-6. The first and last intervals cover some values of input that are outside the range of y_i. The PDF of these out of range errors are shown in red. It is desirable to operate the quantizer such that the out of range inputs occur very rarely.

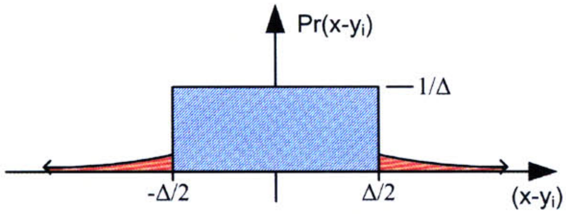

Figure 2-6: Probability distribution of quantization error in uniform quantizer (see text).

The full-scale range is notionally the range between $[-\Delta\frac{L}{2}, \Delta\frac{L}{2}]$. As the analog modulation schemes require the input signal to be normalized within $[-1, 1]$ let us operate the quantizer with the same full-scale range. Therefore the quantizer step size is

$$\Delta = 2^{-b+1} \quad b \in \mathbb{N}^* \tag{2.37}$$

Ignoring out of range inputs, the mean square error due to quantization is [33]

$$\begin{aligned} \xi_q &\approx \int_{-\Delta/2}^{\Delta/2} (x-0)^2 \tfrac{1}{\Delta} \mathrm{d}x \\ &= \frac{\Delta^2}{12} \\ &= \tfrac{1}{3} 2^{-2b} \end{aligned} \tag{2.38}$$

To treat the quantization error as an additive noise process the quantization error must be independent from the input signal. When the number of quantization levels is large this is a reasonable assumption, but for small L we cannot expect independence. However, we can enforce independence by using subtractive dither. A dither signal with amplitude Δ is generated and added to the signal prior to quantization and subtracted back out of the quantized signal.[48] Subtractive dither can also assist in guaranteeing a flat quantization noise spectrum

Finally, we determine the noise power spectrum of a uniform amplitude quantizer. Bennett showed that the spectrum is not necessarily flat, but a flat approximation is reasonable.[5, 49] Thus divide the MSE over the sampling bandwidth, B, of the quantizer.

$$S_{n_{\text{quant}}}(f) = \frac{1}{3B} 2^{-2b} \quad |f| \leq B \tag{2.39}$$

A b-bit analog to digital converter operating at a sampling rate of $2B$ will generate a quantized data rate R_q of $2\,B\,b$ bits per second. For an ADC adjacent to the array processor we can safely ignore R_q. When the ADC is located at the remote antenna we must transport R_q bits per second back to the array processor with high fidelity. Thus the value of b may be different between analog transport and digital transport architectures for a given optical transport power.

2.4.2 Digital Optical Transport

The performance of digital free-space optical communications links is a significant area of study. We may consider the digital link to operate in three regions; high enough power to have effectively zero bit errors, moderate power with occasional errors causing slight degradation of the link, and too little power so the link is unreliable and effectively down. Given that detectors now exist with single photon counting capabilities, let us consider the performance limit of a digital link.[41, 17] We also have the option of using an error correcting code in the digital optical link Coding gains when the link is operating in marginal conditions can be great with reliable communication at one photon per bit.[19] However, as the capacity calculations for coded systems are more complex we will assume uncoded digital transport for now.

The performance limit of an uncoded on-off keying (OOK) optical link is derived in [9, 11]. Photons arrive with a Poisson distribution. For equiprobable signals, we choose to detect a one whenever any photons are detected in a bit interval. The noiseless probability of error, $\Pr\{\varepsilon\}$ in the OOK link is approximately [9, 13]

$$\Pr\{\varepsilon\} = \tfrac{1}{2}e^{-N_s} \tag{2.40}$$

where N_s is the number of photons expected per signal interval. We can approximate this value by dividing the received optical power by number of bits per second, R_q, and the energy per photon, $h\nu$.

$$N_s = \frac{\eta P_u}{R_q\, h\nu} \tag{2.41}$$

2.4.3 End-to-End Performance

Bit errors in the optical transport link corrupt the quantizer words. A bit error in the least significant digit of a quantizer word will cause an error in the signal value of Δ in that sample. However a bit error elsewhere in the word or more than one bit error will cause more significant signal degradation, even up to the full-scale range of the quantizer. At some point the signal errors caused by the transport link is overwhelming and we can consider the link down.

While the transport probability of error, p_ε, is moderate we can calculate the mean square error. For each b-bit sample word i, calculate the probability that transport errors will cause it to be received as word k.

$$Pr\{\mathrm{Word}_k|\mathrm{Word}_i\} = (1 - \mathrm{p}_\varepsilon)^{b-\mathsf{N}_e}(\mathrm{p}_\varepsilon)^{\mathsf{N}_e} \tag{2.42}$$

Here the quantity N_e is a count of the number of binary digits that are different between i and k. The complete mean square error caused by occasional bit errors in uncoded digital transport is therefore

$$\xi_{\mathrm{dig}} = \sum_{i=0}^{2^b-1} Pr\{\mathrm{Word}_i\} \sum_{k=0}^{2^b-1} Pr\{\mathrm{Word}_k|\mathrm{Word}_i\}(y_i - y_k)^2 \tag{2.43}$$

As b increases the computation of ξ_{dig} becomes increasingly costly. For $b = 1$, $\xi_{\mathrm{dig}} = \mathrm{p}_\varepsilon$. By numerically computing ξ_{dig} for increasing b we found it converged to an upper bound of $\frac{4}{3}\mathrm{p}_\varepsilon$ asymptotically. The bound was accurate to five decimal places for $b = 7$ and verified up to $b = 14$. The bound is independent of the ordering of the quantization words (e.g. 2s complement, sign-magnitude) and tested over the range $\mathrm{p}_\varepsilon \in [10^{-20}, 0.5]$.

$$\mathrm{p}_\varepsilon \leq \xi_{dig} \leq \tfrac{4}{3}\mathrm{p}_\varepsilon \tag{2.44}$$

We can reasonably put the degradation due to transport in terms of an additive noise term with power spectral density:

$$\begin{aligned} S_{n_{\mathrm{dig}}}(f) &= \frac{\xi_{dig}}{B} \quad |f| \leq B \\ &\approx \frac{4\mathrm{p}_\varepsilon}{3B} \end{aligned} \tag{2.45}$$

As p_ε in the digital transport link grows the degradation quickly becomes more severe. This is analogous to the FM discriminator anomaly.

2.5 RF Front–End Electronics

2.5.1 Baseband Versus Band Pass Systems

In the analysis of both analog and digital transport subsystems we have used the simplification that the antenna observations were baseband signals. In practice the RF communication signals are modulated onto a high carrier frequency, f_0, with some single sided pass band bandwidth of B. There is no need to transport the entire DC to $f_0 + B$ as much of the range carries no information.

Consider the FM–CD link discussed previously in Figure 2-3. If we were to modify it and directly inject the pass band signal into the modulator the signal chain would now look like Figure 2-7. As the bandwidth to the FM modulator is now $f_0 + B$ the total optical bandwidth is very large which will significantly increase the required optical power. Furthermore, after the FM discriminator the quadratic noise will be much stronger in the band of interest significantly degrading the performance of the link.

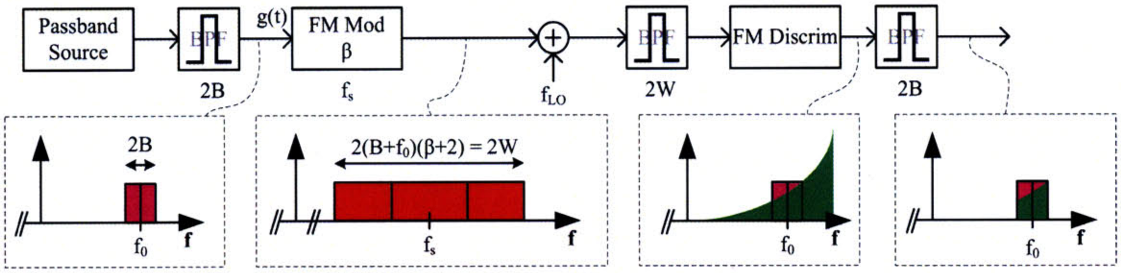

Figure 2-7: Direct front-end FM signal chain with signal and noise spectrums (see text).

The recovered signal at the array processor will be a very high frequency requiring either a very fast sample rate or some form of heterodyning or quadrature sampling (discussed below) The IM–DD transport does not suffer from the effects of quadratically distributed noise but it still suffers from a very large bandwidth.

A more practical way to deal with the high center frequency is to mix the signal down to baseband. As the array processor will need the phase information, we must split the signal into an in-phase (I) and quadrature (Q) component. This is easily done by using a mixer which has one output shifted 90° from the other, hence the heterodyne/quadrature label. A signal chain for this method is shown in Figure 2-8. By splitting the signal into two, we must now transport both signal to the array processor using two independent inter-satellite links. This requirement is not an obstacle as wavelength division multiplexing is well understood.

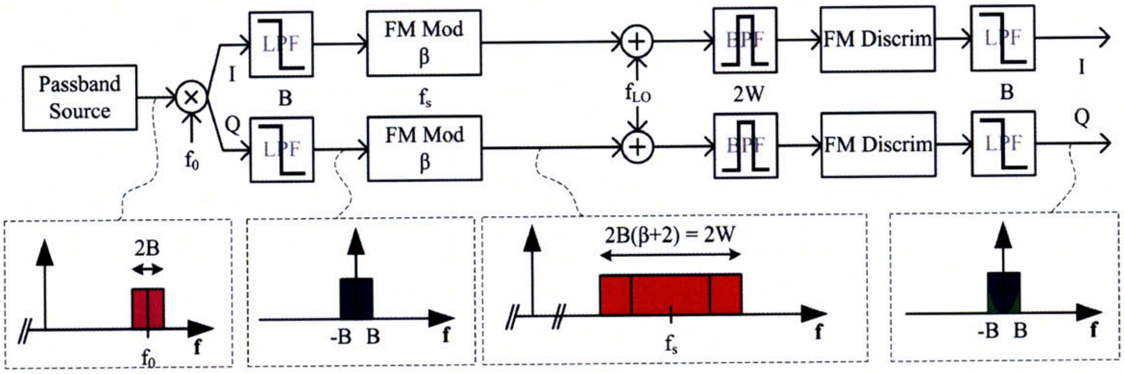

Figure 2-8: Heterodyne (Quadrature) front-end FM signal chain with signal and noise spectrums (see text).

At the array processor the recovered in-phase and quadrature signals may be sampled with standard sampling techniques.

Digital transport is subject to the same issue. It is impractical to sample the raw signal observations given the high required sample rate. Therefore, we can use the same idea of heterodyne mixing with in-phase and quadrature outputs. This is known as complex sampling.[32] A block diagram of this is shown in Figure 2-9.

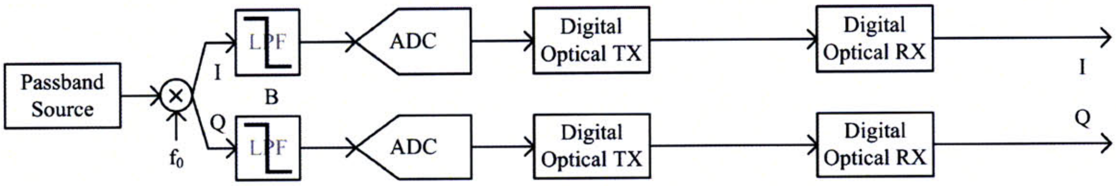

Figure 2-9: Heterodyne (Quadrature) front-end digitizing signal chain (see text).

To compare architectures on equal grounds we will use a heterodyning front-end with separate I and Q channels for both analog and digital transport architectures. Thus, the required optical power will be double that of a single optical link, but this applies to all architectures under investigation.

2.5.2 Gain

The other function of the front-end is to scale the observations appropriately prior to analog or digital transport. Both classes of transport architectures have a fixed full-scale input range between $[-1, 1]$. Signal excursions outside this range can cause overmodulation or out of range issues depending of architecture. Alternately if the signal does not extend to the full-scale range the available dynamic range of the signal transport is unused increasing the relative noise seen at the array processor. Thus, the front-end should also contain a limiting amplifier with controllable amplitude gain.

The observation of the RF environment received by an antenna is noted as $r(t)$. This is the sum of the communication signal, any interfering sources, and environmental and electronic noise due to the front-end electronics. Note the maximum amplitude of $r(t)$ as $r_{\max}$. The amplitude gain, A_{FE}, of the front-end amplifier must be set so that the output, $g(t)$, has a maximum amplitude $g_{\max}$ of no more than 1. See Figure 2-10 for a diagram of the limit amplifier with example input and outputs shown. The three output curves show examples of optimum gain (in blue), too little gain (in green) and too much gain causing clipping (in red). The gain should be set to

$$A_{FE} \leq \frac{1}{r_{\max}} \tag{2.46}$$

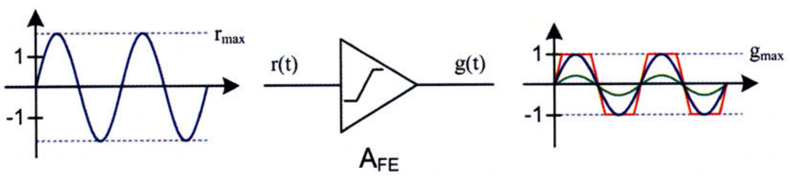

Figure 2-10: Front-end limiting amplifier (see text).

In practice the gain setting of each front-end amplifier will need to be set centrally by the array processor and it will vary greatly as operational conditions change. The controller will need to know the $r_{\max}$ in order to set the gain. Thankfully, $r_{\max}$ should vary slowly relative to the communications bandwidth so the control of A_{FE} can be performed using a lower speed side-channel. For the remainder of this thesis we assume A_{FE} is always set to an optimal level.

2.6 Transport Losses

In Sections 2.3 and 2.4 make note of the propagation loss of the optical inter-satellite link. In order to calculate the power gain, G_{optical}, we assume that the opto-mechanical subsystem operates at the diffraction limit for its size. Therefore, we can use the Friis transmission formula.[15]

$$\frac{P_u}{P_s} = G_{\text{optical}} = \frac{A_{e_t} A_{e_r}}{d^2 \lambda^2} \tag{2.47}$$

Where A_{e_t} and A_{e_r} are the effective aperture area of the transmitter and receiver respectively, d is the separation distance between the apertures and λ is the laser wavelength. The Friis formula is accurate within a few percent so long as the apertures are in the Fraunhofer far-field such that

$$d \geq \frac{2a^2}{\lambda} \tag{2.48}$$

where a is the largest linear dimension of either aperture.[15] If the condition is met and we assume equal circular apertures, the transport gain is simply

$$G_{\text{optical}} = \left(\frac{A_e}{\lambda d}\right)^2 \tag{2.49}$$

This method is the same used by Mecherle & Horstein when comparing RF and optical deep-space communication links.[31]

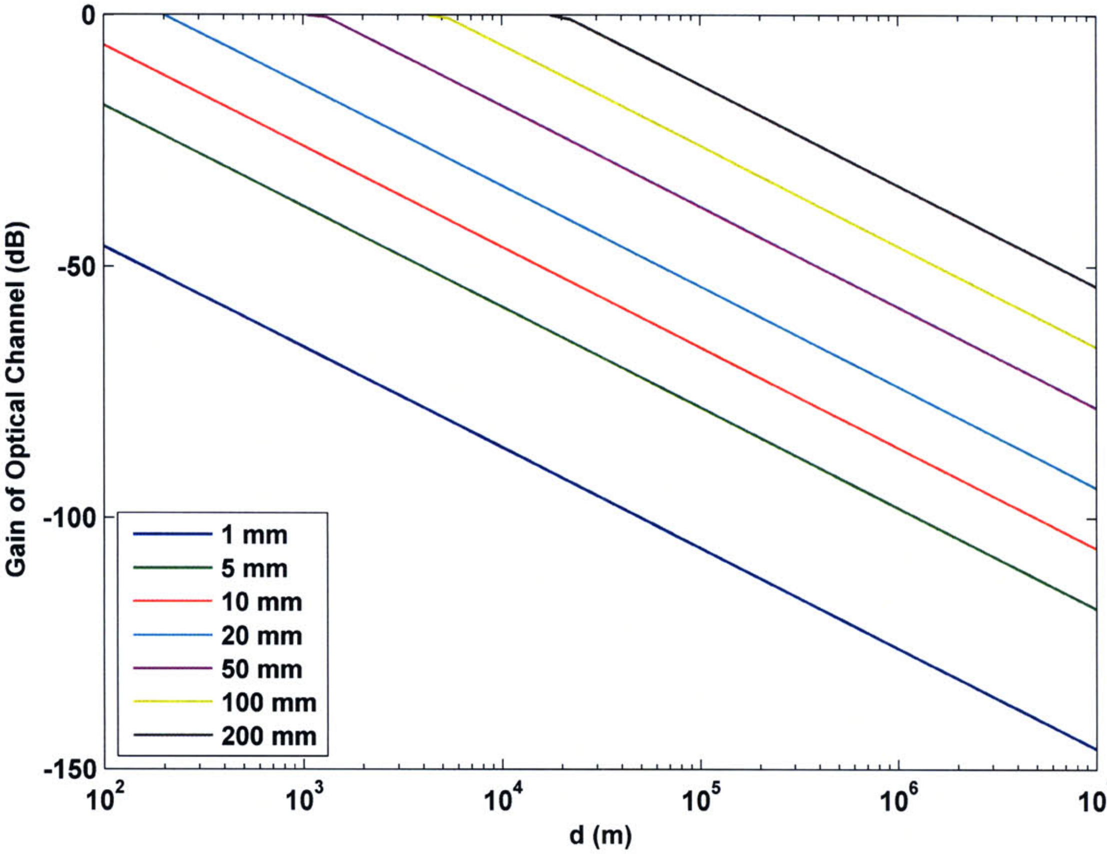

Figure 2-11: Optical propagation loss versus distance and aperture size.

Figure 2-11 shows the gain of the optical channel in decibels versus distance for a selection of aperture diameters based on equation (2.49).

Chapter 3

Array Processing and Detection

3.1 Introduction

This chapter discusses the processing necessary to combine the remote RF antenna observations, mitigate interference and recover the transmitted information from the received signal. We incorporate the constraints analyzed in chapter 2.

Section 3.2 begins the chapter with a review of multi-channel communication receivers in the presence of additive white Gaussian noise. It assumes antipodal modulation of the communication signal and derives the multi-channel correlation receiver. The likelihood ratio test and the probability of error are derived. The analysis is extended to incorporate the a whitening filter for colored noise in Section 3.2.4.

Section 3.3 introduces the antenna-satellite array geometry with a focus on a two antenna configuration. We derive the array response assuming narrow-band plane wave signal and interference sources. The direction of arrival of the RF signals can be derived from the estimated correlation matrix. Here, we assume the direction of arrival is known *a priori*. The array processing is reduced to a complex weighting vector.

Section 3.4 derives the complex array weights for complete nulling of an interferer. The weights are applied to find the resulting bit error probability performance of the communication array. The required additional link margin as compared to the stand-off distance is derived normalized to the wavelength and array size. Finally, the complete system performance is defined.

3.2 Multi-Channel Receiver

In this section we will discuss the design of the multi-channel communication receiver. The approach here follows the methods in Wozencraft & Jacobs for correlation receivers.[51]

Figure 3-1 depicts the signal chain for a basic communication system with two independent receive channels. The data to be transmitted is a stream of discrete symbols, $m[n]$. These modulate a set of known orthonormal basis functions, $\boldsymbol{\varphi}(t)$, to generate the transmitted signal $m(t)$. There are J basis functions denoted individually as $\varphi_j(t)$. The transmitted signal passes through independent channels with additive white Gaussian noise denoted $n_i(t)$ for channels $i = 1$ and 2. The output of each channel is noted as $r_i(t) = m(t) + n_i(t)$. The receiver correlates the received signals against each basis function to generate a vector statistic, $\mathbf{r}_i$, for each channel. This reduces the continuous time waveforms to finite dimensions. Based on these statistics the receiver makes a decision as to which symbol was most likely transmitted. The maximum likelihood receiver yields the minimum error probability.

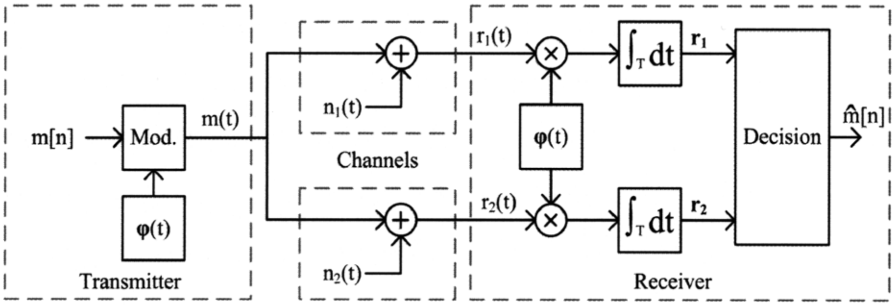

Figure 3-1: Basic communication system signal chain with correlation receiver (see text).

3.2.1 Correlation Receiver

We reduce the received continuous-time signals to finite dimensions by correlating the received signals against the orthonormal basis functions used by the transmitter. Each channel, $i \in [1, \ldots, N]$, has a correlator for each basis function, $j \in [1, \ldots, J]$, generating a receiver statistic $\mathbf{r}_{ij}$.

$$\begin{aligned} \mathbf{r}_{ij} &= \int r_i(t)\varphi_j(t)\mathrm{d}t \\ &= \int m(t)\varphi_j(t)\mathrm{d}t + \int n_i(t)\varphi_j(t)\mathrm{d}t \end{aligned} \tag{3.1}$$

For each transmitted symbol, the first component of equation (3.1) is a constant and the second component is a zero-mean Gaussian random variable. Thus, $\mathbf{r}_{ij}$ is a Gaussian random variable with a mean determined by which symbol was transmitted and a variance of $\sigma^2_{\mathbf{r}_{ij}}$. The received signal for antenna i can be represented by the vector, $\mathbf{r}_i$.

$$\mathbf{r}_i = \begin{bmatrix} \mathbf{r}_{i1} & \ldots & \mathbf{r}_{ij} & \ldots & \mathbf{r}_{iJ} \end{bmatrix} \tag{3.2}$$

For convenience we may refer to the set of receiver vectors for all channels as $\mathbf{r}$.

$$\mathbf{r} = \begin{bmatrix} \mathbf{r}_1 \\ \vdots \\ \mathbf{r}_N \end{bmatrix} \tag{3.3}$$

Consider an antipodal modulation scheme such as binary phase shift keying (BPSK). The baseband basis function for BPSK is a rectangular pulse with unit energy. BPSK uses only one basis function so we drop the subscript, j, and the vector notation of $\varphi(t)$.

$$\varphi(t) = \begin{cases} \frac{1}{T_b} & 0 \leq t \leq T_b \\ 0 & \text{else} \end{cases} \tag{3.4}$$

T_b is the length of a single bit. The Fourier transform of the basis function is[1]

$$\begin{aligned}\mathcal{F}\{\varphi(t)\} &= \Phi(f)\\ &= \int_{-\infty}^{\infty} \varphi(t) e^{-2\pi j f t} \mathrm{d}t\\ &= \int_{-T_b/2}^{T_b/2} \frac{1}{\sqrt{T_b}} e^{-2\pi j f t} \mathrm{d}t\\ &= \sqrt{T_b}\frac{\sin(\pi f T_b)}{\pi f T_b} \qquad (3.5)\end{aligned}$$

The BPSK modulator scales basis function by $\sqrt{E_b}$ with phase controlled by the input symbols, $m[n]$. The modulator uses the following rule.

$$m(t) = \begin{cases} -\sqrt{(}E_b)\varphi(t)\,, & m[0] = 0 \\ \sqrt{(}E_b)\varphi(t)\,, & m[0] = 1 \end{cases} \qquad (3.6)$$

The transmitted symbols have an energy-per-bit of E_b. Assume that all transmitted symbols are equiprobable so $\mathrm{p}_{m=0} = \mathrm{p}_{m=1}$.

As BPSK uses only one basis function (i.e. $J = 1$), the receiver vectors are reduced to scalars and only one correlator per channel is necessary. We calculate the mean and variance of these for each transmitted symbol m on each channel, i. As the noise component is zero-mean, it drops out of the mean calculation.

$$\begin{aligned}\mu_{\mathbf{r}_{i|m=1}} &= \int m(t)\varphi(t)\mathrm{d}t + \int n_i(t)\varphi(t)\mathrm{d}t\\ &= \sqrt{E_b}\int \varphi(t)\varphi(t)\mathrm{d}t\\ &= \sqrt{E_b} \qquad (3.7)\\ &= -\mu_{\mathbf{r}_{i|m=0}}\end{aligned}$$

To calculate the variance we take the expected value of the square of the noise correlation. The variance depends only on the noise and the basis function and is independent of which symbol was transmitted. Since additive white Gaussian

---

[1] We ignore the time shift of the rectangular pulse.

noise is assumed we write the power spectral density of $n_i(t)$ as $S_{n_i}(f) = \frac{N_0}{2}$. The autocorrelation of the noise in the time domain is then $\frac{N_0}{2}(\tau)$.

$$
\begin{aligned}
\sigma^2_{\mathbf{r}_i} &= \mathsf{Var}\left[\int r_i(t)\varphi(t)\mathrm{d}t\right] = \mathsf{E}\left[\left(\int n_i(t)\varphi(t)\mathrm{d}t\right)^2\right] \\
&= \mathsf{E}\left[\iint n_i(t)\varphi(t)n_i(t')\varphi(t')\mathrm{d}t\mathrm{d}t'\right] \\
&= \iint \tfrac{N_0}{2}\delta(t-t')\varphi(t)\varphi(t')\mathrm{d}t\mathrm{d}t' \\
&= \frac{N_0}{2}\int |\varphi(t)|^2\mathrm{d}t = \frac{N_0}{2}\int |\Phi(f)|^2\mathrm{d}f \\
&= \frac{N_0}{2} \quad \text{For orthonormal basis}
\end{aligned}
\tag{3.8}
$$

3.2.2 Likelihood Ratio

We next determine the likelihood ratio test in order to decide which symbol was transmitted. The joint probability distribution of the $\mathbf{r}$ is a multi-variate Gaussian random variable.

$$
\mathsf{p}_{\mathbf{r}_1\mathbf{r}_2|m}(r_1, r_2|m) = \begin{cases} \dfrac{1}{2\pi\sigma_{\mathbf{r}_1}\sigma_{\mathbf{r}_2}}\exp\left(-\dfrac{(r_1+\sqrt{E_b})^2}{2\sigma^2_{\mathbf{r}_1}} - \dfrac{(r_2+\sqrt{E_b})^2}{2\sigma^2_{\mathbf{r}_2}}\right) & , \quad m=0 \\ \dfrac{1}{2\pi\sigma_{\mathbf{r}_1}\sigma_{\mathbf{r}_2}}\exp\left(-\dfrac{(r_1-\sqrt{E_b})^2}{2\sigma^2_{\mathbf{r}_1}} - \dfrac{(r_2-\sqrt{E_b})^2}{2\sigma^2_{\mathbf{r}_2}}\right) & , \quad m=1 \end{cases}
\tag{3.9}
$$

Thus, the likelihood ratio comparing probability of a transmitted "0" or "1" symbol for the received statistics r_1 and r_2 is

$$
\begin{aligned}
\Lambda(r_1, r_2) &= \frac{\mathsf{p}_{\mathbf{r}_1\mathbf{r}_2|m}(r_1, r_2|0)}{\mathsf{p}_{\mathbf{r}_1\mathbf{r}_2|m}(r_1, r_2|1)} \\
&= \exp\left(\frac{(r_1-\sqrt{E_b})^2}{2\sigma^2_{\mathbf{r}_1}} + \frac{(r_2-\sqrt{E_b})^2}{2\sigma^2_{\mathbf{r}_2}} - \frac{(r_1+\sqrt{E_b})^2}{2\sigma^2_{\mathbf{r}_1}} - \frac{(r_2+\sqrt{E_b})^2}{2\sigma^2_{\mathbf{r}_2}}\right) \\
&= \exp\left(-\frac{2\sqrt{E_b}}{\sigma^2_{\mathbf{r}_1}}r_1 - \frac{2\sqrt{E_b}}{\sigma^2_{\mathbf{r}_2}}r_2\right)
\end{aligned}
\tag{3.10}
$$

The log likelihood ratio (LLR) test is used to define the decision regions of the maximum likelihood receiver where the *a priori* probabilities are known.[16] Since we have assumed equiprobable symbols, the log probability ratio is 0. When LLR is greater than zero, pick $\hat{m} = 0$, else pick $\hat{m} = 1$.

$$\mathrm{LLR}(r_1, r_2) = -\frac{2\sqrt{E_b}}{\sigma^2_{\mathbf{r}_1}} r_1 - \frac{2\sqrt{E_b}}{\sigma^2_{\mathbf{r}_2}} r_2 \underset{\hat{m}=1}{\overset{\hat{m}=0}{\gtrless}} 0 = \log \frac{\mathrm{p}_{m=1}}{\mathrm{p}_{m=0}} \tag{3.11}$$

The LLR test weights the correlation statistic from each antenna inversely proportional to the variance of the noise in that channel.

3.2.3 Probability of Error

We define a single Gaussian random variable, $\mathbf{R}$, to replace the multivariate receiver variables used in the log likelihood ratio test where

$$\begin{aligned} \mathbf{R} &= \mathrm{LLR}(\mathbf{r}) \\ &= \mathrm{LLR}(\mathbf{r}_1, \mathbf{r}_2) \end{aligned} \tag{3.12}$$

This is possible because each component of $\mathbf{r}$ is an independent Gaussian random variable and the LLR is a linear sum of terms. The mean and variance of $\mathbf{R}$ can be calculated as

$$\begin{aligned} \mu_{\mathbf{R}|m=0} = -\mu_{\mathbf{R}|m=1} &= -\tfrac{2\sqrt{E_b}}{\sigma^2_{\mathbf{r}_1}} \mu_{\mathbf{r}_1|m=0} - \tfrac{2\sqrt{E_b}}{\sigma^2_{\mathbf{r}_2}} \mu_{\mathbf{r}_1|m=0} \\ &= \tfrac{2\sqrt{E_b}}{\sigma^2_{\mathbf{r}_1}} \sqrt{E_b} + \tfrac{2\sqrt{E_b}}{\sigma^2_{\mathbf{r}_2}} \sqrt{E_b} \\ &= 2E_b \tfrac{\sigma^2_{\mathbf{r}_1} + \sigma^2_{\mathbf{r}_2}}{\sigma^2_{\mathbf{r}_1} \sigma^2_{\mathbf{r}_2}} \end{aligned} \tag{3.13}$$

$$\begin{aligned} \sigma^2_{\mathbf{R}} &= \left(\tfrac{2\sqrt{E_b}}{\sigma^2_{\mathbf{r}_1}}\right)^2 \sigma^2_{\mathbf{r}_1} + \left(\tfrac{2\sqrt{E_b}}{\sigma^2_{\mathbf{r}_2}}\right)^2 \sigma^2_{\mathbf{r}_2} \\ &= 4E_b \tfrac{\sigma^2_{\mathbf{r}_1} + \sigma^2_{\mathbf{r}_2}}{\sigma^2_{\mathbf{r}_1} \sigma^2_{\mathbf{r}_2}} \end{aligned} \tag{3.14}$$

A decision error occurs when the log likelihood ratio test selects the wrong transmitted symbol. We can calculate the conditional probability error for each symbol

$$\begin{aligned}
\Pr\{\epsilon|m=0\} &= \Pr\{\mathrm{LLR}(\mathbf{r}_1,\mathbf{r}_2) < 0|m=0\} \\
&= \Pr\{\mathbf{R} < 0|m=0\} \\
&= \Pr\{\mathcal{N}(\mu_{\mathbf{R}|m=0}, \sigma_{\mathbf{R}}^2) < 0\} \\
&= \Pr\{\mathcal{N}(0,1) > \tfrac{\mu_{\mathbf{R}|m=0}}{\sigma_{\mathbf{R}}}\} \\
&= Q\left(\tfrac{\mu_{\mathbf{R}|m=0}}{\sigma_{\mathbf{R}}}\right) \\
&= Q\left(\sqrt{E_b \frac{\sigma_{\mathbf{r}_1}^2 + \sigma_{\mathbf{r}_2}^2}{\sigma_{\mathbf{r}_1}^2 \sigma_{\mathbf{r}_2}^2}}\right) \qquad (3.15)
\end{aligned}$$

With equiprobable symbols error probability of a multi-channel receiver in the presence of independent additive white Gaussian noise with antipodal signaling is

$$\Pr\{\epsilon\} = Q\left(\sqrt{E_b \frac{\sigma_{\mathbf{r}_1}^2 + \sigma_{\mathbf{r}_2}^2}{\sigma_{\mathbf{r}_1}^2 \sigma_{\mathbf{r}_2}^2}}\right) \qquad (3.16)$$

For this thesis, we have assumed each channel is independent and identical. Thus, $\sigma_{\mathrm{r}_1}^2 = \sigma_{\mathrm{r}_2}^2$. We specify the noise spectral density of a single channel (calculated in equation (3.8)) as $S_{n_i}(f) = N_{0_C}/2$ so the probability of error reduces to

$$\begin{aligned}
\Pr\{\epsilon\} &= Q\left(\sqrt{E_b \frac{\frac{N_{0_C}}{2} + \frac{N_{0_C}}{2}}{\frac{N_{0_C}}{2}\frac{N_{0_C}}{2}}}\right) \\
&= Q\left(\sqrt{4\frac{E_b}{N_{0_C}}}\right) \qquad (3.17)
\end{aligned}$$

The same derivation for a single-channel receiver using antipodal signaling results in an error probability of

$$\Pr\{\epsilon\} = Q\left(\sqrt{2\frac{E_b}{N_{0_C}}}\right) \qquad (3.18)$$

Making two independent observations of the communication signal with two independent noise sources doubles the effective signal to noise ratio.

3.2.4 Whitening Filter

The analysis of the multi-channel receiver, above, depended on the noise being Gaussian and white. In Section 2.3.2 we showed that the noise spectrum for frequency modulated signal transport was quadratically distributed. We will process the received signal to whiten the noise. In this thesis we have not proved that the whitening receiver is optimum. We assume the noise process is wide-sense stationary and the power spectral density, $S_n(f)$, is known.

A whitening filter added immediately prior to the correlator can be used to flatten the power spectrum of the noise. The whitening filter with transfer function, $H_W(f)$, must have a realizable inverse filter such that

$$|H_W(f)|^2 S_n(f) = \Gamma \quad \forall f \tag{3.19}$$

where Γ is some constant value, nominally 1. The whitening filter suppresses energy at frequencies where the noise is strong and amplifies energy where the noise is weak. However, the whitening filter also affects the correlation with the basis function. As the filter is reversible, we may apply the same whitening filter to the basis function prior to the correlator to recover the correlation receiver. The new receiver structure for a single channel is shown in Figure 3-2b and is known as a filtered-reference receiver. The whitened signal is denoted $r^\circ(t)$ and the whitened basis function is denoted $\varphi^\circ(t)$.

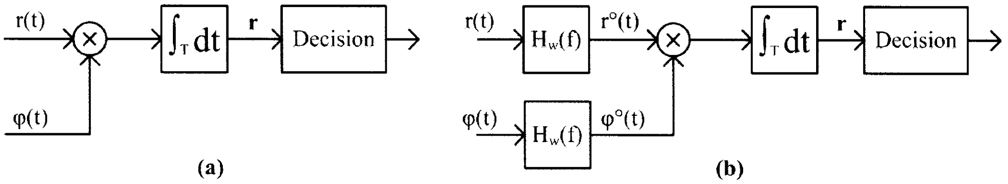

Figure 3-2: Block diagram correlation receiver without (a) and with (b) filtered-reference whitening filter.

We can now calculate the mean and variance of the receiver statistics using the same methods as (3.7) and (3.8). We set $\Gamma = 1$ in equation (3.19) so the power spectral density of the whitened noise at the correlator is unity ($S_{n_r^\circ}(f) = 1$).

$$\begin{aligned}
\mu_{\mathbf{r}^\circ_{m=1}} = -\mu_{\mathbf{r}^\circ_{m=0}} &= \int r^\circ(t)\varphi^\circ(t)\mathrm{d}t \\
&= \int \left[m(t) * h_W(t)\right]\left[\varphi(t) * h_W(t)\right]\mathrm{d}t \\
&= \int M(f)\Phi(f)|H_W(f)|^2\mathrm{d}f \\
&= \sqrt{E_b}\int \frac{|\Phi(f)|^2}{S_n(f)}\mathrm{d}f
\end{aligned} \tag{3.20}$$

$$\begin{aligned}
\sigma^2_{\mathbf{r}^\circ} &= S_{n_r^\circ}(f)\int |\Phi^\circ(f)|^2\mathrm{d}f \\
&= S_{n_r^\circ}(f)\int \frac{|\Phi(f)|^2}{S_n(f)}\mathrm{d}f \\
&= \int \frac{|\Phi(f)|^2}{S_n(f)}\mathrm{d}f
\end{aligned} \tag{3.21}$$

From this we calculate the minimum probability of error for signals in non-white noise using the filtered-reference correlation receiver.

$$\begin{aligned}
\Pr\{\epsilon\} &= Q\left(\frac{\mu_{\mathbf{r}^\circ_{m=0}}}{\sigma_{\mathbf{r}^\circ}}\right) \\
&= Q\left(\frac{\sqrt{E_b}\int \frac{|\Phi(f)|^2}{S_n(f)}\mathrm{d}f}{\sqrt{\int \frac{|\Phi(f)|^2}{S_n(f)}\mathrm{d}f}}\right) \\
&= Q\left(\sqrt{E_b\int \frac{|\Phi(f)|^2}{S_n(f)}\mathrm{d}f}\right)
\end{aligned} \tag{3.22}$$

White Noise

To verify the analysis we substitute a white noise process into equation (3.22). Set $S_n(f) = \alpha = \frac{N_0}{2}$. The result matches equation (3.18).

$$\Pr\{\epsilon\} = Q\left(\sqrt{\frac{E_b}{\alpha}}\right) = Q\left(\sqrt{\frac{2E_b}{N_0}}\right) \tag{3.23}$$

FM–CD Noise

Now, consider the noise process when using a frequency modulated inter-satellite link. In addition to the noise from the analog transport subsystem, there is additive white noise from the RF front-end and from the digitizers. Therefore, we write the power spectral density of the FM–CD system noise in the form

$$S_n(f) = \alpha^2 + (\gamma f)^2 \tag{3.24}$$

where α^2 is the total noise spectral density of white noise and $(\gamma f)^2$ is from equation (2.30) such that

$$\alpha^2 = \frac{N_0}{2} \tag{3.25}$$

$$\gamma^2 = \frac{h\nu}{2\eta P_u B^2 \beta^2} \tag{3.26}$$

To evaluate equation (3.22) we must evaluate the integral in equation (3.21). Recall that the band-limiting filter after the FM discriminator in the FM–CD system cuts off all frequencies above B. The appropriate limits of integration are from $-B$ to B. However, there is no closed form solution to this integral with fixed integration limits when $\gamma \neq 0$. We know in the FM–CD architecture that noise density rapidly increases with frequency and that the whitening filter suppresses large noise. It is then reasonable to investigate the behavior of equation (3.21) with the limits taken to $\pm\infty$. This will represent a strict upper bound.

$$\begin{aligned}
\zeta &= \int_{B}^{B} \frac{|\Phi(f)|^2}{S_n(f)} \mathrm{d}f \\
&\leq \int_{-\infty}^{\infty} \frac{|\Phi(f)|^2}{S_n(f)} \mathrm{d}f \\
&= \int_{-\infty}^{\infty} T_b \frac{\sin^2(\pi f T_b)}{\pi^2 f^2 T_b^2 \left(\alpha^2 + (\gamma f)^2\right)} \mathrm{d}f \\
&= \int_{-\infty}^{\infty} \mathfrak{g}_1(f) \mathfrak{g}_2(f) \mathrm{d}f
\end{aligned} \tag{3.27}$$

Evaluating equation (3.27) directly is somewhat difficult. We make use of Parseval's theorem by representing the integrand as two functions, $\mathfrak{g}_1(f) = |\Phi(f)|^2$ and $\mathfrak{g}_2(f) = 1/S_n(f)$. We take the Fourier transform of each with $\mathfrak{s}$ as the free variable.

$$\begin{aligned}
\mathfrak{G}_1(\mathfrak{s}) &= \int_{-\infty}^{\infty} \mathfrak{g}_1(f) e^{j2\pi f\mathfrak{s}} \mathrm{d}\mathfrak{s} \\
&= \int_{-\infty}^{\infty} T_b \frac{\sin^2(\pi f T_b)}{\pi^2 f^2 T_b^2} e^{j2\pi f\mathfrak{s}} \mathrm{d}\mathfrak{s} \\
&= \begin{cases} 1 - \frac{\mathfrak{s}}{T_b} & 0 < \mathfrak{s} \leq T_b \\ 1 + \frac{\mathfrak{s}}{T_b} & -T_b \leq \mathfrak{s} \leq 0 \\ 0 & \text{else} \end{cases}
\end{aligned} \tag{3.28}$$

$\mathfrak{G}_1(\mathfrak{s})$ can also be derived directly from the autocorrelation of $\varphi(t)$, $\varphi(\mathfrak{s}) * \varphi(\mathfrak{s})$.

$$\begin{aligned}
\mathfrak{G}_2(\mathfrak{s}) &= \int_{-\infty}^{\infty} \mathfrak{g}_2(f) e^{j2\pi f\mathfrak{s}} \mathrm{d}\mathfrak{s} \\
&= \int_{-\infty}^{\infty} \frac{1}{\alpha^2 + \gamma^2 f^2} e^{j2\pi f\mathfrak{s}} \mathrm{d}\mathfrak{s} \\
&= \begin{cases} \frac{\pi}{\alpha\gamma} \exp\left(-\frac{2\pi\alpha\mathfrak{s}}{\gamma}\right) & \mathfrak{s} > 0 \\ \frac{\pi}{\alpha\gamma} \exp\left(\frac{2\pi\alpha\mathfrak{s}}{\gamma}\right) & \mathfrak{s} \leq 0 \end{cases}
\end{aligned} \tag{3.29}$$

Both transforms are symmetric about $\mathfrak{s} = 0$ and real. We now compute ζ from equation (3.27) using Parseval's theorem and equations (3.28) and (3.29).

$$\begin{aligned}
\zeta &= \int_{-\infty}^{\infty} \mathfrak{g}_1(f)\mathfrak{g}_2(f) \mathrm{d}f = \int_{-\infty}^{\infty} \mathfrak{G}_1(\mathfrak{s})\mathfrak{G}_2(\mathfrak{s}) \mathrm{d}\mathfrak{s} \\
&= \int_0^{T_b} \left(1 - \tfrac{\mathfrak{s}}{T_b}\right) \tfrac{\pi}{\alpha\gamma} \exp\left(-\tfrac{2\pi\alpha\mathfrak{s}}{\gamma}\right) \mathrm{d}\mathfrak{s} + \int_{-T_b}^{0} \left(1 + \tfrac{\mathfrak{s}}{T_b}\right) \tfrac{\pi}{\alpha\gamma} \exp\left(\tfrac{2\pi\alpha\mathfrak{s}}{\gamma}\right) \mathrm{d}\mathfrak{s} \\
&= 2\int_0^{T_b} \left(1 - \tfrac{\mathfrak{s}}{T_b}\right) \tfrac{\pi}{\alpha\gamma} \exp\left(-\tfrac{2\pi\alpha\mathfrak{s}}{\gamma}\right) \mathrm{d}\mathfrak{s} \\
&= \left[-\frac{1}{\alpha^2} \exp\left(-\frac{2\pi\alpha\mathfrak{s}}{\gamma}\right) + -\frac{\gamma + 2\pi\alpha\mathfrak{s}}{2\pi\alpha^3 T_b} \exp\left(-\frac{2\pi\alpha\mathfrak{s}}{\gamma}\right)\right]\Bigg|_0^{T_b} \\
&= \frac{1}{2\pi T_b \alpha^3}\left(2\pi T_b\alpha - \gamma + \gamma \exp\left(-\frac{2\pi T_b \alpha}{\gamma}\right)\right)
\end{aligned} \tag{3.30}$$

Substituting in α^2 and γ^2 results in

$$\boxed{\zeta = \frac{\sqrt{2}}{\pi T_b N_0^{3/2}} \left(\pi T_b \sqrt{2N_0} + \frac{\sqrt{h\nu}}{B\beta\sqrt{2\eta P_u}} \left(\exp\left(-2\pi T_b B\beta \sqrt{\frac{N_0 \eta P_u}{h\nu}} \right) - 1 \right) \right)} \tag{3.31}$$

The probability of error for the whitened FM–CD system with one channel is then

$$\boxed{\Pr\{\epsilon\} = Q\left(\sqrt{E_b \zeta}\right)} \tag{3.32}$$

This assumes the receiver is operating in the weak noise regime and the probability of FM anomaly is small (i.e. $\Pr\{\mathcal{A}\} \approx 0$).

The effect of the bandwidth approximation used to find equation (3.30) can be determined to see how close the upper bound is. Table 3.1 contains ratios of band-limited numerical integration of equation (3.30) to the analytic result with limits at $\pm\infty$. Ratios are computed for a range of colored noise strengths and a range of band limits. For a baseband BPSK signal in white noise only just over 90% of the signal energy is contained within $[-B, B]$, as shown by the underlined value in the first row. As the strength of the quadratic noise term increases, the whitening correlation receiver extracts more energy from within the $[-B, B]$ limits. Therefore, we can conclude that the approximation in equation (3.30) is reasonable and the upper bound gets progressively tighter as γ increases.

		Normalized Bandwidth ($B = 1/T_b$)			
α^2	γ^2	1	1.5	2	5
1	0	$\underline{0.903}$	0.931	0.95	0.98
1	0.01	0.916	0.945	0.963	0.991
1	0.1	0.94	0.966	0.981	0.998
1	1	0.978	0.99	0.996	1
1	10	0.995	0.998	0.999	1
1	100	0.999	1	1	1

Table 3.1: Ratio of band-limited numerical integration to analytic expression (see text).

3.3 Array Processing

In Section 3.2 we derived the multi-channel correlation receiver for a signal transmitted in additive Gaussian noise. We must now modify our analysis to account for the geometry of the transmitting and receiving antennas and deal with interfering sources. Our analysis is heavily based on chapter 2 in [46].

Figure 3-3 depicts an array receiver system with two RF sources. One transmitter, representing the user of the communication system, has data modulated onto passband signal $s(t)$. We may consider $s(t)$ to be $m(t)$, discussed in Section 3.2, appropriately frequency translated to a center frequency of f_0 Another transmitter, spatially distinct from the first, sends a signal that interferes with the communication system, $z(t)$. We make no assumptions on the content of the interfering signal. Spatially distinct antennas in the receiver array pick up two different observations of the RF signals. Noise at the front end, $n_{i_F}(t)$, and from signal transport, $n_{i_T}(t)$, are shown separately but in the following analysis we consider the total noise on each channel as $n_i(t)$.

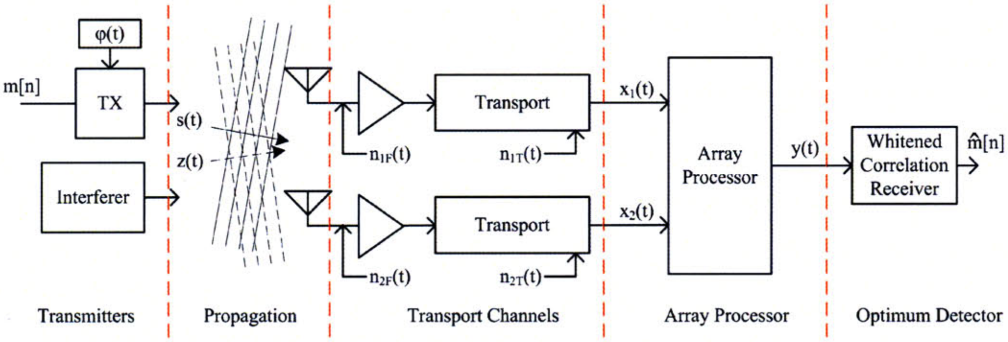

Figure 3-3: Block diagram of two channel receiver with user and interferer (see text).

3.3.1 Array Geometry

For convenience we place the array of receive antennas around the origin of a Cartesian coordinate system. The three dimensional positions of N receive antennas are denoted by the $[3 \times N]$ matrix $\mathbf{p}$. The position of antenna i can be written as $\mathbf{p}_i$, the i^{th} column of $\mathbf{p}$.

$$\mathbf{p} = \begin{bmatrix} x_0 & & x_{N-1} \\ y_0 & \ldots & y_{N-1} \\ z_0 & & z_{N-1} \end{bmatrix} = \begin{bmatrix} \mathbf{p}_0 & \mathbf{p}_1 & \ldots & \mathbf{p}_{N-1} \end{bmatrix} \tag{3.33}$$

In our two channel setup, two antennas are located on the z axis distance $d/2$ from the origin. The antennas are shown as blue circles in Figure 3-4.

$$\mathbf{p} = \begin{bmatrix} 0 & 0 \\ 0 & 0 \\ -\frac{d}{2} & \frac{d}{2} \end{bmatrix} \tag{3.34}$$

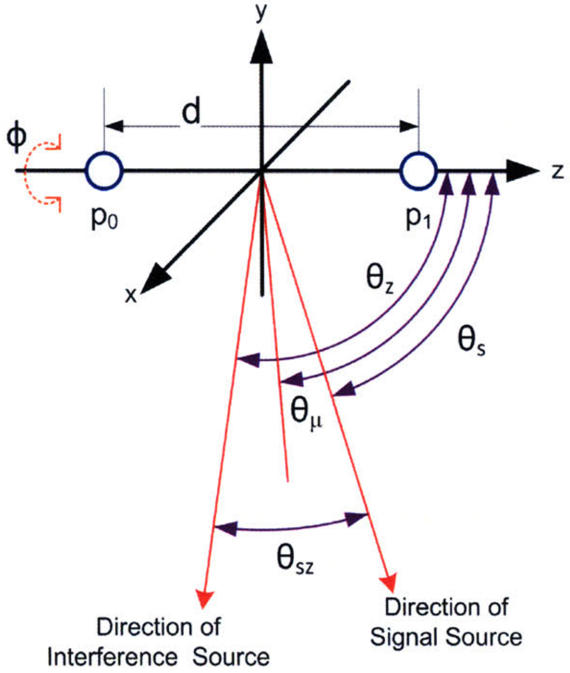

Figure 3-4: Two channel antenna geometry with signal and interference angles.

We assume that the transmitting sources are far enough away from the antenna array that the propagating RF signals may be treated as plane waves. For ground-to-space communication this is a very reasonable approximation. We also assume the amplitude of the RF signals are uniform over entire array. For a transmitted plane-wave signal, $s(t)$, we represent the signal at the origin as $s(t, \mathbf{0})$. The signal received at antenna i is then $s(t, \mathbf{p}_i) = s(t - \tau_{si}, \mathbf{0})$, where τ_{si} is the time delay of the signal between the origin and the antenna. The set of signals (from $s(t)$) received by each antenna may be represented in matrix form as

$$\mathbf{s}(t, \mathbf{p}) = \begin{bmatrix} s(t, \mathbf{p}_0) \\ \vdots \\ s(t, \mathbf{p}_{N-1}) \end{bmatrix} = \begin{bmatrix} s(t - \tau_{s0}, \mathbf{0}) \\ \vdots \\ s(t - \tau_{s(N-1)}, \mathbf{0}) \end{bmatrix} \tag{3.35}$$

We write the matrix $\mathbf{z}(t, \mathbf{p})$ to represent interference and $\mathbf{z}(t, \mathbf{p})$ to represent the noise in the same manner. The sum of all received signals, $\mathbf{x}(t, \mathbf{p})$, follows the rules of superposition.[35]

$$\mathbf{x}(t, \mathbf{p}) = \mathbf{s}(t, \mathbf{p}) + \mathbf{z}(t, \mathbf{p}) + \mathbf{n}(t, \mathbf{p}) \tag{3.36}$$

If the noise at each antenna is from internal sources (e.g. thermal noise in front-end amplifier) and not from the received RF signal then the noise term does not directly depend on $\mathbf{p}$. Each antenna has independent noise so to maintain independence without specifying position we can rewrite the noise term as

$$\mathbf{n}(t) = \begin{bmatrix} n_1(t) & \dots & n_i(t) & \dots & n_N(t) \end{bmatrix}^{\mathrm{T}} \tag{3.37}$$

We calculate the delay values of τ_{si} and τ_{zi} based on propagation directions of signal and interference. Define a unit directional vector, $\mathbf{u}_s$, that points in the direction of the signal source s. It is convenient to use spherical coordinates to define the direction.

$$\mathbf{u}_s = \begin{bmatrix} \sin\theta_s \cos\phi_s \\ \sin\theta_s \sin\phi_s \\ \cos\theta_s \end{bmatrix} \tag{3.38}$$

The delay of the plane wave s at $\mathbf{p}_i$ is the inner product $\tau_{si} = -\mathbf{u}_s^{\mathrm{T}} \mathbf{p}_i / c$. The direction vector for the interference is $\mathbf{u}_z$ defined similarly.

The second assumption we make is that the bandwidth of the RF signal is narrow relative to its center frequency. This enables us to approximate the plane wave as a single sinusoid of frequency f_0 Hz. We can also refer to the spatial frequency, k, of the sinusoid where $k = 2\pi f_0/c$ in cycles per meter. The spatial frequency and the direction of propagation can be combined to define a single frequency plane wave with wavenumber $\mathbf{k}$. The wavenumber is a vector normal to the phase front of the plane wave in the direction of propagation and is defined for signal s as

$$\mathbf{k}_s = -\frac{2\pi}{\lambda}\mathbf{u}_s \quad \text{where} \quad ||\mathbf{k}|| = \frac{2\pi f_0}{c} = \frac{\omega_0}{c} = \frac{2\pi}{\lambda} \tag{3.39}$$

where λ is the spatial wavelength in meters.

We define the plane wave signal $s(t)$ at the origin for convenience as

$$s(t, \mathbf{0}) = A_s e^{j2\pi f_0 t} \tag{3.40}$$

with amplitude A_s. The time delay, τ_{si}, can be reduced to a phase shift for a sinusoid.

$$\begin{aligned} s(t, \mathbf{p}_i) &= A_s e^{j2\pi f_0 (t-\tau_{si})} \\ &= A_s e^{j2\pi f_0 t} e^{-j2\pi f_0 \tau_{si}} \\ &= A_s e^{j2\pi f_0 t} e^{-j\mathbf{k}_s^{\mathrm{T}}\mathbf{p}_i} \end{aligned} \tag{3.41}$$

To simplify notation we define the array manifold vector, $\mathbf{v}_{\mathbf{k}}(\mathbf{k})$ for plane waves as the phase shift for plane wave $\mathbf{k}_s$ at the array $\mathbf{p}$.[46]

$$\mathbf{v}_{\mathbf{k}}(\mathbf{k}_s) = \begin{bmatrix} e^{-j\mathbf{k}_s^{\mathrm{T}}\mathbf{p}_0} \\ \vdots \\ e^{-j\mathbf{k}_s^{\mathrm{T}}\mathbf{p}_{N-1}} \end{bmatrix} \tag{3.42}$$

Thus, we can rewrite equation (3.35) using the array manifold vector as

$$\mathbf{s}(t, \mathbf{p}) = A_s e^{j2\pi f_0 t} \mathbf{v}_{\mathbf{k}}(\mathbf{k}_s) \tag{3.43}$$

Similarly, we incorporate the array manifold vector notation into equation (3.36).

$$\mathbf{x}(t,\mathbf{p}) = e^{j2\pi f_0 t}\left(A_s\mathbf{v_k}(\mathbf{k}_s) + A_z\mathbf{v_k}(\mathbf{k}_z)\right) + \mathbf{n}(t) \tag{3.44}$$

The array manifold vector for the two antenna case in Figure 3-4 for a plane wave arriving from $\mathbf{u}_s$ is

$$\mathbf{v_k}(\mathbf{k}_s) = \begin{bmatrix} \exp\left(-j\frac{\pi f_0}{c}d\cos\theta_s\right) \\ \exp\left(j\frac{\pi f_0}{c}d\cos\theta_s\right) \end{bmatrix} \tag{3.45}$$

Notice that this remains completely independent of azimuth angle ϕ_s as would be expected with isotropic antennas given the array geometry.

3.3.2 Processing

The array processor is comprised of a bank of linear time-invariant filters and a summing node to combine each filtered antenna element. The transfer functions of the filter bank are represented in vector form as $\mathbf{H}(f)$, with impulse responses as $\mathbf{h}(t)$. The output of the array processor is then

$$y(t) = \mathbf{h}^{\mathrm{T}} * \mathbf{x}(t,\mathbf{p}) \tag{3.46}$$

$$Y(f) = \mathbf{H}^{\mathrm{T}}\mathbf{X}(f,\mathbf{p}) \tag{3.47}$$

Given the plane wave approximation we can simplify these expressions. As we are interested to the response of the array to each independent signal, let us look at the response to a single plane wave with wavenumber, $\mathbf{k}_s$.[46]

$$\begin{aligned} y_s(t,\mathbf{k}_s) &= \int \mathbf{h}^{\mathrm{T}}(t-\tau)\mathbf{s}(\tau,\mathbf{p})\mathrm{d}\tau \\ &= \int \mathbf{h}^{\mathrm{T}}(t-\tau)e^{j2\pi f_0 t}\mathrm{d}\tau\mathbf{v_k}(\mathbf{k}_s) \\ &= \int \mathbf{h}^{\mathrm{T}}(\tau)e^{j2\pi f_0(t-\tau)}\mathrm{d}\tau\mathbf{v_k}(\mathbf{k}_s) \\ &= \mathbf{H}^{\mathrm{T}}(f_0)\mathbf{v_k}(\mathbf{k}_s)e^{j2\pi f_0 t} \qquad (3.48) \\ &= \mathbf{H}^{\mathrm{T}}(\|\mathbf{k}_s\|\tfrac{c}{2\pi})\mathbf{v_k}(\mathbf{k}_s)e^{jc\|\mathbf{k}_s\|t} \end{aligned}$$

The integral reduces to a Fourier transform of $\mathbf{h}^{\mathrm{T}}(t)$ evaluated at $f = f_0$. This result shows us the linear filters can be reduced to a bank of complex weights (magnitude and phase). The weighting vector is

$$\mathbf{w}^H = \mathbf{H}^{\mathrm{T}}(f_0) \tag{3.49}$$

We derive the weights for complete nulling in Section 3.4.

3.3.3 Covariance Matrix

In order to determine the weights used the array processor we need the array manifold vectors and power for each received signal. Recall that these values capture the array geometry and the directional information on each RF signal. In practice the array processor does not have *a priori* knowledge of these values. It can calculate the input covariance matrix, $\mathcal{R}_{xx}$ based on the received signals.[35]

$$\mathcal{R}_{xx} = \mathsf{E}[\mathbf{x}\mathbf{x}^H] = \mathcal{R}_{mm} + \mathcal{R}_{zz} + \mathcal{R}_{nn} \tag{3.50}$$

where

$$\mathcal{R}_{mm} = \mathsf{E}[\mathbf{m}(t, \mathbf{p})\, \mathbf{m}(t, \mathbf{p})^H] \tag{3.51}$$

$$\mathcal{R}_{nn} = \mathsf{E}[\mathbf{n}(t)\mathbf{n}(t)^H] = \sigma_n^2 \mathbf{I} \tag{3.52}$$

This assumes the noise is independent and identically distributed at each antenna. $\mathbf{I}$ is the identity matrix.

Initially, we assume that the array processor knows $\mathcal{R}_{xx}$ with certainty. The covariance matrix can be factored into pairs of eigenvalues and eigenvectors.[46] The eigenvalues are the relative signal power and the eigenvectors are related to the array manifold vectors. In general we can separate up to K separate signals where $K \leq N$ given N antennas as long as $\mathcal{R}_{xx}$ is at least of rank K.

Knowledge of $\mathcal{R}_{xx}$ is never perfect. Instead it is usually estimated by taking a series of snapshots of $\mathbf{x}(t)$. Finding the dominant eigenvalues of the estimate can be used to determine the number and strengths of separate signals arriving at the array.[46] Then algorithms such as Multiple Signal Classification (MUSIC) can estimate the direction of arrival for each signal.[37] This information is used to generate the complex array weights.

3.4 Complete Nulling

In this section, we determine the complex weights for completely suppressing a single strong interference signal. This processing is not optimum but has reasonably good performance and greatly simplifies calculation We use the two-antenna geometry from Figure 3-4 and assume the narrow-band plane wave approximation is adequate. To completely suppress, or null, an interfering signal with wavenumber $\mathbf{k}_z$ we set the constraint such that

$$y_z(t, \mathbf{k}_z) = 0 \tag{3.53}$$

$$\mathbf{w}^H \mathbf{v}_{\mathbf{k}}(\mathbf{k}_z) = 0 \qquad \text{Nulling Constraint} \tag{3.54}$$

For N antennas this constraint requires solving N equations with N unknown complex variables. In the two-antenna case it can be solved by inspection. The antenna weights may be scaled by any constant and still satisfy equation (3.54). For convenience we set the scale factor such that $\|\mathbf{w}_{\text{null}}\| = 1$ so

$$\mathbf{w}_{\text{null}} = \frac{1}{\sqrt{2}} \mathbf{v}_{\mathbf{k}}(\mathbf{k}_z) \begin{bmatrix} 1 \\ -1 \end{bmatrix} \tag{3.55}$$

Thus, the array gain (amplitude) for the interfering signal is zero.

$$\begin{aligned}
A_z &= \mathbf{w}_{\text{null}}^H \mathbf{v}_{\mathbf{k}_z} \\
&= \frac{1}{\sqrt{2}} \left[\exp\left(j\tfrac{\pi f_0}{c} d\cos\theta_z\right) - \exp\left(-j\tfrac{\pi f_0}{c} d\cos\theta_z\right) \right] \begin{bmatrix} \exp\left(-j\tfrac{\pi f_0}{c} d\cos\theta_z\right) \\ \exp\left(j\tfrac{\pi f_0}{c} d\cos\theta_z\right) \end{bmatrix} \\
&= \frac{1}{\sqrt{2}} \exp\left(j\frac{\pi f_0}{c} d\cos\theta_z - j\frac{\pi f_0}{c} d\cos\theta_z\right) - \frac{1}{\sqrt{2}} \exp\left(j\frac{\pi f_0}{c} d\cos\theta_z - j\frac{\pi f_0}{c} d\cos\theta_z\right) \\
&= \frac{1}{\sqrt{2}} (e^0 - e^0) \\
&= 0
\end{aligned} \tag{3.56}$$

With the interfering signal completely nulled only the communication signal and system noise remain. The signal gain is calculated in the same manner

$$\begin{aligned}
A_s &= \mathbf{w}_{\text{null}}^H \mathbf{v}_{\mathbf{k}_s} \\
&= \frac{1}{\sqrt{2}} \exp\left(j\frac{\pi f_0}{c} d\cos\theta_z - j\frac{\pi f_0}{c} d\cos\theta_s\right) - \frac{1}{\sqrt{2}} \exp\left(j\frac{\pi f_0}{c} d\cos\theta_z - j\frac{\pi f_0}{c} d\cos\theta_s\right) \\
&= -\sqrt{2} j \sin\left(\frac{\pi f_0 d}{c} (\cos\theta_z - \cos\theta_s)\right) \\
&= -\sqrt{2} j \sin\left(\frac{\pi d}{\lambda} (\cos\theta_z - \cos\theta_s)\right)
\end{aligned} \tag{3.57}$$

The noise gain is calculated differently as the noise on each channel is independent. Recall that for independent random variables the variances add. Likewise, for independent noise the powers add so we may use the norm of the array weights as the noise gain.

$$\begin{aligned}
A_n &= \|\mathbf{w}_{\text{null}}\| \\
&= 1
\end{aligned} \tag{3.58}$$

Now we apply these gains to the calculation the vector receiver mean and variance as in equations (3.7) and (3.8). The mean due to signal is

$$\begin{aligned}\mu_{\mathbf{y}} &= \int y_s(t)\varphi(t)\mathrm{d}t \\ &= |A_s|\sqrt{E_b} \\ &= \sqrt{2}\sin\left(\frac{\pi d}{\lambda}(\cos\theta_z - \cos\theta_s)\right) \qquad (3.59)\end{aligned}$$

Recall that the noise process is white or has been whitened so $S_n(f)$ is a constant, nominally $N_0/2$. The variance from the noise is

$$\begin{aligned}\sigma_{\mathbf{y}}^2 &= A_n^2 S_n(f)\int|\Phi(f)|^2\mathrm{d}f \\ &= A_n^2\sigma_n^2 \\ &= \sigma_n^2 \qquad (3.60)\end{aligned}$$

We can now calculate the probability of error for a two-antenna system with a nulled interferer. This assumes identical white noise for each antenna channel.

$$\begin{aligned}\Pr(\epsilon) &= Q\left(\frac{\mu_{\mathbf{y}}}{\sigma_{\mathbf{y}}}\right) \\ &= Q\left(\sqrt{\frac{E_b}{\sigma_n^2}2\sin^2\left(\frac{\pi d}{\lambda}(\cos\theta_z - \cos\theta_s)\right)}\right) \qquad (3.61)\end{aligned}$$

In the ground-to-satellite communication scenario the absolute angle of the signal and interference source is not as important as the angle between two. We define the angle between the signal and the interferer as θ_{sz} and the average of the signal and interference angle as θ_μ. These relationships are shown in Figure 3-4. Given the geometry, θ_μ will usually be near 90° as the satellites will be approximately parallel to the ground and generally overhead. The probability of error can be rewritten as

$$\Pr(\epsilon) = Q\left(\sqrt{\frac{E_b}{\sigma_n^2}2\sin^2\left(\frac{\pi d}{\lambda}2\sin(\theta_\mu)\sin(\tfrac{1}{2}\theta_{sz})\right)}\right) \qquad (3.62)$$

Lastly, we account for the whitening filter in equation (3.30). The probability of error now accounts for white and non-white noise. However, the effects of FM anomaly or failures of the digital link are not included. When either event occurs, then at least one of the transport channels is down and the nulling process fails.

$$\boxed{\Pr(\epsilon|\mathcal{A}^C) = Q\left(\sqrt{E_b\,\zeta\,2\sin^2\left(\frac{\pi d}{\lambda}2\sin(\theta_\mu)\sin(\tfrac{1}{2}\theta_{sz})\right)}\right)} \tag{3.63}$$

3.4.1 Stand-off Distance and Link Margin

The obvious problem with complete nulling is when the interferer and user are in close proximity leading to signal suppression and high probability of error. The amount of suppression was calculated in equation (3.63). For a more general understanding of the stand-off distance we normalize the stand-off angle as a function of $\frac{\lambda}{d}$. We can use the small angle approximation, $\sin(\vartheta) = \vartheta$, as we want to minimize the θ_{sz}.

The normalized stand-off angle is defined as θ_Δ where

$$\theta_\Delta = \frac{\lambda}{d}u_{sz} \tag{3.64}$$

where u_{sz} is the fraction of a beam width based on a single diffraction limited aperture between 0 and 1.[43] The stand-off distance is χ or approximately $\theta_\Delta Z$ where Z is the satellite altitude (i.e. the distance between the transmitters and the receive array).

We assume the mean angle of the interference and signal are broadside to the array, approximately 90°. Therefore, we assume $\sin(\theta_\mu) = 1$. The suppression of signal means that additional signal energy is required to maintain the same probability of error. This additional margin is noted as ϱ and incorporated into equation (3.63) so

$$\Pr\{\epsilon\} = Q\left(\sqrt{E_b\,\zeta\,\varrho\,2\sin^2\left(\frac{\pi d}{\lambda}2\sin(\tfrac{1}{2}\theta_\Delta)\right)}\right) \tag{3.65}$$

The required margin can be determined by observation to be

$$\varrho^{-1} = 2\sin^2\left(\frac{\pi d}{\lambda}2\sin(\tfrac{1}{2}\theta_\Delta)\right) \tag{3.66}$$

Figure 3-5 shows the required margin for a stand-off angle between 0 and $\frac{\lambda}{d}$ ($u \in [0, \frac{1}{2}]$). Obviously, at very small angles the signal suppression is very high requiring a very large margin. At $\frac{\lambda}{4d}$ the required margin is only a very reasonable 3 dB. At $\frac{\lambda}{2d}$ the array geometry is such that complete nulling with no suppression is possible. Increasing the angle beyond $\frac{\lambda}{2d}$ causes the phase to wrap around increasing the required margin. This is an effect of using a narrow band approximation.

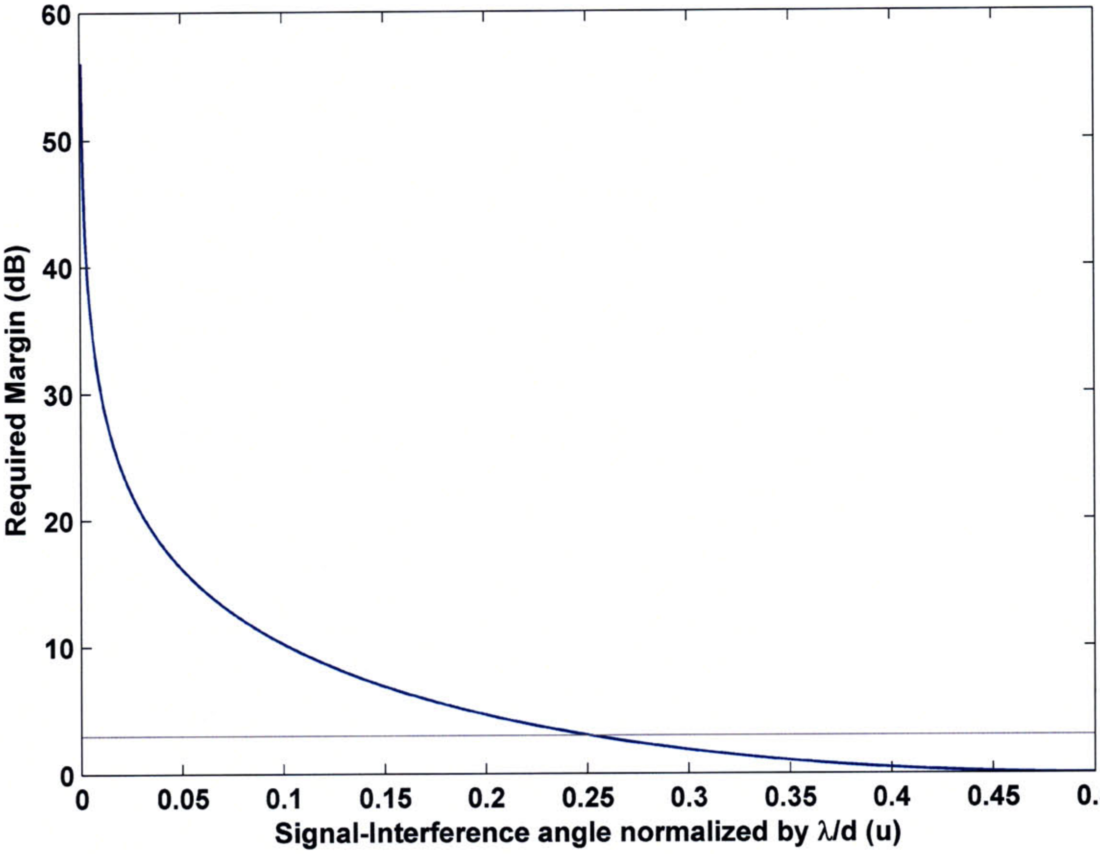

Figure 3-5: SNR Margin required to maintain performance with nulling for close distance (see text).

THIS PAGE INTENTIONALLY LEFT BLANK

Chapter 4

Example Parameterized Analysis

4.1 Introduction

This chapter combines the results of Chapter 2 and Chapter 3 to express a complete parameterized model of each architecture. We compare the architectures under example conditions and select the best architecture. The chapter begins in Section 4.2 by defining the parameters for analyzing each architecture in terms of the inter-satellite link, the array processing and the system spatial geometry. We discuss an approximation to relate simple uncoded BPSK modulation with a channel coded RF modulation scheme.

In Section 4.3 we compare the minimum received optical power necessary to meet a set performance goal for each architecture. First, we look at an example in Section 4.3.1 with a very low required probability of error as a baseline. Scenarios without interference and with very strong interference are considered. Then, in Section 4.3.2 we consider a much higher required error probability to approximate the performance of a coded system. Performance is evaluated over a wide range of interference amplitudes. Next, in Section 4.3.3 we relate the system performance to the RF transmitter and remote antenna satellite geometry and show a performance threshold of digital versus FM–CD transport architectures.

4.2 System Parameters

In Chapters 2 and 3, we dissected the effects of signal transport, array processing and detection. As in Section 3.4 on complete nulling, we continue to assume a two-antenna system with a communication user and an interfering signal. To investigate the relative performance of each transport architecture in a given application, we specify two sets of parameters. The first set of parameters defines the communication system and the second defines the satellite and transmitter geometry.

There are six communication system parameters:

1. *The symbol duration (bit duration), T_b, in the RF communication signal.* As seen on page 66, the bandwidth approximation of $B = 1/T_b$ is reasonable. Thus, this parameter specifies the user bit rate and the necessary signal transport bandwidth.

2. *The signal-to-noise ratio per bit at the remote receiver antennas in terms of E_b/N_0.* This ratio is specified per antenna and accounts for transmitted energy, RF propagation losses, antenna efficiency and noise present at the front-end.

3. *The ratio of the interference amplitude to the signal amplitude, ISAR.* To specify the necessary front-end gain in Section 2.5.2 we need to know the worst case amplitude of the interference relative to the signal. This makes no assumption on the correlation of the noise and interference or the interference waveform. Thus, the maximum amplitude of the signal plus interference at the front-end amplifier is $r_{\max} = s_{\max}(1 + \text{ISAR})$ where $s_{\max}$ is the maximum amplitude of the user signal. By combining the first three parameters the required front-end gain is then

$$G_{FE} = \frac{T_b}{E_b} \frac{1}{(1 + \text{ISAR})^2} \tag{4.1}$$

4. The normalized angular spacing of the signal and interference, u_{sz} relative to $\frac{\lambda}{d}$. This is defined in Section 3.4.1. When $u_{sz} = 0.5$ perfect nulling without

suppression is possible but as u_{sz} decreases it causes suppression of the user signal. If ISAR = 0, there is no interference so nulling is not necessary and u_{sz} is a degenerate parameter we set to 0.5 to maximize system performance.

5. *The number of bits, b, used to quantize each antenna channel.* The quantizer may be at the remote antenna or the array processor depending on which architecture is used (i.e. digital or analog transport).

6. *The received optical power at the array processor, P_u, for an inter-satellite link.* We assume a symmetric system so both optical transport channels have the same received optical power. Higher optical power results in better performance of the signal transport subsystem.

From these six parameters, we can calculate the probability of error in equation (3.63). This assumes that both inter-satellite links are operational. The probability that both links are operational and the signal transport is "good" in the FM–CD case is

$$\Pr(\text{good}) = (1 - \Pr\{\mathcal{A}\})^2 \tag{4.2}$$

where $\Pr\{\mathcal{A}\}$ is the probability of an FM anomaly on one channel from equation (2.31). When either ISL is down the array processor is unable to null the interference. To simplify our analysis, we will consider that the loss of either ISL results in unrecoverable errors in the detection process. We model this behavior by assuming an error probability of 1/2 when the signal transport system is not "good". The complete probability of error for the FM–CD link is then

$$\Pr(\epsilon) = \Pr(\text{good})\Pr(\epsilon|\mathcal{A}^C) + (1 - \Pr(\text{good}))\tfrac{1}{2} \tag{4.3}$$

Notice that the frequency modulation index, β, is not one of the listed parameters. For each operational point in the FM–CD architecture we optimize β to minimize the probability of error. As $\Pr(\epsilon)$ does not have an analytic form[1], we find the optimum

---

[1] This is due to the upper bound of $\mathcal{A}$ of equation (2.31)

frequency modulation index, β_{opt}, through numerical search.

Although occasional errors in the digital link were treated in Section 2.4.3, decreasing received power eventually causes the digital link to fail. We can reasonably consider the digital link as non-operational when the bit-error probability is greater than 0.1. As in the analog FM–CD architecture above, we consider the loss of either digital link to degrade the error probability to 1/2. For two identical channels we can use a simple threshold test where digital transport is considered "good" when $\Pr\{\varepsilon\} < (0.1)(0.1)$ is satisfied.

We now have a set of parameterized models to calculate the probability of error for decoding the information from the user. For any given set of parameters, we can determine which architecture results in the lowest probability of error. However, this is not the most useful comparison for the end-user nor is it the most instructive for the system designer. The probability of error calculation is based on using an uncoded BPSK modulation scheme for the RF signal. In practice, any advanced communication system will use error correcting codes to better utilize the RF channel.

Channel coding allows for arbitrarily low bit error rates in the presence of noise as long as the signal to noise ratio is above a threshold.[39] The analysis of the multitude of coding schemes and their performance is outside the scope of this thesis. However, it is important to note that the performance of present day coding systems can be very close to the limit provided by Shannon. It is instructive to note the coding gain possible over uncoded BPSK. A coded system can offer effectively zero error probability while uncoded BPSK has a probability of error of approximately 0.1.[20]

This leads us to consider an error probability goal, p_{goal}, as a surrogate to more advanced coding and modulation schemes. If the calculated error probability for uncoded BPSK meets the goal, then we consider that a coded system can achieve an arbitrarily low error rate under the under the same parameters. The threshold test is then

$$\Pr(\epsilon) \leq \text{p}_{\text{goal}} \quad \mapsto \quad \text{Success}$$

As the transport laser power is one of the constraints we would like to minimize, let us consider it as the performance metric. For a given $\mathrm{p}_{\mathrm{goal}}$ we wish to find the minimum received optical power that meets the threshold. This swaps parameter 6 above with the error probability goal.

As the determination of the minimum received optical power, P_u, for a given set of parameters is computed numerically and based on a number of assumptions, the precision of the result may not be high. We are attempting to compare the performance between architectures and if the difference between minimum optical power is approximately a single decibel or less, we may consider the architectures to be tied. Therefore, the following results are rounded to the nearest dBm.

The transmitter and satellite geometry parameters are:

7. *The distance between the remote antenna satellites, d.*

8. *The center frequency of the RF communication signal, f_0.* We use this value to determine the wavelength, λ_0, of the signal where $\lambda_0 = c/f_0$.

9. *The distance from the RF transmitters to the satellite constellation, Z.* As this distance is large, we assume the transmitters are on one plane and the satellites are on another parallel plane

10. *The distance between the interfering transmitter and the user transmitter, χ.*

11. The optical transport loss between each remote antenna satellite and the array processor, G_{optical}, as calculated in Section 2.6. This accounts for the propagation spreading loss, the optical telescope aperture size and any losses in the optical subsystems. The distance between the antenna and array satellites is at least $\frac{d}{2}$ when the processor is directly in between the antenna satellites.

These parameters can be partially reduced. The geometry parameters d, λ_0, Z and χ (items 7 through 10) can be reduced to the distance d and the angular spacing, u_{sz} (see Section 3.4.1). This is the same as parameter 4.

4.3 Example Applications

First, we look at the performance of the communication system itself ignoring the system geometry. In Section 4.3.3 we incorporate the system geometry of the transmitter and receiver antenna spacing.

The following analyses use these general system parameters. The baseband bandwidth, B, is set at 1 GHz for an uncoded data rate of 1 Gbps and therefore $T_b = 10^{-9}$ (parameter 1). The RF carrier frequency is set at 30 GHz (parameter 8). The optical inter-satellite link is at the common wavelength of 1.55 μm. The optical detectors have a quantum efficiency of 0.9. An optical pre-amplifier is used to achieve the shot noise limit for IM–DD. We assume the constellation is in a geosynchronous orbit (GEO) at an altitude of $Z = 36 \cdot 10^6$ m.

4.3.1 Uncoded User

First, we compare architectures where the communication user is using uncoded BPSK. We set an error probability goal of $\mathrm{p}_{\mathrm{goal}} = 10^{-9}$. To get an idea of how such a system would work, we first investigate the case where there is no interfering user.

No Interference

Figure 4-1 shows the probability of error for the FM–CD architecture versus received optical power and modulation index, β, where $E_b/N_0 = 10$ dB and $b = 3$ bits. As the optical power increases, the performance gets better until it plateaus due to the quantizer and SNR per bit limitations. We can see that there is almost no benefit in this scenario for $\beta > 1$.

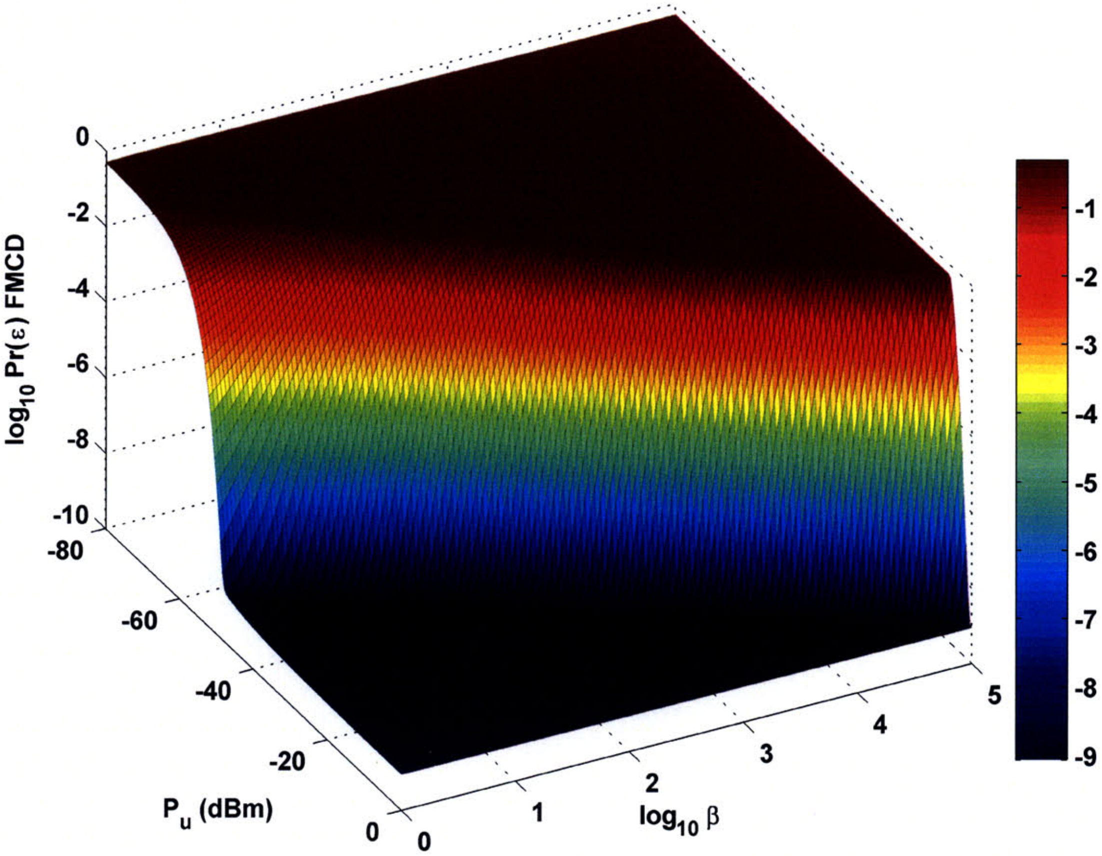

Figure 4-1: $\Pr(\epsilon)$ for FM–CD versus P_u and β, no interference, 3-bits, $E_b/N_0 = 10$ dB.

Under these conditions, we can compare the error performance between architectures where the optimum β is always used for FM–CD. Figure 4-2 shows the probability of error for each system versus the received optical power. In addition to the three transport architectures, we show the baseline reference performance of the two antenna receiver with a lossless noiseless wire connecting the antennas to the array processor. The performance goal is shown as a dotted line. In the top graph, the quantizer noise is only included in the digital architecture. This shows the best case performance where one might have a very high rate quantizer (> 3-bits) at the array processor for the analog transport. The lower graph includes the effects of quantization in all systems and the reference performance.

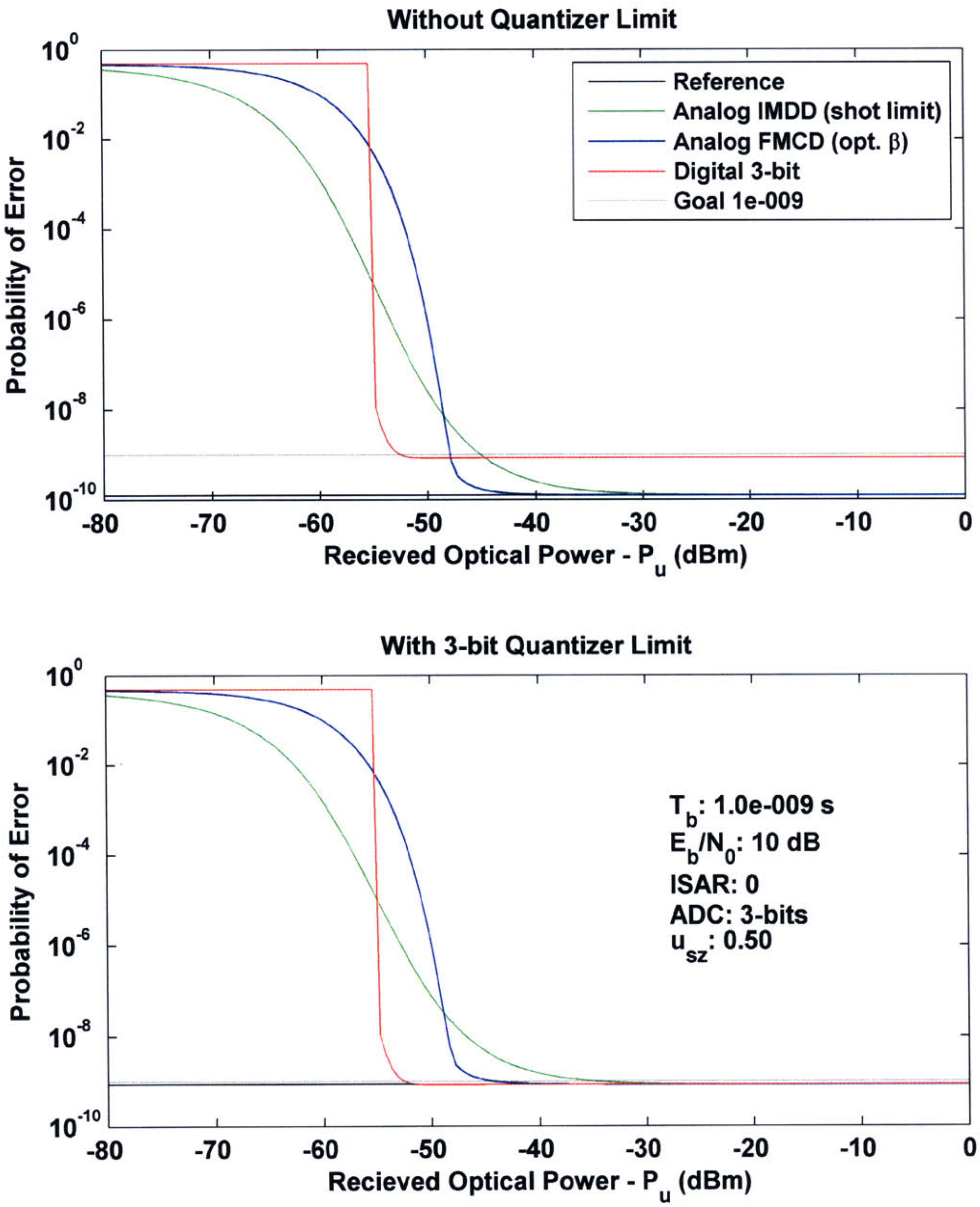

Figure 4-2: Pr(ϵ) for uncoded systems with no interference (see text).

In this example the sharp cutoff of the digital system is evident at about -55 dBm. The analog FM–CD system requires more power to reach the performance goal, but it falls off much less steeply. The analog IM–DD system has a shallow falloff as well but requires the most power of any system to achieve the performance goal.

Table 4.1 shows the minimum received optical power for each architecture at various operating points. The first four columns represent system parameters 2 through 5. The first value of b (for each unique value of E_b/N_0) is the minimum number of bits necessary to meet the performance goal. The next three columns are the minimum optical received power for each architecture, with the lowest being highlighted in green. The last column is the optimal frequency modulation index for the FM–CD architecture.

E_b/N_0	ISAR	u_{sz}	b-bits	Digital	IM–DD	FM–CD	β_{opt}
(dB)					P_u (dBm)		
10	0	$\star$[2]	3	-52	-33	-44	4.3
10	0	$\star$	4	-52	-44	-48	1
15	0	$\star$	2	-57	-50	-48	1
15	0	$\star$	3	-55	-53	-48	1
15	0	$\star$	4	-53	-53	-48	1
20	0	$\star$	2	-57	-52	-48	1
20	0	$\star$	3	-55	-54	-48	1
20	0	$\star$	4	-53	-54	-48	1

Table 4.1: Minimum P_u for $\text{p}_{\text{goal}} = 10^{-9}$ with no interference, $T_b = 10^{-9}$.

In the uncoded case with no interference, it is apparent that the digital architecture is superior to either analog architectures by at least 3 dB. Observe that the best runner-up architecture is FM–CD for lower E_b/N_0 and IM–DD for higher E_b/N_0. The preferred architecture for uncoded BPSK with no interference uses digital transport and 3-bit quantizers requiring -52 dBm of optical received power.

Moderate Interference

We analyze the performance of each architecture in the presence of moderate interference where ISAR $= 10$. For an $E_b/N_0 = 10$ dB at least 7-bit quantization is

---

[2] The signal-interference angle is a do-not-care value in this case as there is no interfering signal amplitude. Effectively $u_{sz} = 0.5$.

necessary to meet the error probability goal. The normalized signal-interference angle is set at 0.5, which is the best case for nulling. The probability of error of the FM–CD architecture is shown in Figure 4-3 versus received optical power and the frequency modulation index. Slices of the surface are shown in Figure 4-4 to clarify to dependence on β.

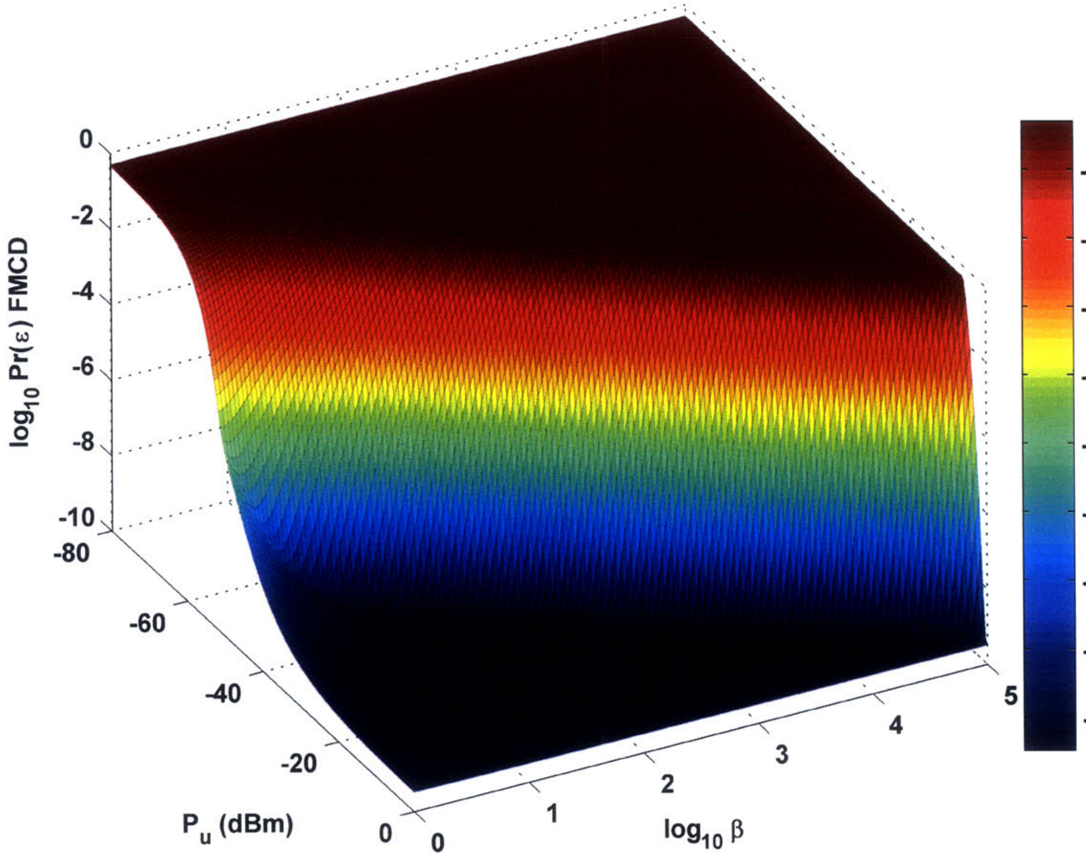

Figure 4-3: Pr(ϵ) for FM–CD versus P_u and β, ISAR = 10, 7-bits, $E_b/N_0 = 10$ dB, $u_{sz} = 0.5$.

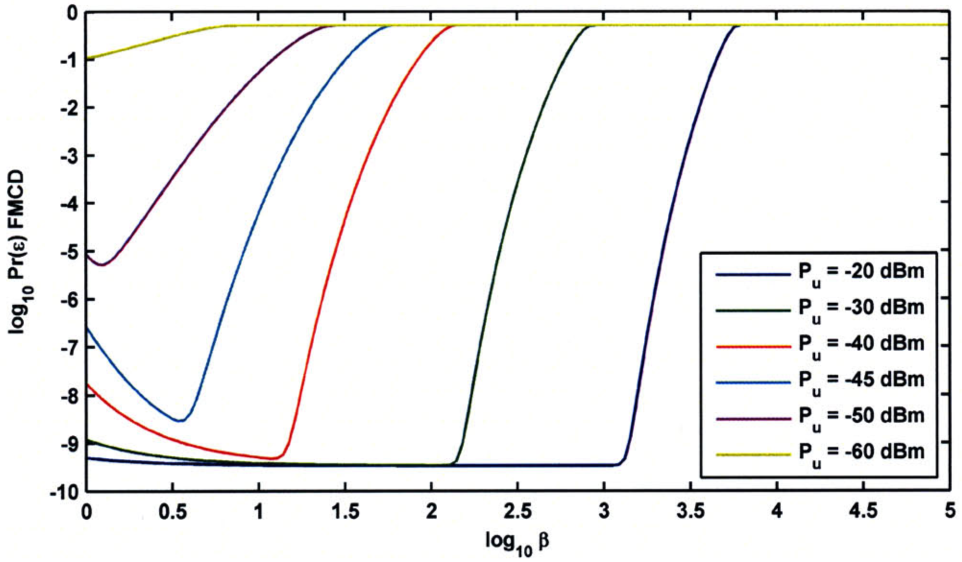

Figure 4-4: $\Pr(\epsilon)$ for FM–CD versus β, ISAR $= 10$, 7-bits, $E_b/N_0 = 10$ dB, $u_{sz} = 0.5$.

There are three behaviors seen with β. When P_u is small, the error probability is high and increasing β only further harms performance. β_{opt} in this region is 1. As P_u increases the FM bandwidth expansion effect improves performance until the FM discriminator anomaly causes a drop-off (refer to Section 2.3.2). This results in an obvious minimum probability of error used to determine β_{opt}. Finally, P_u is large enough that the FM–CD transport process is no longer limiting and the error probability is relatively flat. Here, the performance is relatively insensitive to β as long as it is low enough to avoid the drop-off from the FM anomaly. In Figure 4-5, the minimum probability of error is plotted against P_u along with the optimum frequency modulation index, β_{opt}.

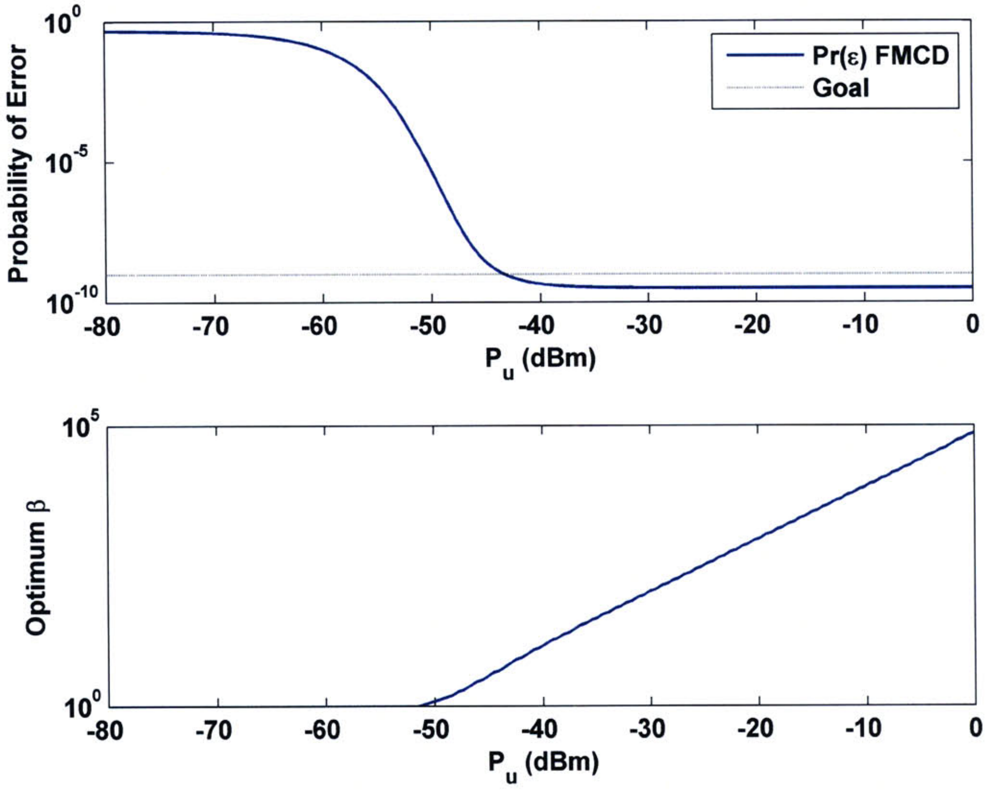

Figure 4-5: Optimum β versus P_u for FM–CD, ISAR = 10, 7-bits, $E_b/N_0 = 10$ dB, $u_{sz} = 0.5$.

Figure 4-6 shows the performance of each architecture under the same parameters. Table 4.2 has the performance over a range parameters with ISAR = 10. The effects of both front-end signal to noise ratio and normalized signal-interferer angle are evaluated. Decreasing u_{sz} requires an increase in the effective front-end signal to noise ratio due to the signal suppression effect of complete nulling. This is why an E_b/N_0 of 20 dB and 9-bit quantization is needed to support $u_{sz} = 0.1$.

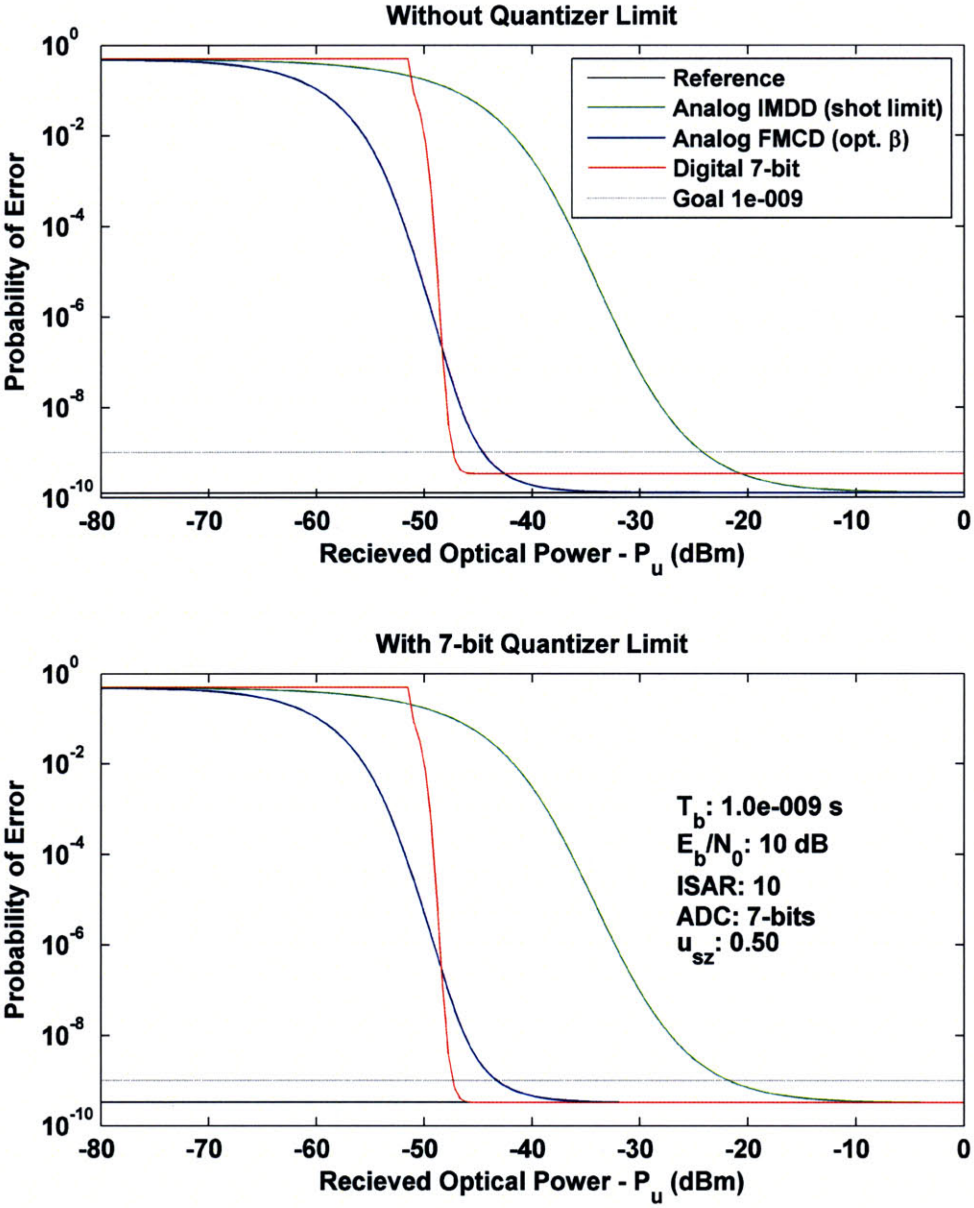

Figure 4-6: $\Pr(\epsilon)$ for uncoded systems with moderate interference.

		u_{sz}	0.5				0.25				0.1			
E_b/N_0	ISAR	b	Dig.	IM	FM	β_{opt}	Dig.	IM	FM	β_{opt}	Dig.	IM	FM	β_{opt}
(dB)		bits	P_u (dBm)				P_u (dBm)				P_u (dBm)			
10	10	7	-47	-22	-43	5.6	–	–	–	–	–	–	–	–
10	10	8	-47	-24	-44	4.2	–	–	–	–	–	–	–	–
10	10	9	-46	-24	-45	3.8	–	–	–	–	–	–	–	–
15	10	5	-48	-13	-38	22	–	–	–	–	–	–	–	–
15	10	6	-49	-31	-48	1.1	-47	-20	-43	5.9	–	–	–	–
15	10	8	-48	-33	-48	1	-47	-27	-47	1.8	–	–	–	–
20	10	5	-49	-27	-46	2.3	–	–	–	–	–	–	–	–
20	10	6	-49	-33	-48	1	-48	-28	-47	1.7	–	–	–	–
20	10	9	-47	-34	-48	1	-47	-30	-48	1	-45	-8.6	-38	19

Table 4.2: Minimum P_u for $p_{\text{goal}} = 10^{-9}$ with moderate interference, $T_b = 10^{-9}$.

For each operating point evaluated here the digital architecture is best. The FM–CD architecture performs as well as digital in some cases but otherwise trails slightly. The performance of the IM–DD architecture is at least 20 dB poorer than either digital or FM–CD architectures. This is a change from the no-interference case analyzed previously. The preferred architecture for uncoded BPSK with moderate interference uses digital transport with at least -47 dBm and uses 7-bit digitizers.

Strong Interference

We now analyze the performance of each architecture with strong interference where ISAR = 100. When $E_b/N_0 = 15$ dB, at least 9-bit quantization is necessary to meet the uncoded performance goal. The normalized signal-interference angle is set at 0.5. The probability of error for the FM–CD architecture under these parameters is shown in Figure 4-7 and Figure 4-8 as β varies. The minimum probability of error and β_{opt} is shown in Figure 4-9.

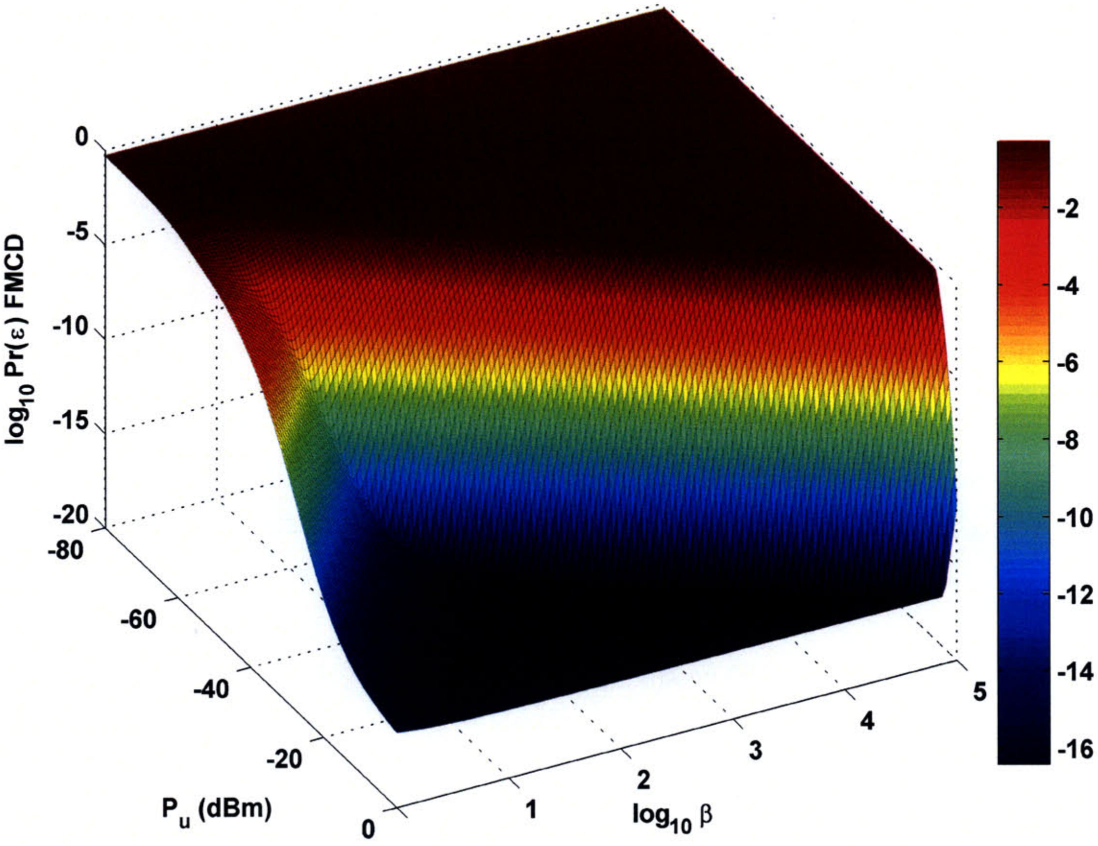

Figure 4-7: $\Pr(\epsilon)$ for FM–CD versus P_u and β, ISAR = 100, 9-bits, $E_b/N_0 = 15$ dB, $u_{sz} = 0.5$.

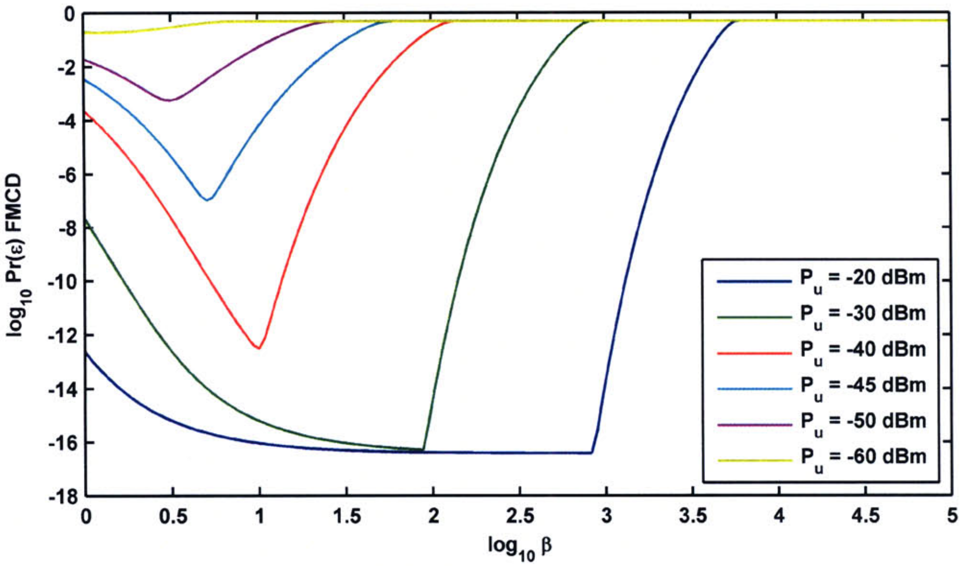

Figure 4-8: $\Pr(\epsilon)$ for FM–CD versus β, $\text{ISAR} = 100$, 9-bits, $E_b/N_0 = 15$ dB, $u_{sz} = 0.5$.

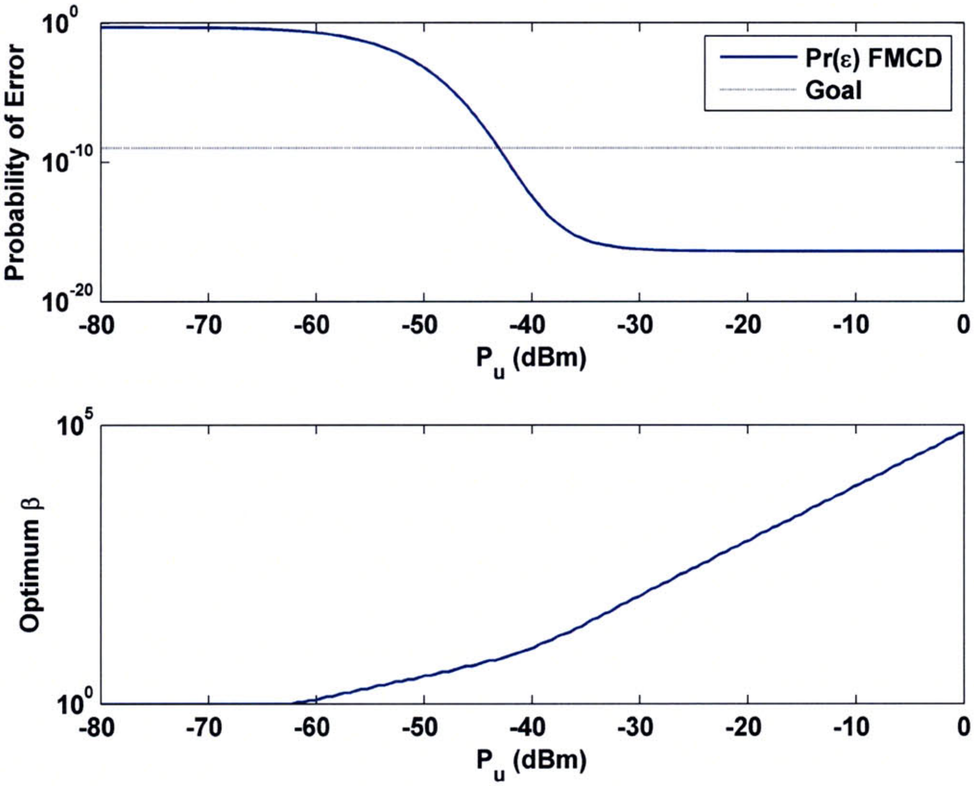

Figure 4-9: Optimum β versus P_u for FM–CD, ISAR $= 100$, 9-bits, $E_b/N_0 = 15$ dB, $u_{sz} = 0.5$.

Figure 4-10 shows the performance of each architecture under the same parameters. Table 4.3 has the performance over a range parameters with ISAR $= 100$.

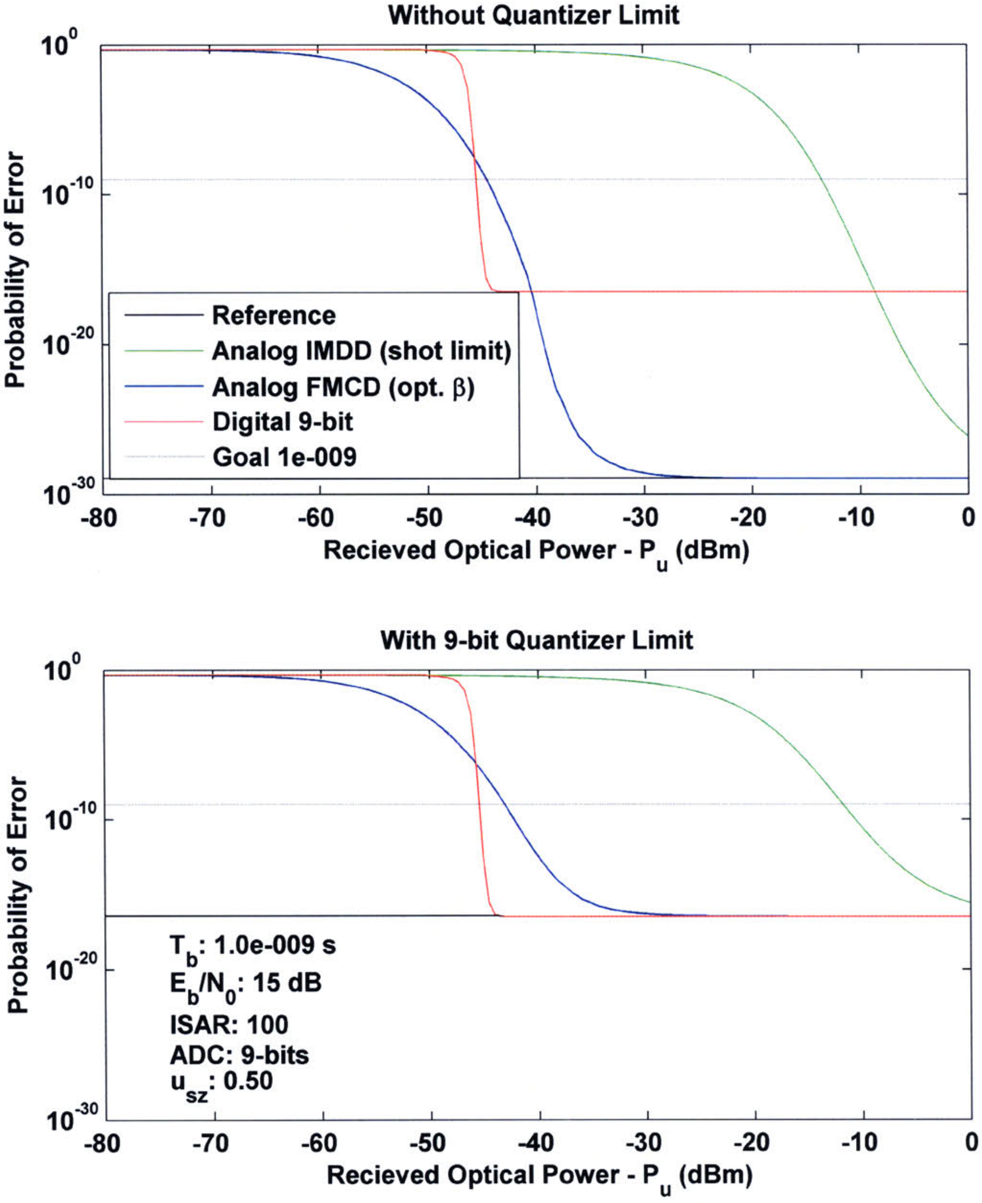

Figure 4-10: $\Pr(\epsilon)$ for uncoded systems with strong interference.

		u_{sz}	0.5				0.25				0.1			
E_b/N_0	ISAR	b	Dig.	IM	FM	β_{opt}	Dig.	IM	FM	β_{opt}	Dig.	IM	FM	β_{opt}
(dB)		bits	P_u (dBm)				P_u (dBm)				P_u (dBm)			
10	100	10	-44	-1.1	-36	31	–	–	–	–	–	–	–	–
10	100	11	-43	-4.2	-38	19	–	–	–	–	–	–	–	–
10	100	12	-43	-4.7	-39	18	–	–	–	–	–	–	–	–
15	100	9	-45	-12	-43	6.4	–	–	–	–	–	–	–	–
15	100	10	-45	-13	-44	4.8	-44	-6.8	-41	11	–	–	–	–
15	100	11	-44	-13	-44	4.5	-44	-7.9	-42	9.3	–	–	–	–
20	100	9	-45	-13	-44	4.6	-45	-7.4	-41	10	–	–	–	–
20	100	10	-45	-14	-45	3.1	-44	-10	-44	5.7	–	–	–	–
20	100	11	-44	-14	-46	2.6	-44	-11	-44	4.7	–	–	–	–
20	100	12	-44	-14	-46	2.5	-44	-11	-44	4.5	-42	12	-31	110
20	100	13	-44	-14	-46	2.5	-43	-11	-44	4.3	-42	8.4	-33	62

Table 4.3: Minimum P_u for $p_{\text{goal}} = 10^{-9}$ with strong interference, $T_b = 10^{-9}$.

In general, the digital architecture provides the best performance. The FM–CD architecture performance is almost as good as digital and in one instance beats it. The IM–DD architecture, however, is very poor by comparison, almost down by 30 to 40 dB. Therefore, digital architecture is preferred with 10-bit quantization and at least -44 dB received optical power.

Very Strong Interference

Now consider the uncoded system performance in the presence of very strong interference, where ISAR = 1000. Figure 4-11 shows the FM–CD performance versus optical power and β when ISAR = 1000, $E_b/N_0 = 15$ dB and $b = 12$ bits. The normalized signal-interference angle is set at 0.5. The optimum β_{opt} which minimizes the probability of error is shown versus received optical power in Figure 4-12.

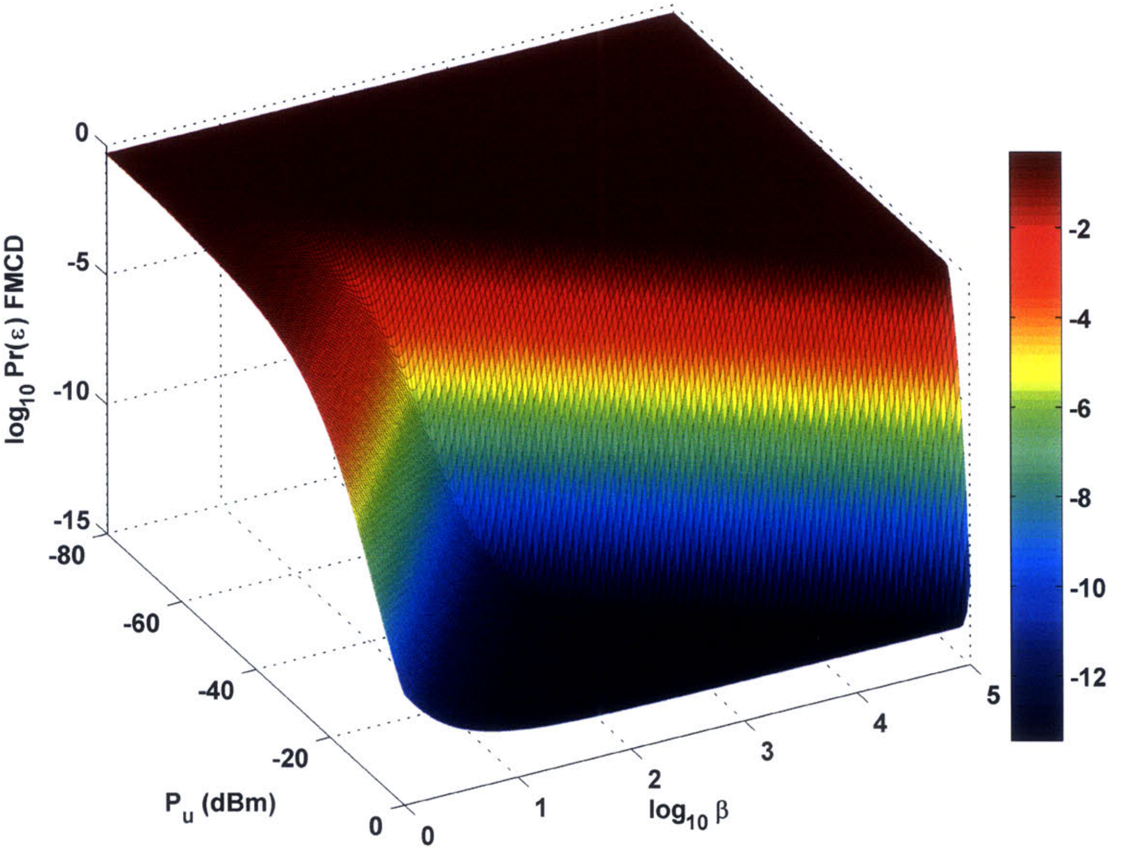

Figure 4-11: $\Pr(\epsilon)$ for FM–CD versus P_u and β, ISAR $= 1000$, 12-bits, $E_b/N_0 = 15$ dB, $u_{sz} = 0.5$.

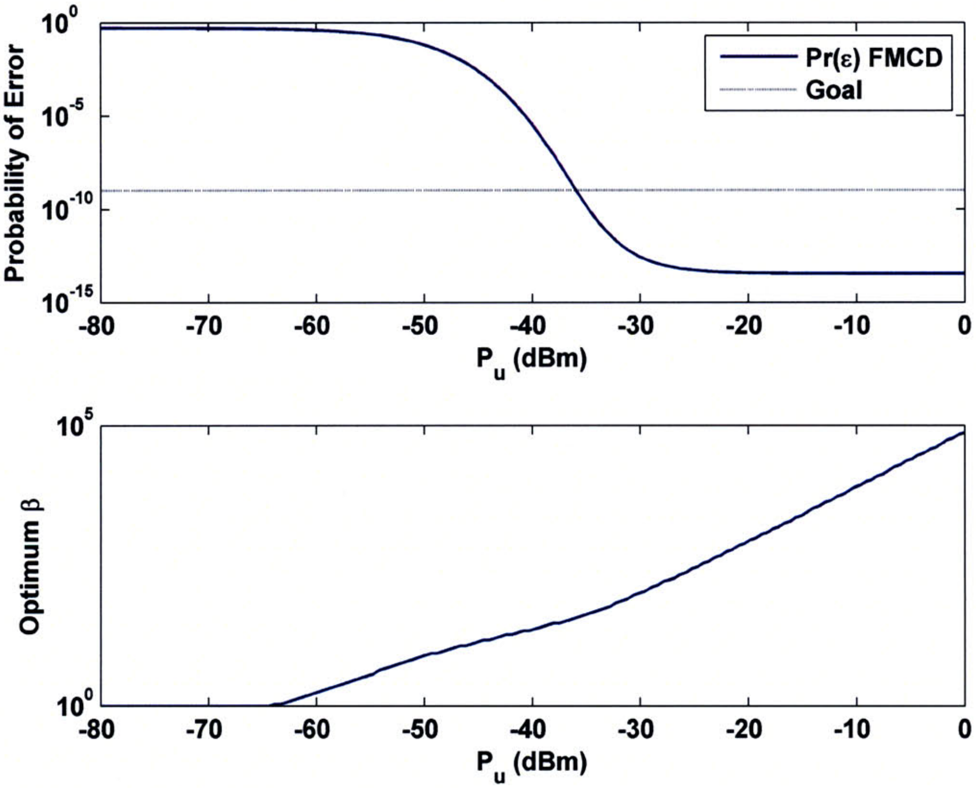

Figure 4-12: Optimum β versus P_u for uncoded FM–CD, ISAR = 1000, 12-bits, $E_b/N_0 = 15$ dB, $u_{sz} = 0.5$.

We compare the performance of each architecture under these parameters with and without quantization in Figure 4-13. The IM–DD architecture has a significant performance penalty compared to the FM–CD and digital architectures.

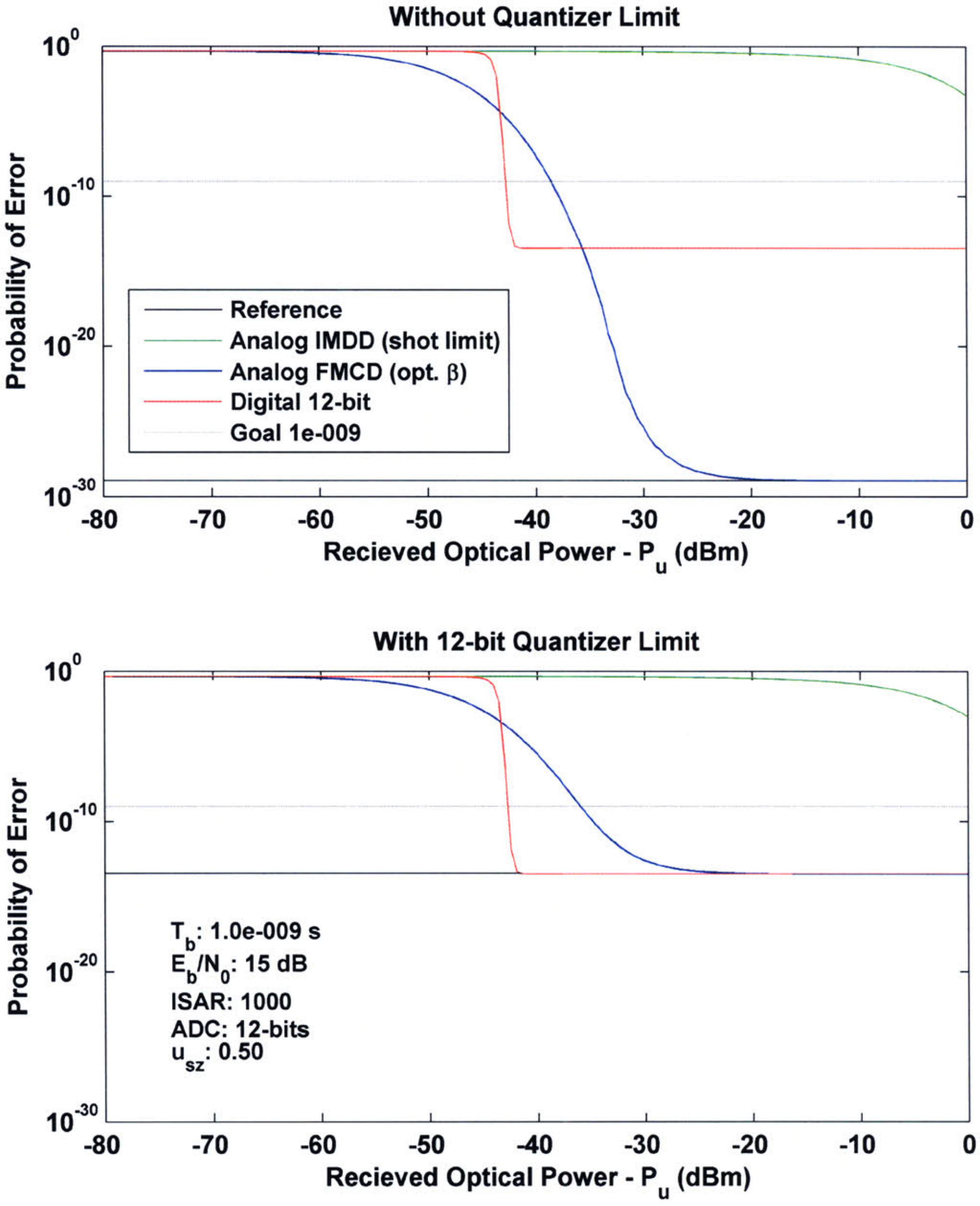

Figure 4-13: $\Pr(\epsilon)$ for uncoded systems with very strong interference.

Table 4.3 contains a range of both front-end signal to noise and normalized signal-interferer angle evaluated with quantizer effects. Only the digital and FM–CD architectures are compared. The IM–DD architecture is excluded from the table, as its performance is at least 40 dB worse under all parameters.

		u_{sz}	0.5			0.25			0.1		
E_b/N_0	ISAR	b	Dig.	FM	β_{opt}	Dig.	FM	β_{opt}	Dig.	FM	β_{opt}
(dB)		bits	P_u (dBm)			P_u (dBm)			P_u (dBm)		
10	1000	13	-41	-26	335	–	–	–	–	–	–
10	1000	14	-41	-32	94	–	–	–	–	–	–
10	1000	16	-41	-32	84	–	–	–	–	–	–
15	1000	12	-42	-36	39	–	–	–	–	–	–
15	1000	13	-42	-38	24	-42	-34	59	–	–	–
15	1000	14	-42	-38	22	-41	-35	45	–	–	–
20	1000	12	-42	-42	27	-42	-31	102	–	–	–
20	1000	13	-42	-42	17	-42	-37	32	–	–	–
20	1000	16	-41	-41	13	-41	-38	22	-40	-26	298
20	1000	17	-41	-31	13	-41	-38	22	-40	-27	261

Table 4.4: Minimum P_u for $p_{\text{goal}} = 10^{-9}$ with very strong interference, $T_b = 10^{-9}$.

The best performing uncoded architecture with a strong interferer under these conditions is digital. In some cases, the FM–CD performance is behind by only about 4–10 dB. However, the digital architecture consistently outperforms analog architectures over a wide range of E_b/N_0 and u_{sz}. A digital architecture with 16-bit quantization and at least -40 dBm of received optical power will support the strong and weak interference applications.

4.3.2 Coded User

We now compare architectures for coded RF systems using the surrogate error goal of $p_{\text{goal}} = 0.1$. A wide range of interference strengths are considered. The behavior of FM–CD and its dependence on β as ISAR increases is similar to the uncoded examples. The following examples are assume β_{opt} and figures showing FM–CD performance versus β are suppressed.

No Interference

We first compare the performance of each architecture without interference. Figure 4-14 shows the performance for $E_b/N_0 = 0$ dB and a 1-bit quantizer. As there is no interference, $u_{sz} = 0.5$. Under these parameters, the IM–DD architecture clearly offers the best performance. The digital and FM–CD architectures each have 6 dB penalty as compared to IM–DD.

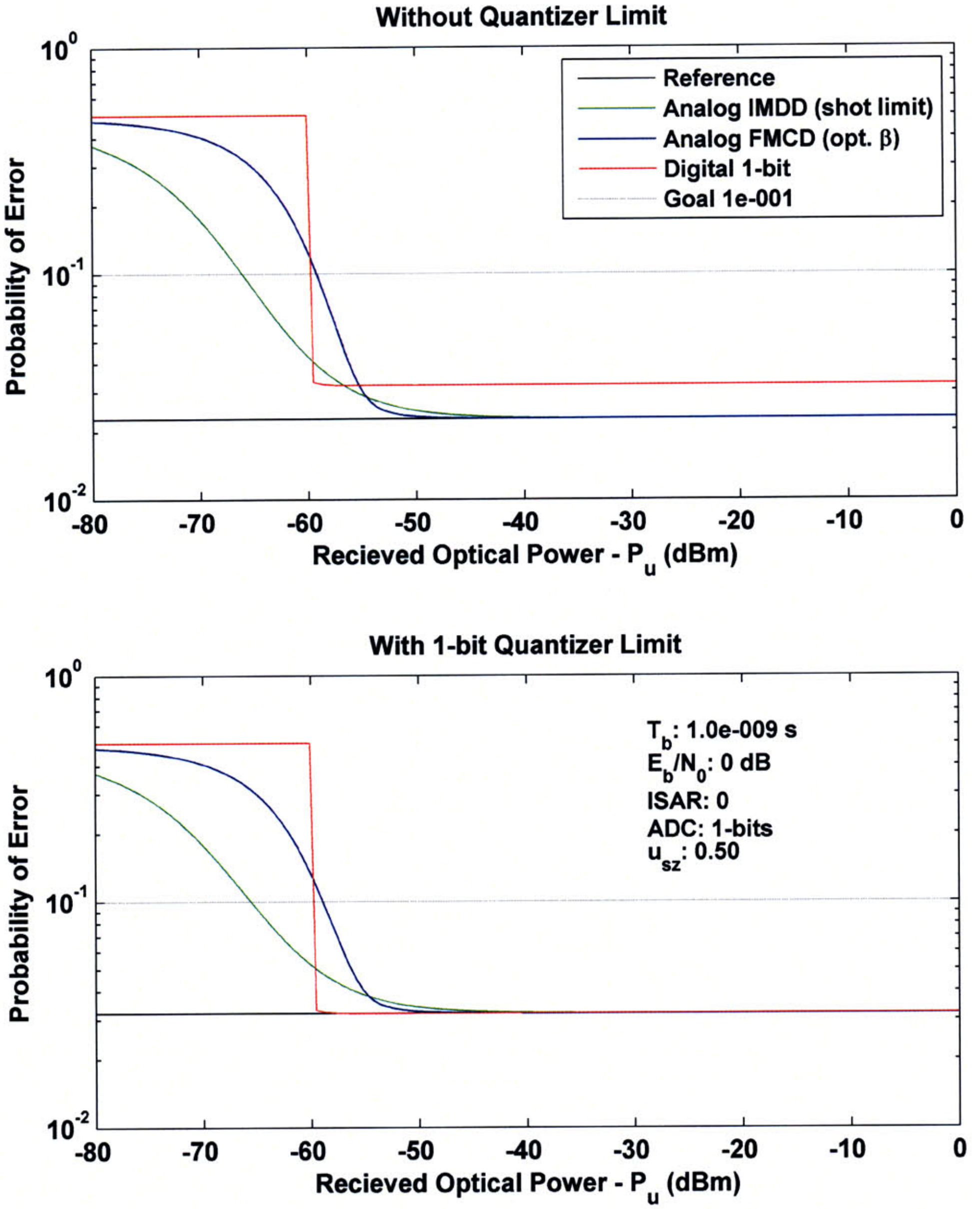

Figure 4-14: $\Pr(\epsilon)$ for coded systems with no interference.

Table 4.5 shows the performance over a range of parameters. For coded systems without interference, the FM–CD and digital architectures are generally tied for performance at about -60 dBm received optical power. As the necessary dynamic range of the signal is small the optimum value of β_{opt} is 1. As the IM–DD architecture has a

6 dB to 8 dB advantage, the preferred architecture is IM–DD with 2-bit quantization and at least -66 dBm of received optical power.

E_b/N_0	ISAR	u_{sz}	b-bits	Digital	IM–DD	FM–CD	β_{opt}
(dB)				P_u (dBm)			
0	0	$\star$[3]	1	-60	-66	-59	1
0	0	$\star$	2	-57	-66	-59	1
0	0	$\star$	3	-55	-66	-59	1
5	0	$\star$	1	-60	-67	-60	1
5	0	$\star$	2	-57	-68	-60	1
5	0	$\star$	3	-55	-68	-60	1
10	0	$\star$	1	-60	-68	-60	1
10	0	$\star$	2	-57	-68	-60	1
10	0	$\star$	3	-55	-68	-60	1

Table 4.5: Minimum P_u for $\text{p}_{\text{goal}} = 10^{-9}$ with no interference, $T_b = 10^{-9}$.

Small Interference

Next, we consider small interference where the interfering signal is approximately the same as amplitude as the user signal. Table 4.6 shows these results for ISAR = 1. Figure 4-14 shows the performance of each architecture in a stressing case where the signal-interference angle is very narrow, $u_{sz} = 0.1$, and signal suppression due to nulling is high. Here, $E_b/N_0 = 10$ dB and 1-bit quantization is used. In order of performance, the FM–CD architecture is best, followed by digital and then IM–DD.

---

[3] The signal-interference angle is a do-not-care value in this case as there is no interfering signal amplitude. Effectively $u_{sz} = 0.5$.

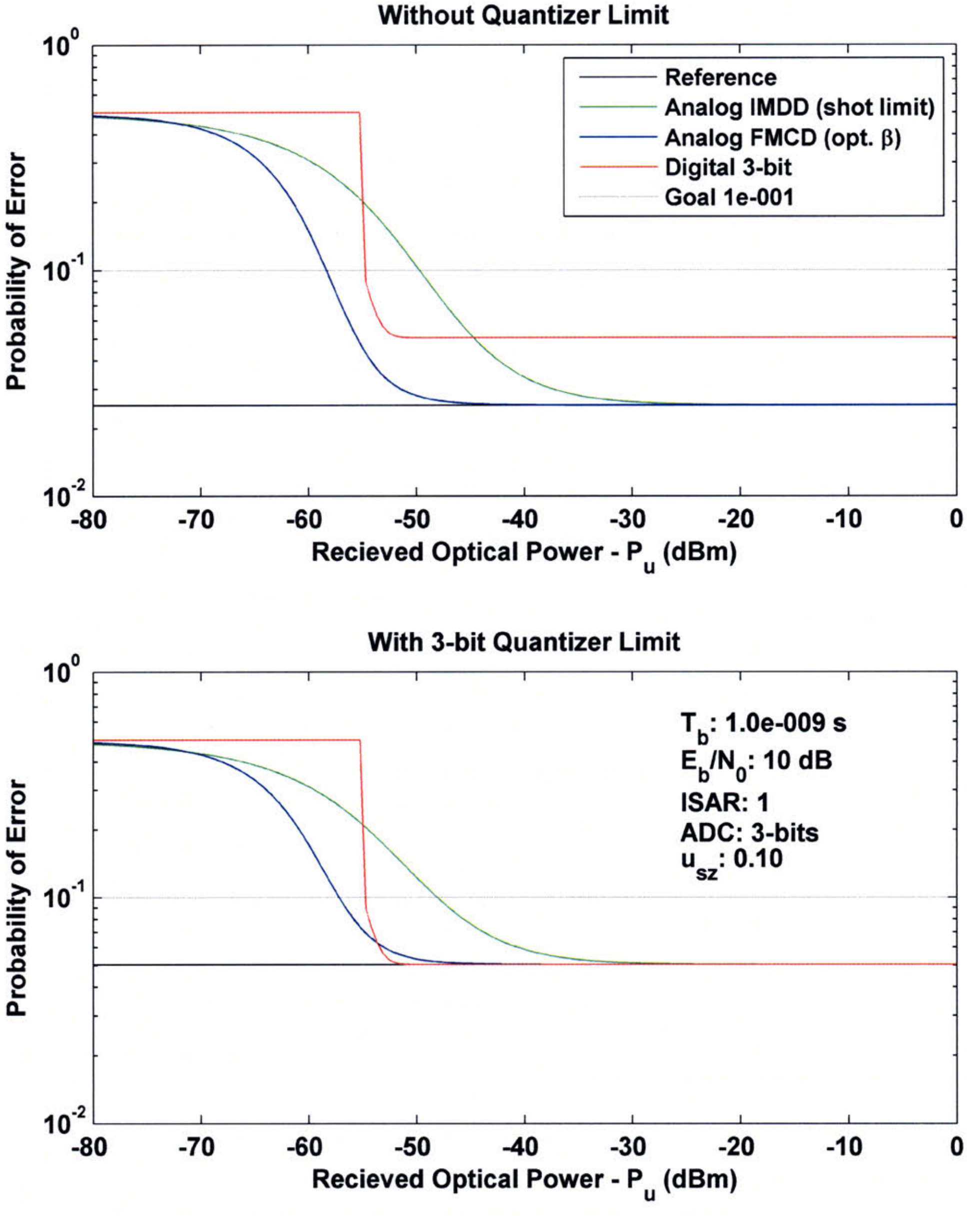

Figure 4-15: $\Pr(\epsilon)$ for coded systems with small interference, narrow angle.

		u_{sz}	0.5				0.25				0.1			
E_b/N_0	ISAR	b	Dig.	IM	FM	β_{opt}	Dig.	IM	FM	β_{opt}	Dig.	IM	FM	β_{opt}
(dB)		bits	P_u (dBm)				P_u (dBm)				P_u (dBm)			
0	1	1	-59	-57	-58	1	–	–	–	–	–	–	–	–
0	1	2	-56	-59	-59	1	-56	-46	-53	1.6	–	–	–	–
0	1	3	-55	-60	-59	1	-55	-51	-56	1	–	–	–	–
5	1	1	-59	-60	-59	1	-59	-52	-56	1	–	–	–	–
5	1	2	-57	-61	-60	1	-57	-57	-59	1	–	–	–	–
5	1	3	-55	-62	-60	1	-55	-58	-59	1	–	–	–	–
10	1	1	-59	-61	-59	1	-59	-55	-58	1	–	–	–	–
10	1	2	-57	-62	-60	1	-57	-58	-60	1	–	–	–	–
10	1	3	-55	-62	-60	1	-55	-59	-60	1	-55	-48	-57	1
10	1	4	-54	-62	-60	1	-53	-59	-60	1	-53	-49	-58	1

Table 4.6: Minimum P_u for $p_{\text{goal}} = 10^{-1}$ with small interference, $T_b = 10^{-9}$.

The best choice of architecture in the small interference case varies over the range of parameters analyzed. For $u_{sz} = 0.5$ the IM–DD architecture is best by about 1 dB. Smaller signal-interference angles favor the digital and FM–CD architectures slightly. There is no clearly preferred architecture unless u_{sz} is small, which favors FM–CD. FM–CD also offers less complex remote antenna satellites and lower prime power requirements due to the lack of remote analog to digital converters.

Moderate Interference

As the interference increases the performance become more differentiated between architectures. Figure 4-16 shows the performance with ISAR = 10, $E_b/N_0 = 0$, 3-bit quantization and $u_{sz} = 0.5$. The penalty of using 3-bit quantization in the FM–CD system is apparent when comparing the top and bottom figures. By using a higher resolution quantizer at the array processor with the FM–CD system, will result in performance gains.

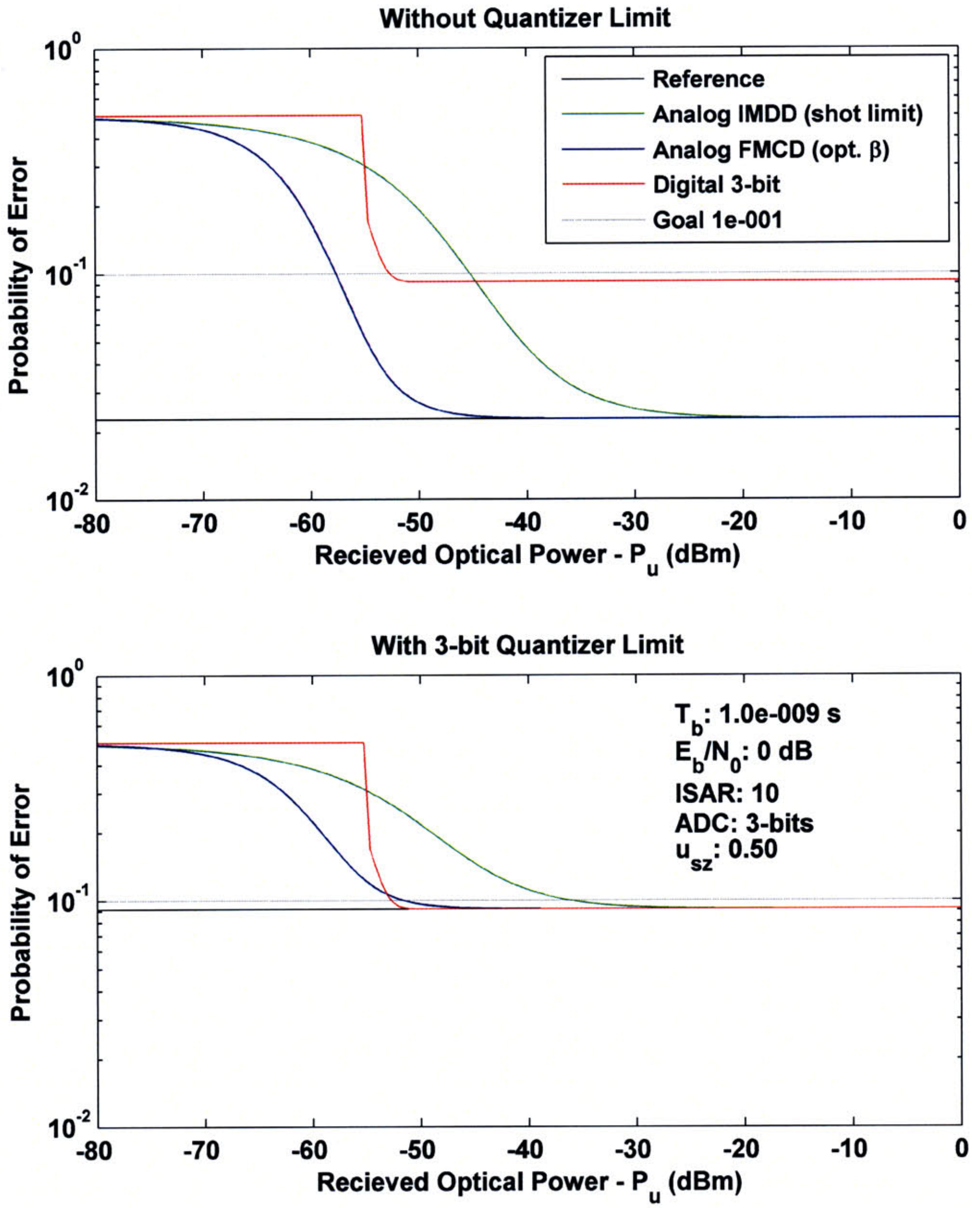

Figure 4-16: $\Pr(\epsilon)$ for coded systems with moderate interference.

In Table 4.7 shows FM–CD versus digital transport performance for a range of parameters when ISAR $= 10$. Under the parameters used in Figure 4-16, we see that using 6-bit quantization and FM–CD transport will outperform any digital transport by 6 dB. Also notice that the optimum β_{opt} in most cases is greater than 1.

		u_{sz}	0.5				0.25				0.1			
E_b/N_0	ISAR	b	Dig.	IM	FM	β_{opt}	Dig.	IM	FM	β_{opt}	Dig.	IM	FM	β_{opt}
(dB)		bits	P_u (dBm)				P_u (dBm)				P_u (dBm)			
0	10	3	-52	-36	-52	3	–	–	–	–	–	–	–	–
0	10	4	-52	-44	-57	1.2	–	–	–	–	–	–	–	–
0	10	5	-52	-45	-57	1.1	-50	-35	-52	2.8	–	–	–	–
0	10	6	-51	-45	-58	1.1	-49	-37	-53	2.4	–	–	–	–
5	10	3	-53	-43	-56	1.3	–	–	–	–	–	–	–	–
5	10	4	-53	-46	-59	1	-52	-41	-56	1.4	–	–	–	–
5	10	5	-52	-47	-59	1	-51	-43	-58	1.2	–	–	–	–
5	10	6	-51	-47	-59	1	-50	-43	-58	1.2	–	–	–	–
10	10	3	-54	-44	-57	1.3	–	–	–	–	–	–	–	–
10	10	4	-53	-47	-59	1	-52	-43	-58	1.3	–	–	–	–
10	10	5	-52	-47	-60	1	-51	-44	-59	1	-49	-31	-52	2.4
10	10	6	-51	-47	-60	1	-51	-59	1	-49	-34	-44	-55	2.3

Table 4.7: Minimum P_u for $\text{p}_{\text{goal}} = 10^{-1}$ with moderate interference, $T_b = 10^{-9}$.

Strong Interference

Increasing the interference further we look at ISAR = 100. The FM–CD transport architecture continues to outperform the digital transport architecture. The performance of IM–DD much worse than either FM–CD or digital. In Figure 4-17 we show an example with $E_b/N_0 = 5$ dB, 7-bit quantization and a reduced signal-interferer angle of 0.25.

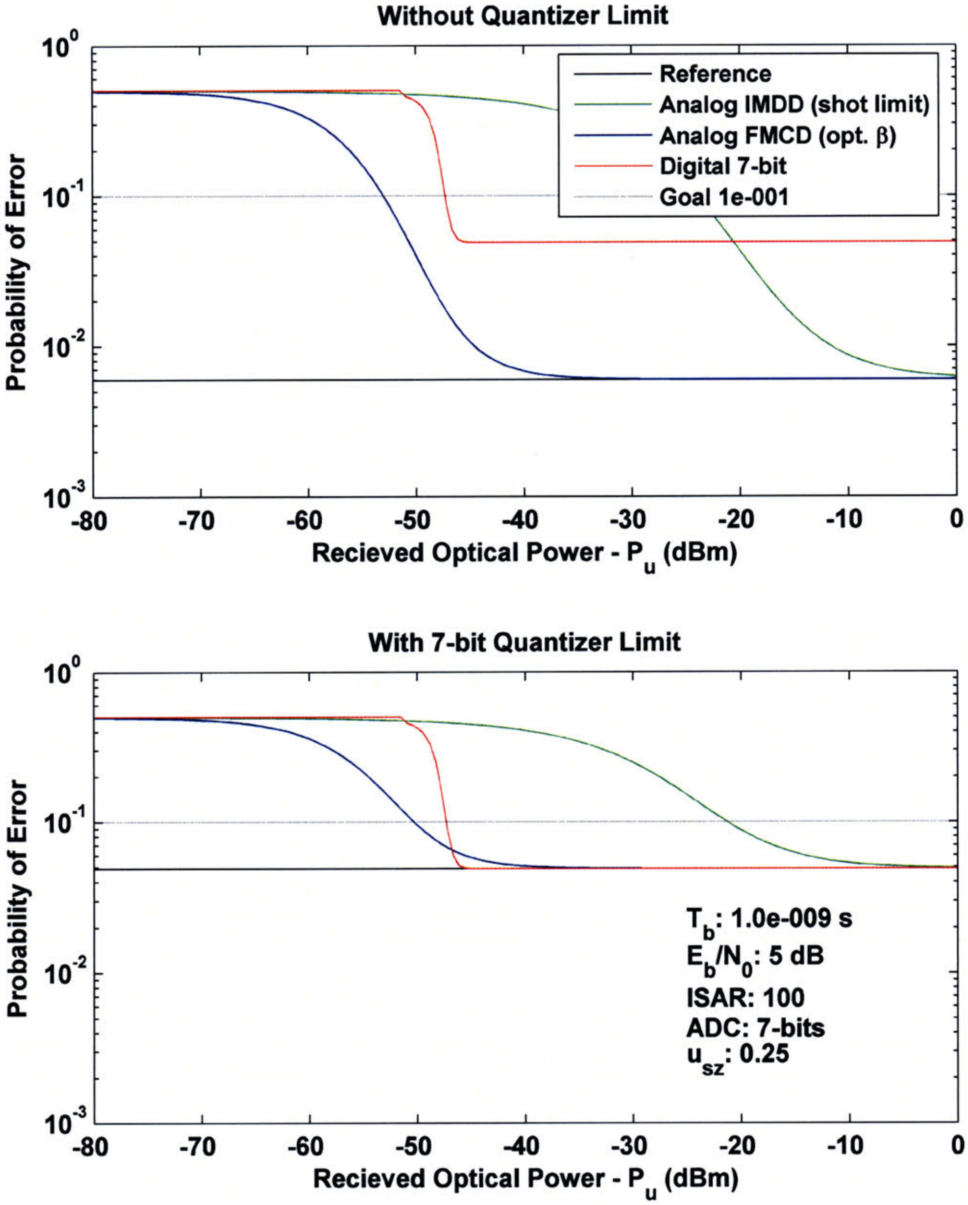

Figure 4-17: $\Pr(\epsilon)$ for coded systems with strong interference.

Table 4.8 has the parametric results for strong interference. In all cases we see that FM–CD transport is the best architecture by at least 1 dB but usually more.

		u_{sz}	0.5				0.25				0.1			
E_b/N_0	ISAR	b	Dig.	IM	FM	β_{opt}	Dig.	IM	FM	β_{opt}	Dig.	IM	FM	β_{opt}
(dB)		bits	P_u (dBm)				P_u (dBm)				P_u (dBm)			
0	100	7	-47	-25	-51	5	–	–	–	–	–	–	–	–
0	100	8	-47	-26	-52	4.3	-46	-15	-46	14	–	–	–	–
0	100	9	-47	-26	-53	4.2	-45	-17	-47	10	–	–	–	–
5	100	6	-47	-21	-49	7.7	–	–	–	–	–	–	–	–
5	100	7	-47	-27	-54	3.6	-47	-21	-50	6.6	–	–	–	–
5	100	8	-47	-27	-55	2.9	-47	-23	-52	4.7	–	–	–	–
5	100	9	-46	-28	-55	2.7	-46	-24	-53	4.3	–	–	–	–
10	100	6	-48	-23	-50	6.3	–	–	–	–	–	–	–	–
10	100	7	-47	-27	-54	3.2	-47	-22	-52	5.2	–	–	–	–
10	100	8	-47	-28	-56	2.3	-47	-25	-54	3.6	-45	-9	-44	20
10	100	9	-47	-28	-57	2	-46	-25	-55	3	-45	-15	-48	10
10	100	10	-46	-28	-57	1.8	-46	-25	-55	3	-45	-15	-49	9

Table 4.8: Minimum P_u for $p_{\text{goal}} = 10^{-1}$ with strong interference, $T_b = 10^{-9}$.

Very Strong Interference

We finally consider the performance of each architecture under very strong interference, ISAR = 1000. Figure 4-18 shows the comparison results for $E_b/N_0 = 5$ dB, 10-bit quantization and $u_{sz} = 0.5$. Again, we see that FM–CD transport outperforms digital transport and IM–DD transport lags significantly

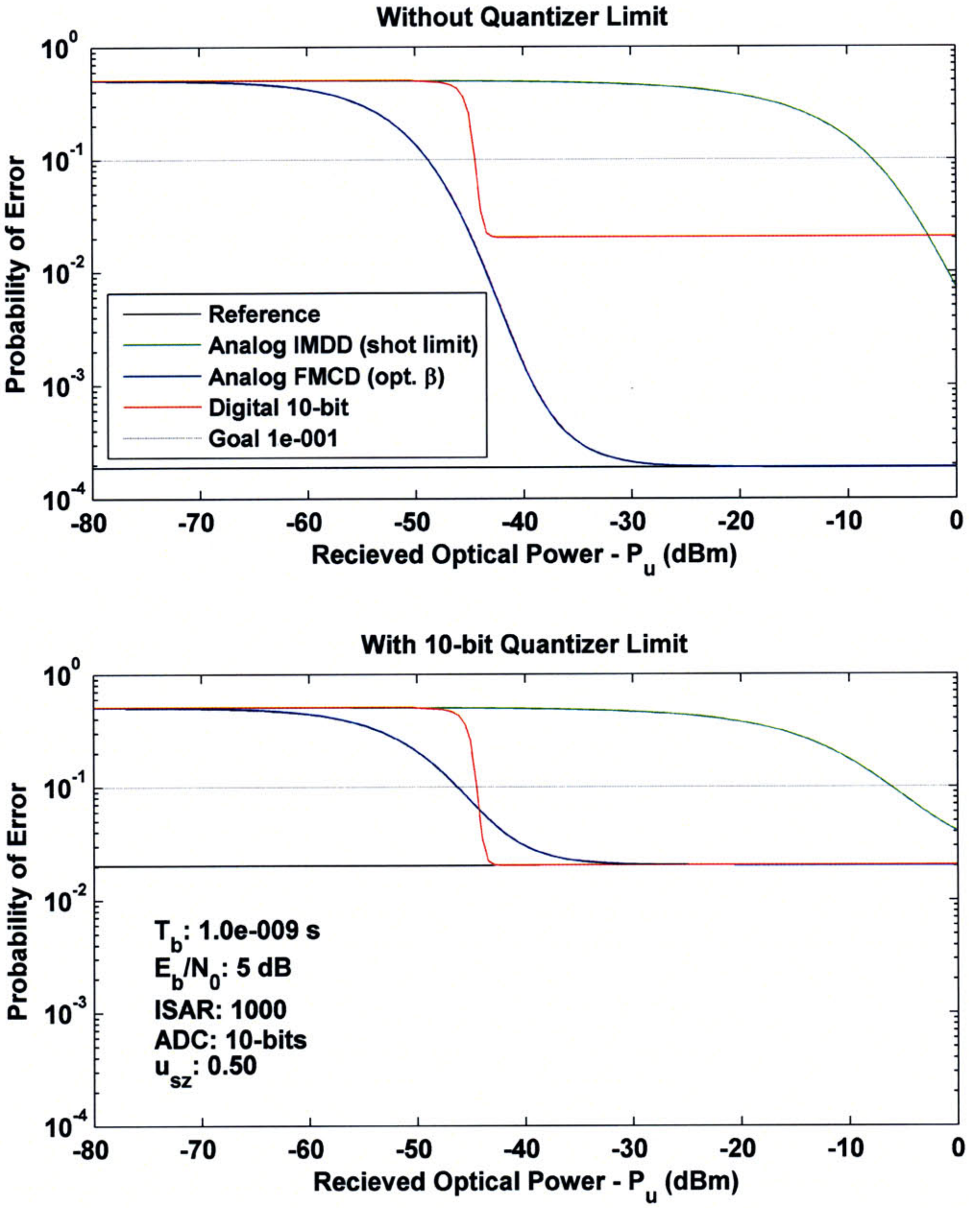

Figure 4-18: $\Pr(\epsilon)$ for coded systems with very strong interference.

Table 4.9 shows the performance of the digital and FM–CD systems over a range of parameters. As the IM–DD performance results are worse by at least 30 dB in all cases they are not presented in the table. The FM–CD transport architecture as at least as good if not better performance than the digital transport architecture in all cases.

		u_{sz}	0.5			0.25			0.1		
E_b/N_0 (dB)	ISAR	b bits	Dig. P_u (dBm)	FM	β_{opt}	Dig. P_u (dBm)	FM	β_{opt}	Dig. P_u (dBm)	FM	β_{opt}
0	1000	10	-44	-44	24	–	–	–	–	–	–
0	1000	11	-44	-46	19	-43	-37	87	–	–	–
0	1000	12	-43	-46	17	-43	-40	47	–	–	–
5	1000	10	-44	-46	17	-44	-41	37	–	–	–
5	1000	11	-44	-48	12	-43	-45	21	–	–	–
5	1000	12	-43	-49	11	-43	-46	18	–	–	–
10	1000	10	-44	-47	15	-44	-43	27	–	–	–
10	1000	11	-44	-49	10	-43	-47	16	–	–	–
10	1000	12	-43	-50	8	-43	-48	13	-42	-41	47
10	1000	13	-43	-51	7.4	-43	-48	11	-42	-42	39
10	1000	14	-43	-51	7.1	-43	-49	11	-42	-42	37
15	1000	10	-44	-47	14	-44	-44	26	–	–	–
15	1000	11	-44	-50	9.0	-43	-47	14	-43	-38	72
15	1000	12	-43	-51	6.6	-43	-49	10	-43	-43	31
15	1000	13	-43	-52	5.4	-43	-50	8.3	-42	-45	24

Table 4.9: Minimum P_u for $p_{\text{goal}} = 10^{-1}$ with very strong interference, $T_b = 10^{-9}$.

4.3.3 System Geometry

We now incorporate the transmitter and receiver system geometry for a satellite array in Geosynchronous orbit. We assume that the array processor is equidistant from each remote antenna satellite where the free-space optical links are both of length d (the three satellites are in an equilateral triangle configuration). The received optical power is calculated, initially, using a 1 mW (i.e. 0 dBm) source laser with 1 cm apertures for the FSO transmitters and receivers.

The minimum d presented is 100 meters. This is a good starting point over single satellite array applications where the maximum satellite size is tens of meters. As each antenna in the array should be within the main beam of the transmitted signals from the ground, there is a practical upper limit to d. If we roughly consider a 30 GHz signal and 1 m ground antennas the maximum practical d is on the order of 10^5.

Moderate Interference

In Figure 4-19 we plot the probability of error response versus receive antenna separation distance, d, and the normalized antenna-interference angle u_{sz}. Quantizer resolution is suppressed by only plotting the lowest error probability after numerically computing the optimum value of b for each operating point. In this example we assume $E_b/N_0 = 0$ dBm and a moderate interference with ISAR = 10.

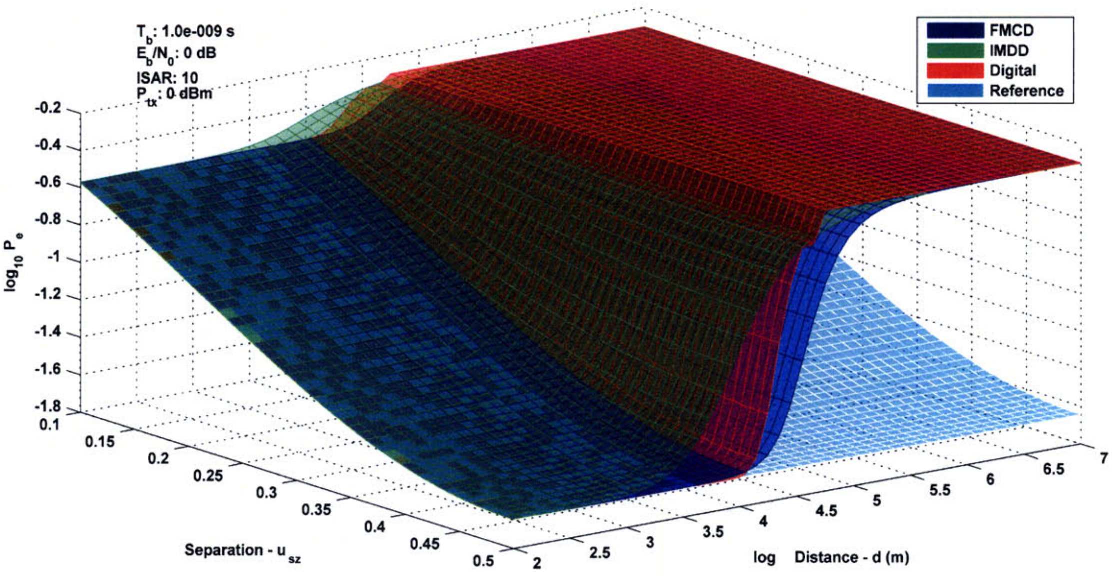

Figure 4-19: $\Pr(\epsilon)$ versus ground separation angle and satellite separation distance, $E_B/N_0 = 0$ dB, ISAR $= 10$, $P_s = 0$ dBm (see text).

We can first see the significant effect of decreasing u_{sz} where for these operating parameters $p_{\text{goal}} = 0.1$ cannot be met for $u_{sz} < 0.25$ even when d is small. As long as $d < 10^4$ m, the performance of both FM–CD and digital transport architectures are identical to the reference system (limited only by E_b/N_0 and u_{sz}). The IM–DD system has significantly lower performance everywhere. As the distance increases, we see digital and FM–CD start to fall off rapidly, with the FM–CD architecture outperforming the digital architecture. Numerical precision limits result in the mosaic artifact in the left side of the figure where FM–CD and digital architectures are limited by the reference.

There are four operating regimes based on the antenna separation distance. In order of increasing d the four regimes are:

1. *Performance limited by E_b/N_0 and u_{sz} (reference).* Performance is generally insensitive to the transport architecture in this regime. For higher ISAR only digital and FM–CD transport architectures are reach the reference performance limit due to the poor performance of IM–DD.

2. *Best performance with digital transport.* The FM–CD and IM–DD analog transport performance starts to taper off.

3. *Best performance with FM–CD transport.* Decreasing received optical power causes the digital transport link to fail with a sharp cutoff.

4. *Communication system down.* At some point performance is degraded enough that communication is not possible regardless of the transport architecture.

Thus, we can use the threshold between regimes 2 and 3 to determine the optimum transport architecture for any application. As we discussed in Section 4.2 having the lowest bit-error probability may not be necessary as long as the goal is reached.

The actual ground separation in meters between the signal and the interference source, χ, is shown in Figure 4-20 as a function of the antenna spacing, d, and the normalized angle, u_{sz}. Results for RF center frequencies of both 30 GHz and 3 GHz are shown.

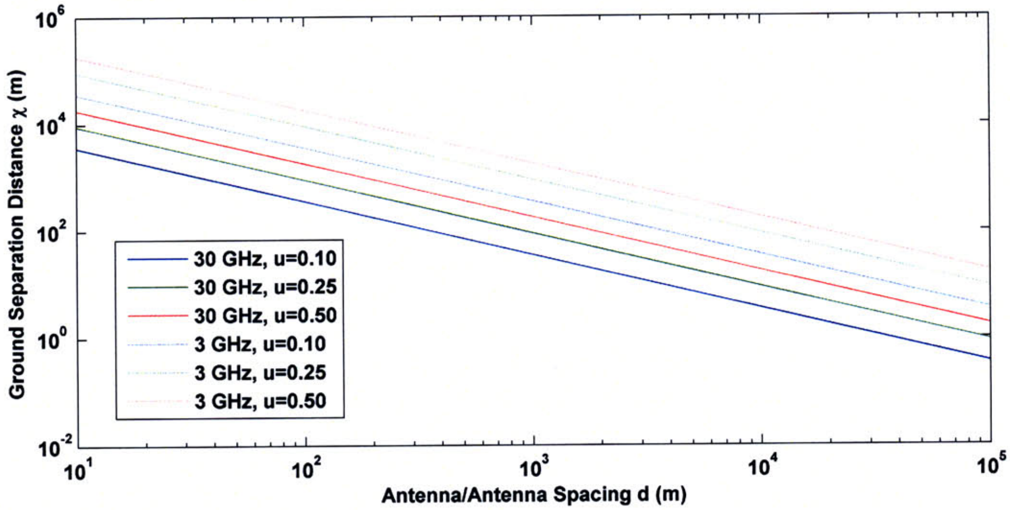

Figure 4-20: Ground separation distance versus satellite separation at GEO, f_0 = 30 GHz (see text).

We can use these two figures to determine which geometry configurations are supported. For example, to achieve a ground separation distance of 10 m with p_{goal} = 0.1, d must be at least 8 km (for $u_{sz} = 0.25$).

As the front-end signal to noise ratio improves the achievable probability of error decreases rapidly. This enables much narrower signal-interferer angles without increasing d or the transmit optical power. Figure 4-21 and Figure 4-22 show the same performance comparison with an E_b/N_0 of 10 dB and 20 dB respectively.

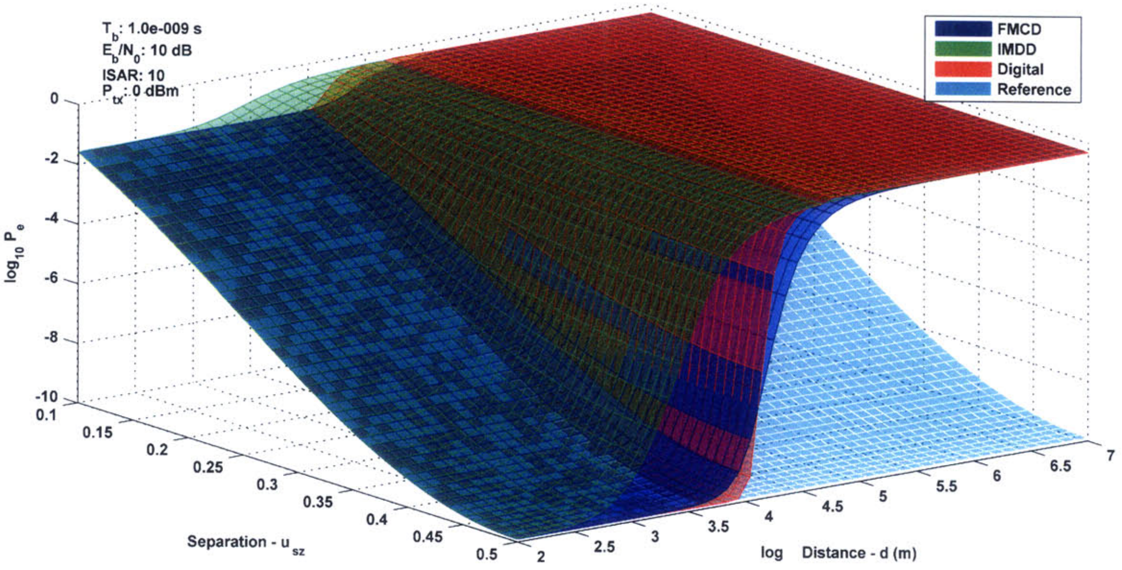

Figure 4-21: $\Pr(\epsilon)$ versus ground separation angle and satellite separation distance, $E_B/N_0 = 10$ dB, ISAR $= 10$, $P_s = 0$ dBm.

Figure 4-23 is a closer detail view of Figure 4-22. The IM–DD results are suppressed from this figure. The comparable baseline distance for low and high $\mathrm{p_{goal}}$ values are shown.

An alternate way to decrease the ground spacing between the user signal and interference signal, χ, is to increase the baseline, d. Selecting the best architecture enables the smallest ground spacing. A 6 dB decrease in minimum received optical power doubles the maximum baseline distance and therefore decreasing the close in distance by a factor of two. If the system is limited by received optical power then either the optical apertures or the transmitted optical power must be increased. As a 1 mW transmit laser is conservative, we may consider higher transmit powers. Figure 4-24 increases the transmit optical power to 100 mW (20 dBm). The result is an increase in d by a factor of 10, translating to a decrease in signal-interferer distance

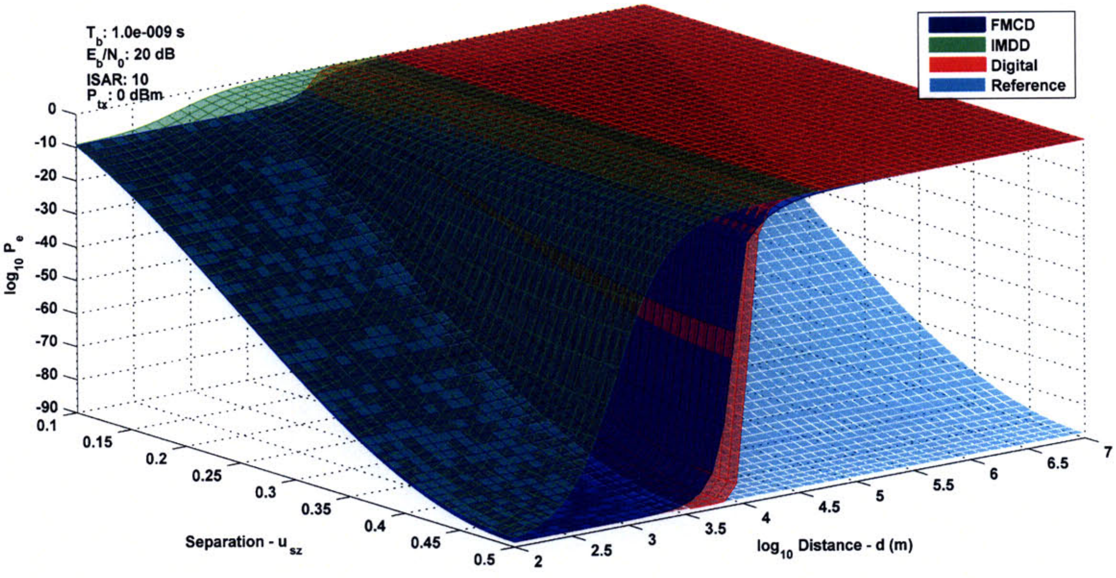

Figure 4-22: $\Pr(\epsilon)$ versus ground separation angle and satellite separation distance, $E_B/N_0 = 20$ dB, ISAR = 10, $P_s = 0$ dBm.

by a factor of ten.

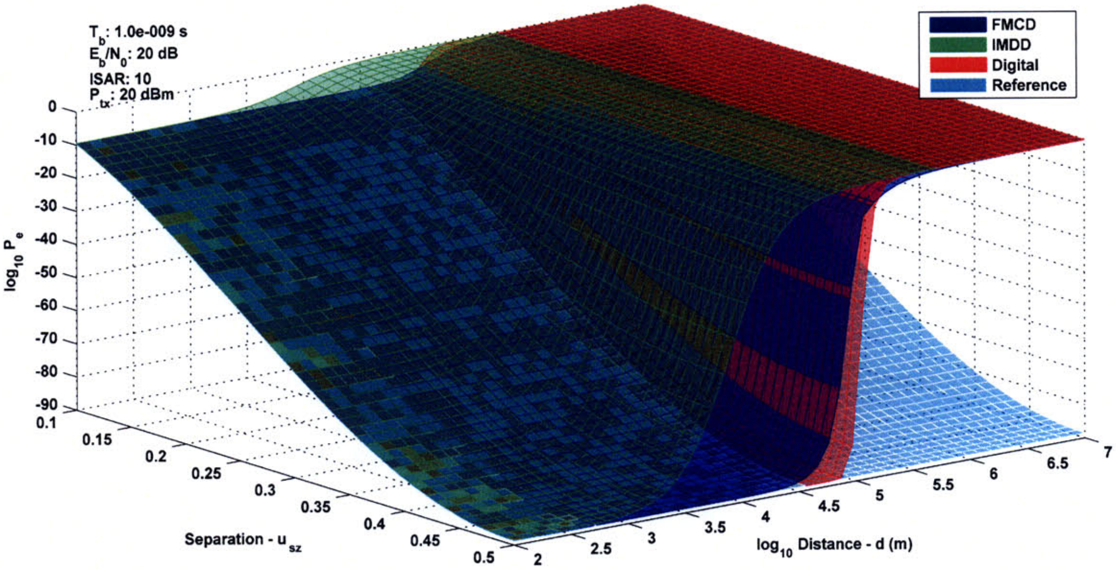

Figure 4-24: $\Pr(\epsilon)$ versus ground separation angle and satellite separation distance, $E_B/N_0 = 20$ dB, ISAR = 10, $P_s = 20$ dBm.

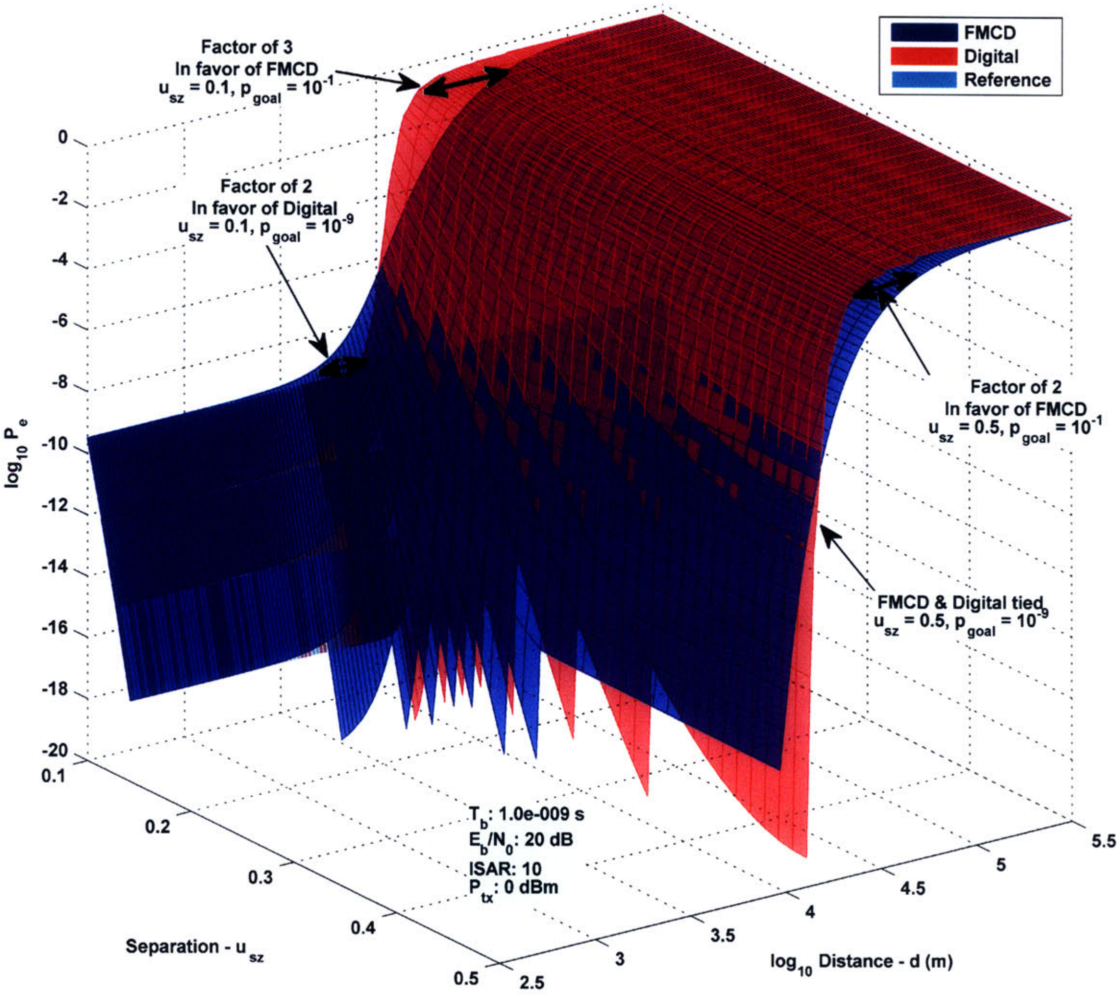

Figure 4-23: $\Pr(\epsilon)$ versus ground separation angle and satellite separation distance, $E_B/N_0 = 20$ dB, ISAR $= 10$, $P_s = 0$ dBm, detail.

Small Interference

We consider small interference with ISAR = 1 in Figure 4-25 to Figure 4-28 for a range of front-end signal to noise ratios. It interesting to note how the best choice of transport architecture may be IM–DD for weak front-end signal to noise and digital for strong signal to noise. This behavior is only seen when ISAR is small. The last figure shows the increase in achievable d by increasing the transmitted optical power.

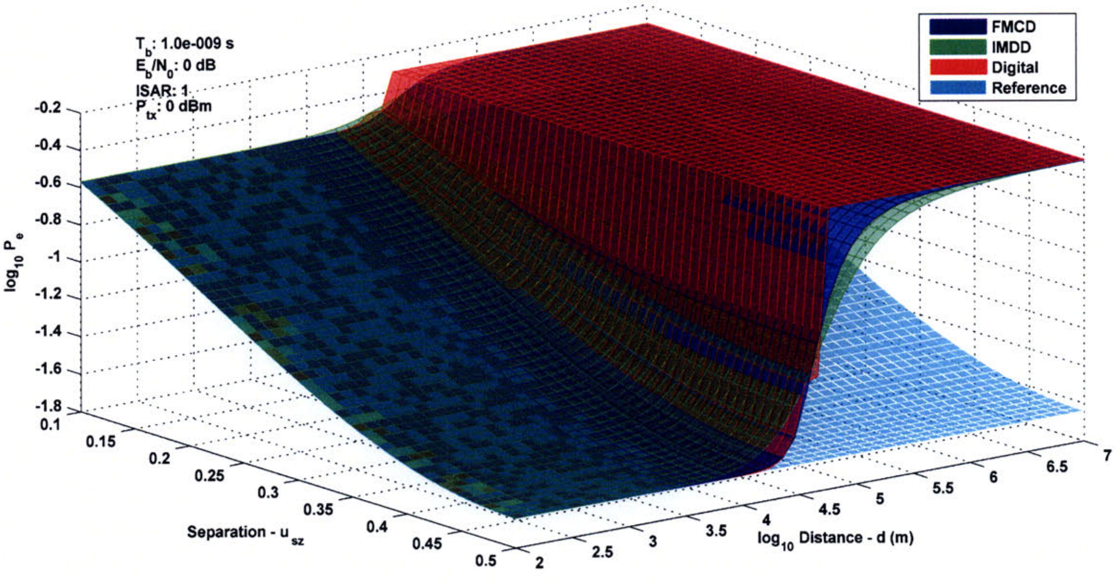

Figure 4-25: $\Pr(\epsilon)$ versus ground separation angle and satellite separation distance, $E_B/N_0 = 0$ dB, ISAR $= 1$, $P_s = 0$ dBm.

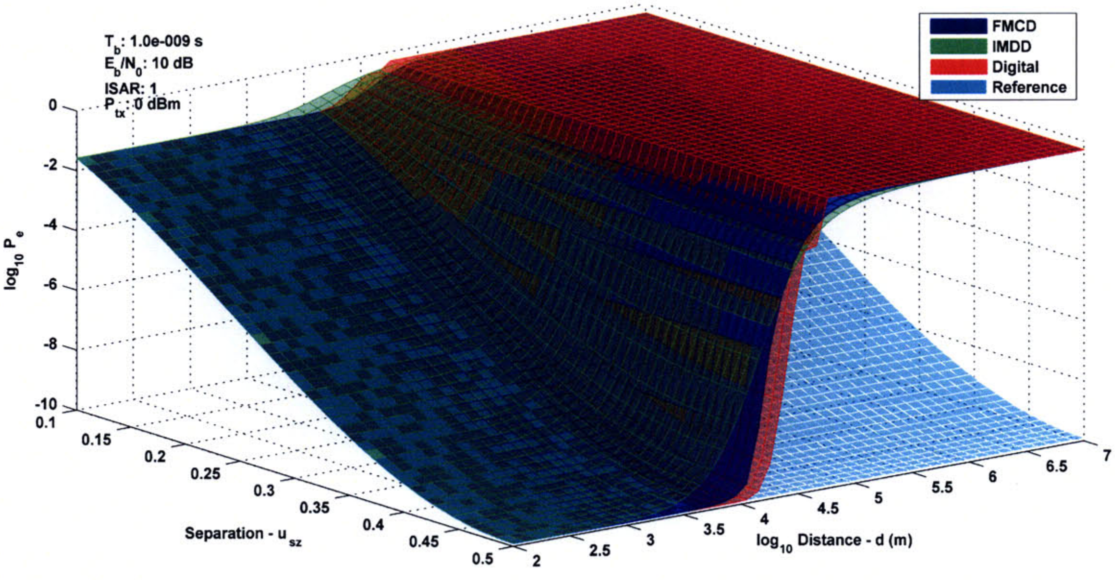

Figure 4-26: $\Pr(\epsilon)$ versus ground separation angle and satellite separation distance, $E_B/N_0 = 10$ dB, ISAR $= 1$, $P_s = 0$ dBm.

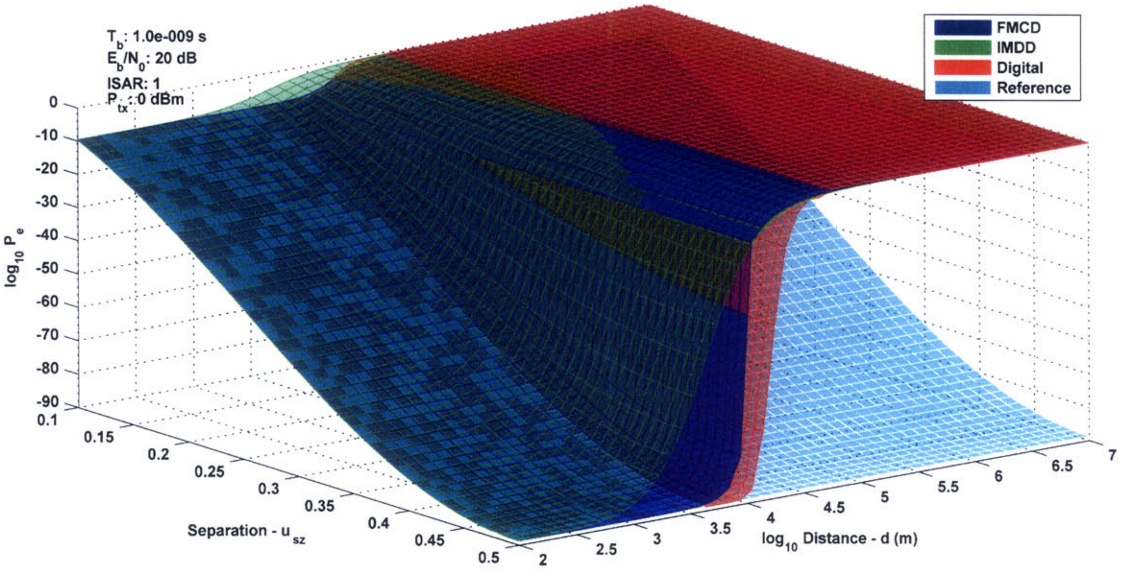

Figure 4-27: $\Pr(\epsilon)$ versus ground separation angle and satellite separation distance, $E_B/N_0 = 20$ dB, ISAR $= 1$, $P_s = 0$ dBm.

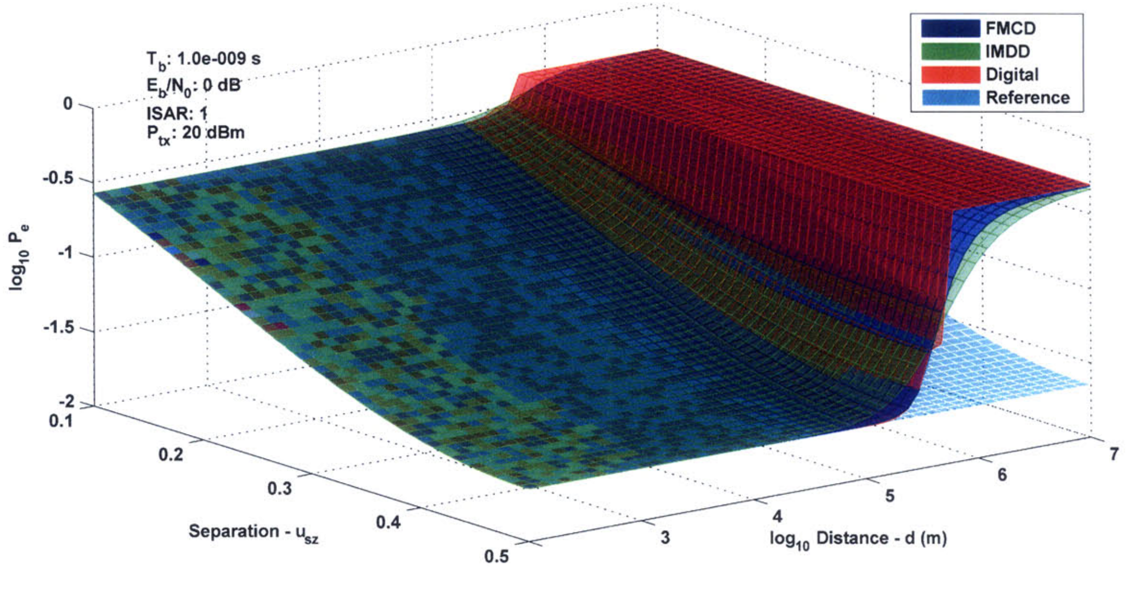

Figure 4-28: $\Pr(\epsilon)$ versus ground separation angle and satellite separation distance, $E_B/N_0 = 0$ dB, ISAR $= 1$, $P_s = 20$ dBm.

Strong Interference

We consider strong interference with ISAR = 100 in Figure 4-29 to Figure 4-31 for a range of front-end signal to noise ratios. Figure 4-32 shows a more detailed view of Figure 4-31 with a few comparisons (IM–DD results are suppressed). The poor performance of IM–DD is obvious and the FM–CD versus digital threshold is very clear.

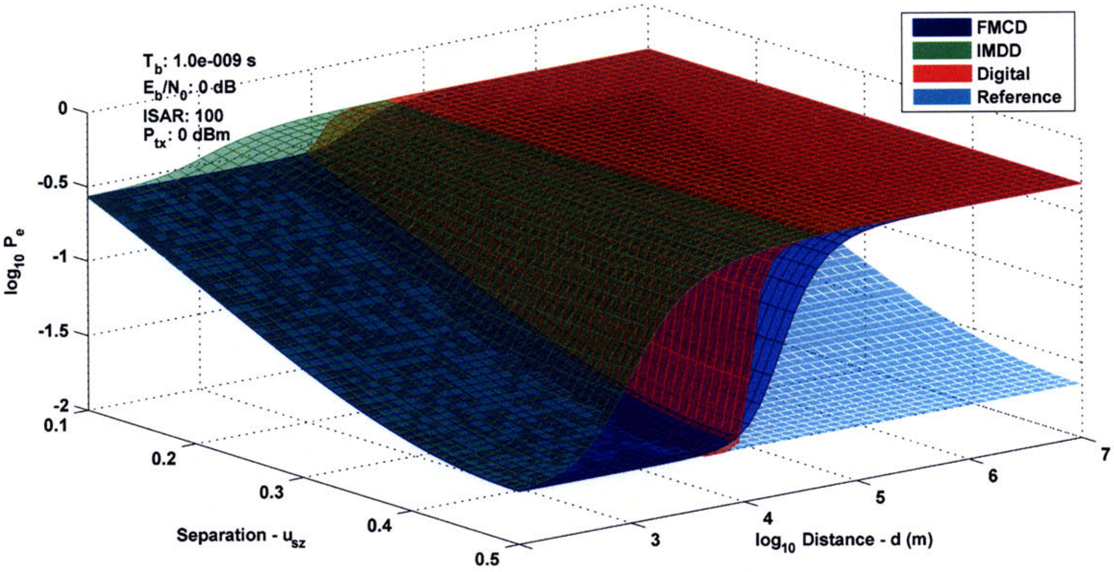

Figure 4-29: $\Pr(\epsilon)$ versus ground separation angle and satellite separation distance, $E_B/N_0 = 0$ dB, ISAR $= 100$, $P_s = 0$ dBm.

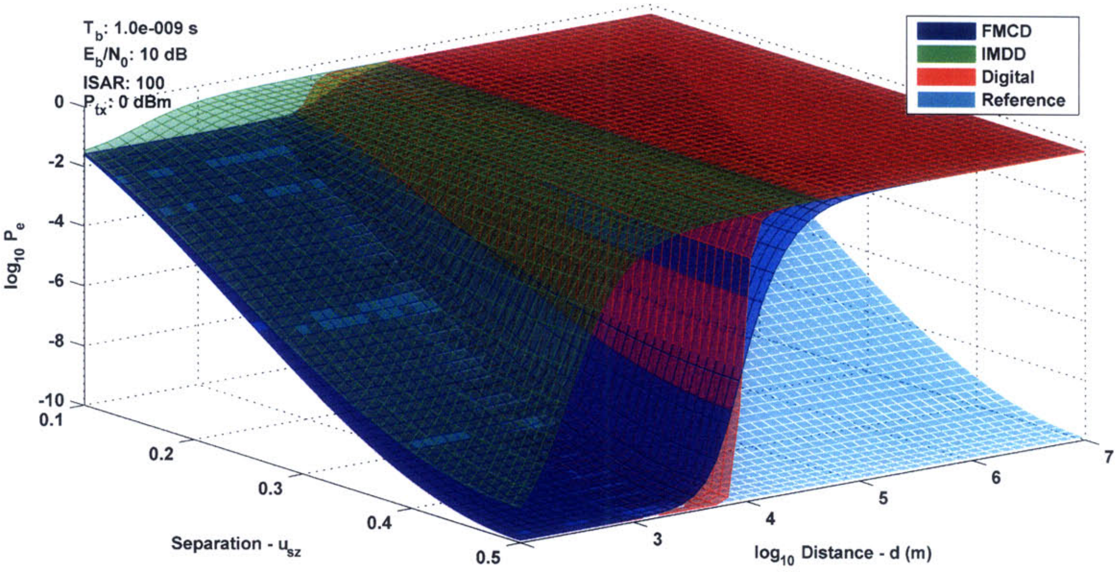

Figure 4-30: $\Pr(\epsilon)$ versus ground separation angle and satellite separation distance, $E_B/N_0 = 10$ dB, ISAR = 100, $P_s = 0$ dBm.

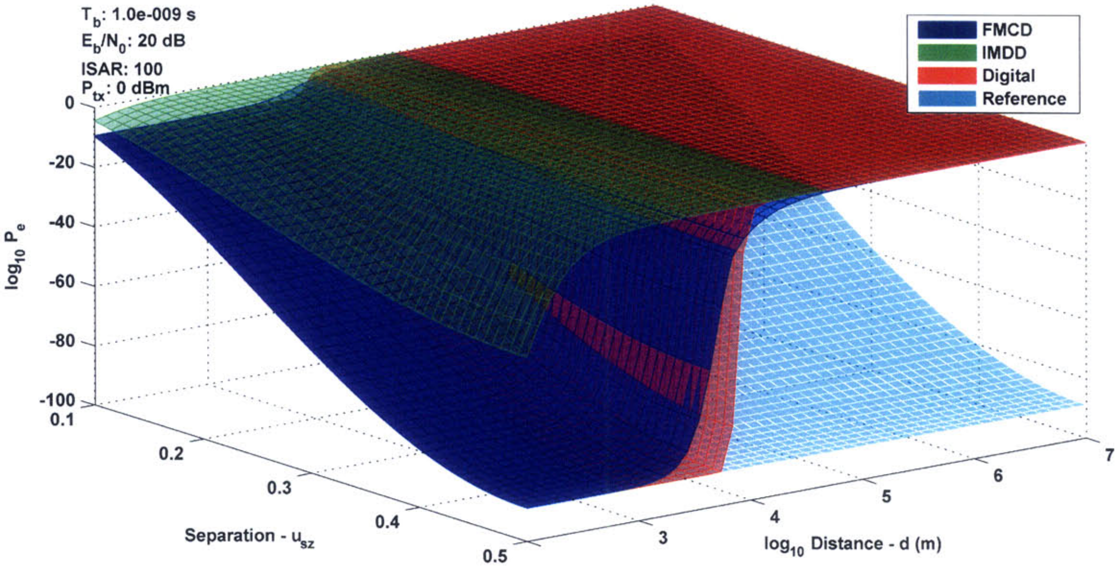

Figure 4-31: $\Pr(\epsilon)$ versus ground separation angle and satellite separation distance, $E_B/N_0 = 20$ dB, ISAR = 100, $P_s = 0$ dBm.

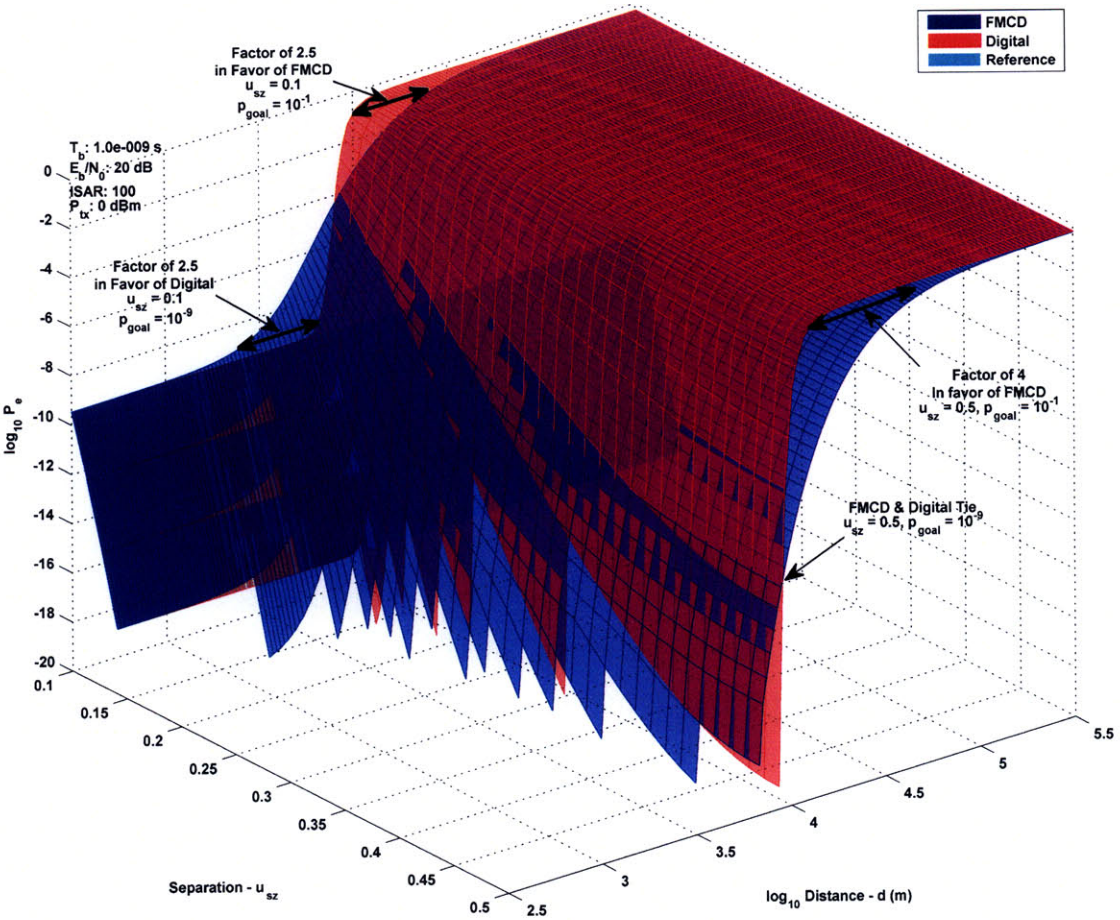

Figure 4-32: $\Pr(\epsilon)$ versus ground separation angle and satellite separation distance, $E_B/N_0 = 20$ dB, ISAR = 100, $P_s = 0$ dBm, detail.

Very Strong Interference

We consider very strong interference with ISAR = 1000 in Figure 4-33 to Figure 4-35 for a range of front-end signal to noise ratios. In the last figure the surface for IM–DD is removed for clarity.

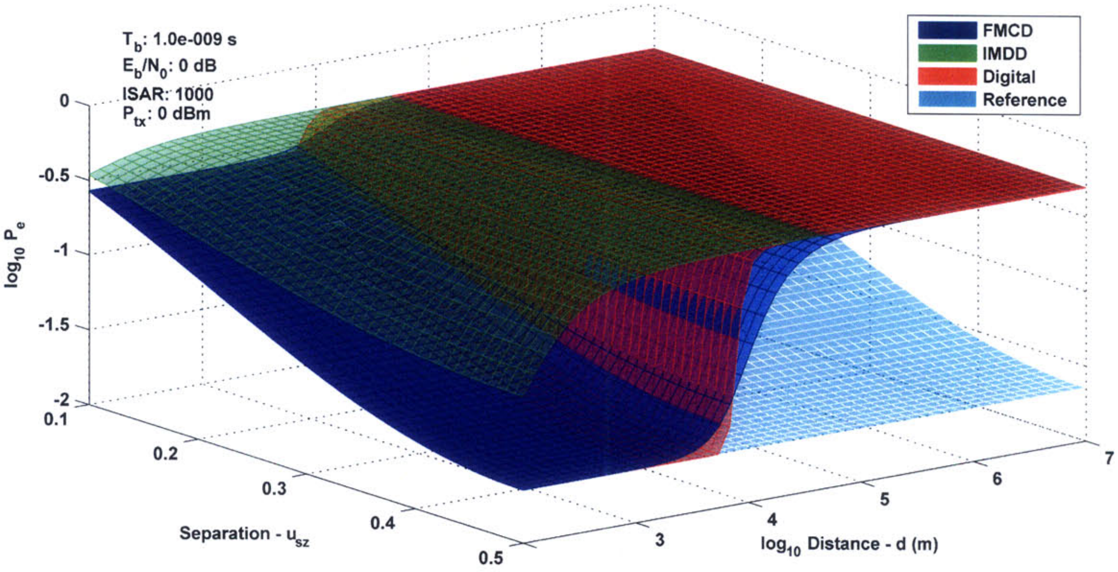

Figure 4-33: $\Pr(\epsilon)$ versus ground separation angle and satellite separation distance, $E_B/N_0 = 0$ dB, ISAR = 1000, $P_s = 0$ dBm.

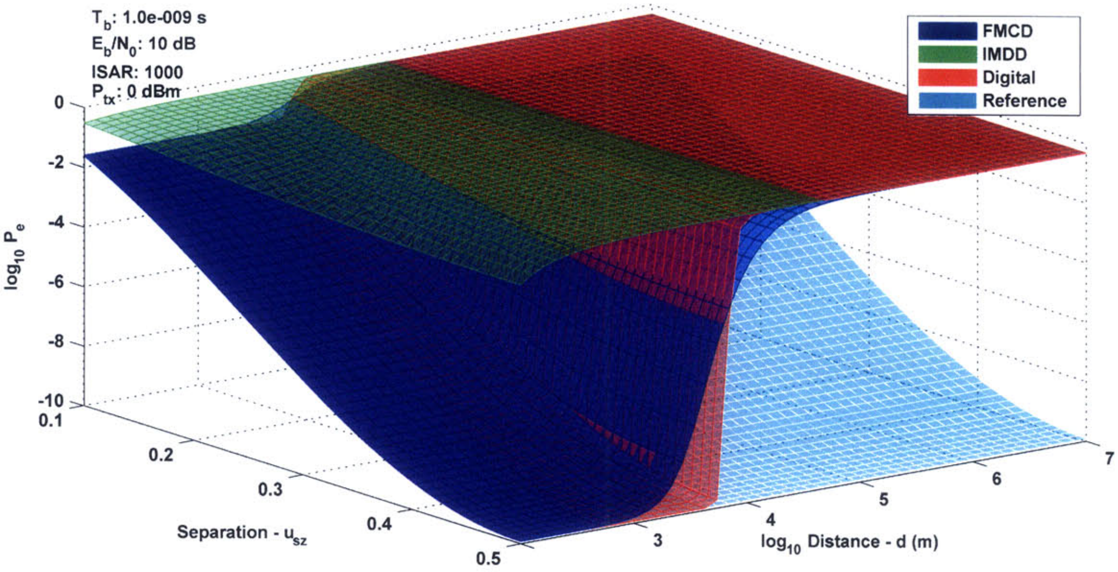

Figure 4-34: $\Pr(\epsilon)$ versus ground separation angle and satellite separation distance, $E_B/N_0 = 10$ dB, ISAR = 1000, $P_s = 0$ dBm.

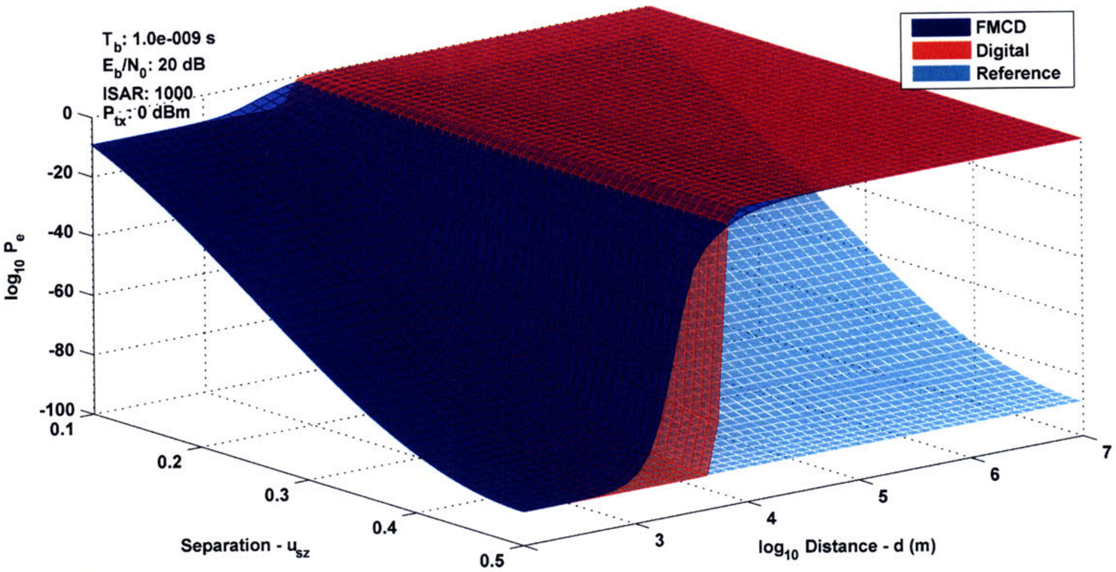

Figure 4-35: $\Pr(\epsilon)$ versus ground separation angle and satellite separation distance, $E_B/N_0 = 20$ dB, ISAR $= 1000$, $P_s = 0$ dBm.

Chapter 5

Results and Conclusions

In this thesis we have constructed reasonable parameterized models for satellite communication arrays using free-space optical inter-satellite links. A range of system architectures were discussed. We have focused on architectures using digital array processing with analog and digital modulated ISLs. For analysis, we used a two-channel receiver with two independent signal sources (a user and an interferer) and used complete nulling to suppress the interferer. Reasonable system performance goals were set and used to compare architectures.

We have shown that free-space optical inter-satellite links are capable of supporting high resolution satellite communication arrays. The required optical power, specifically for digital and analog frequency modulated links, is on the order of a milliwatt. This enables the use of centimeter class optical apertures and very low transmit laser power. It also allows the system engineer to trade optical power for complexity in the optical system. When the interference amplitude was low, analog intensity modulation works as well (and in some cases better) than FM–CD or digital. However, for moderate to strong interference IM–DD transport requires orders of magnitude more received optical power.

We found when a low probability of error goal was set for RF signals with uncoded BPSK ($\mathrm{p_{goal}} = 10^{-9}$) the digital transport architecture was significantly favored when comparing required minimum received optical power. This was true for both low and high interference levels.

When the probability of error goal was relaxed ($p_{\text{goal}} = 10^{-1}$) as a surrogate to assuming a coded RF modulation scheme we found the FM–CD transport architecture had better performance than the digital system in almost all scenarios. In some cases the digital and FM–CD architectures were tied.

Finally, we found a threshold satellite spacing, d, useful for selecting digital or analog FM–CD transport as the best architecture. Below the threshold, digital transport has the smallest bit-error probability and above the threshold FM–CD transport has lower error probability.

5.1 Limitations

We have made a number of simplifying assumptions in this thesis that may partially limit the direct application of our results. The first is the simple two-channel array model in Figure 3-1. Practical satellite communication arrays may have more antennas. They may also be asymmetric where some antennas are local to the array processor and do not suffer the degradation from optical transport as in Figure 1-2b. We have assume also assumed the digital optical inter-satellite link is uncoded binary.

We have not proved the complex weighted array processing followed by a whitened correlation receiver to be optimum. When the array is asymmetric, it is likely that this configuration is not optimum. The use of complete nulling is known to be non-optimum for very close signal and interference sources but it greatly simplifies analysis. We have also assumed we know the direction of arrival for each signal. The estimation of the direction of arrival (DOA) is necessary in practical systems. As the DOA is estimated from the received signal, it is also degraded by signal transport so this would need to be taken into account.

5.2 Future Research

Continuing research on high resolution satellite communication systems using optical inter-satellite links is likely, beginning with address the limitations shown above.

Furthermore, architectures with analog optical array processing may be considered as a method of dealing with very large interference before digitization and more traditional digital processing. Similar analysis may also be applied to terrestrial radio communication systems with fiber-optic links between remote antennas and the array processor. Finally, one may actually build a high resolution satellite communication constellation and demonstrate the results presented here.

THIS PAGE INTENTIONALLY LEFT BLANK

Appendix A

SNR of FM–CD Transport

Nick Andrikogiannopoulos analyzed the performance of a frequency modulated optical link with coherent detection in terms of its raw signal to noise ratio.[4] This thesis extends the analysis to the performance of a full communication system using FM–CD. As part of our analysis, we found discrepancies in Mr. Andrikogiannopoulos SNR analysis. This appendix has the corrected results.

Anomaly-free SNR

Section 2.3.2 derived the power spectral density of the post-discriminator noise in an FM–CD link. The results in equation (2.30) is not flat. However, the signal to noise ratio can be derived independently of the noise color.

First integrate the noise PSD over the bandwidth, B, to determine the total post discriminator noise power, N_D. Shot noise limited homodyne coherent detection is assumed.

$$\begin{aligned} N_D &= \int_{-B}^{B} S_{n_{\mathrm{FMCD}}}(f) \\ &= \frac{h\nu}{2\eta P_u} \int_{-B}^{B} \frac{f^2}{f_\Delta^2} \mathrm{d}f \\ &= \frac{h\nu}{2\eta P_u} \frac{2}{3} \frac{B^3}{f_\Delta^2} \\ &= \frac{h\nu B}{3\eta P_u \beta^2} \\ &= \frac{1}{3\beta^2(\beta+2)\,\mathrm{CNR}} \end{aligned} \tag{A.1}$$

The total signal power can be calculated in the time domain by taking the mean square amplitude of the modulating signal, $\overline{g^2(t)}$. A full-scale sinusoid has $\overline{g^2(t)} = \frac{1}{2}$ and uniformly distributed random signal between $[-1, 1]$ has $\overline{g^2(t)} = \frac{1}{3}$. The value of $\overline{g^2(t)}$ is limited to a maximum value of 1 by the front-end limiting filter to prevent over-modulation. It is reasonable to approximate the signal power as 1. Thus, the signal to noise ratio is then

$$\begin{aligned} \mathrm{SNR}_{\mathrm{FMCD}} &= \frac{\overline{g^2(t)}}{N_D} \\ &= 3\overline{g^2(t)}\beta^2(\beta+2)\mathrm{CNR} \\ &= 3\overline{g^2(t)}\frac{\beta^2}{B}\frac{\eta}{h\nu}P_u \\ &\approx 3\frac{\beta^2}{B}\frac{\eta}{h\nu}P_u \end{aligned} \tag{A.2}$$

Effect of FM Anomaly

The output of the link, $\hat{g}(t)$, is independent of the input when an FM phase anomaly occurs as discussed in section 2.3.2. The probability of this event is bounded in equation (2.31). Effectively the signal at the output, nominally $\overline{g^2(t)}$, is noise. Although this is not a perfect representation of the true signal to noise ratio (it does not account for the recovery time after an anomaly), it does allow the peak SNR to be determined with reasonable accuracy. The complete FM–CD signal to noise ratio is approximated by

$$\begin{aligned} \mathrm{SNR}_{\mathrm{FMCD}} &= \frac{\overline{g^2(t)}}{(1-\Pr\{A\})N_D + \Pr\{A\}\overline{g^2(t)}} \\ &= \frac{\overline{g^2(t)}}{(1-\Pr\{A\})\frac{h\nu B}{3\eta P_u \beta^2} + \Pr\{A\}\overline{g^2(t)}} \end{aligned} \tag{A.3}$$

Results

A set of example results are shown below evaluated for a range of values of bandwidth expansion, β, and received optical power, P_u. The following graphs assume a signal bandwidth of 1 GHz and signal energy of 1.

Figure A-1 shows the SNR response as the received optical power is increased from -80 dBm to 0 dBm for various values of β. There is an obvious knee point where the SNR rapidly increases and then becomes linear in received power. Figure A-2 shows the SNR as β varies from 1 to 10^6 for a range of optical power levels. For each power level the performance increases linearly with β until the FM threshold is reached and the SNR drops rapidly. The peak represents the optimum β and SNR for a given optical power level. As shown above, the SNR following the peak is only a rough approximation link reliability in this region is poor. Figure A-3 is a combination of the prior two figures to better see the effect of β. Finally in Figure A-4, we show the optimal selection of β for a given optical power and the resulting best case SNR. These results are numerically computed.

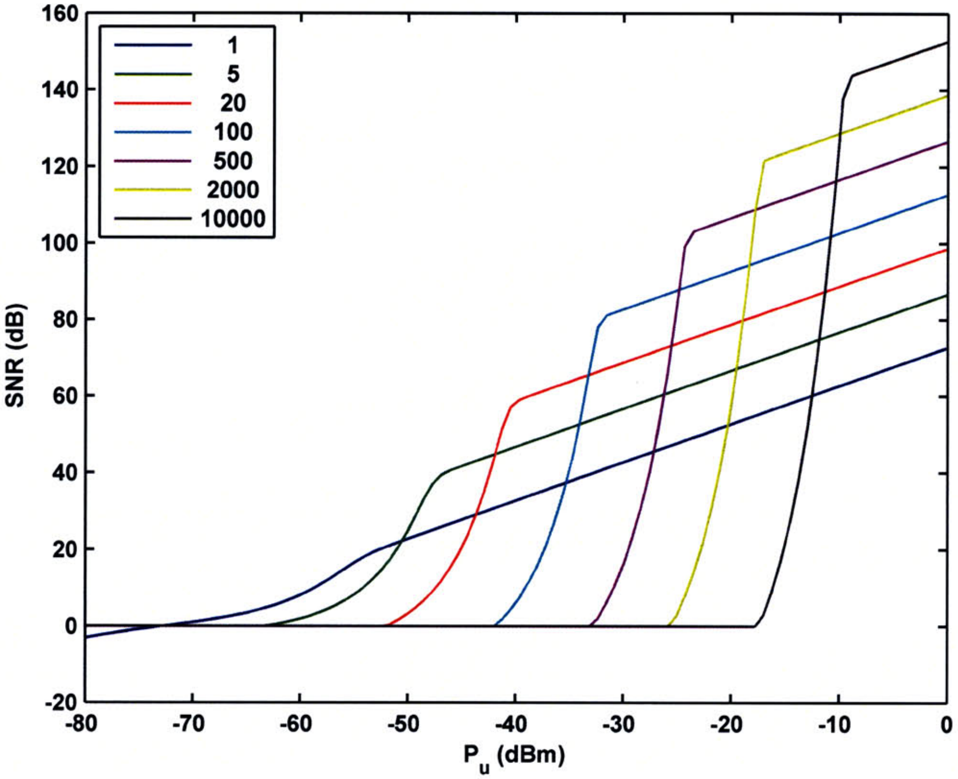

Figure A-1: SNR of FM–CD link versus received optical power at various β.

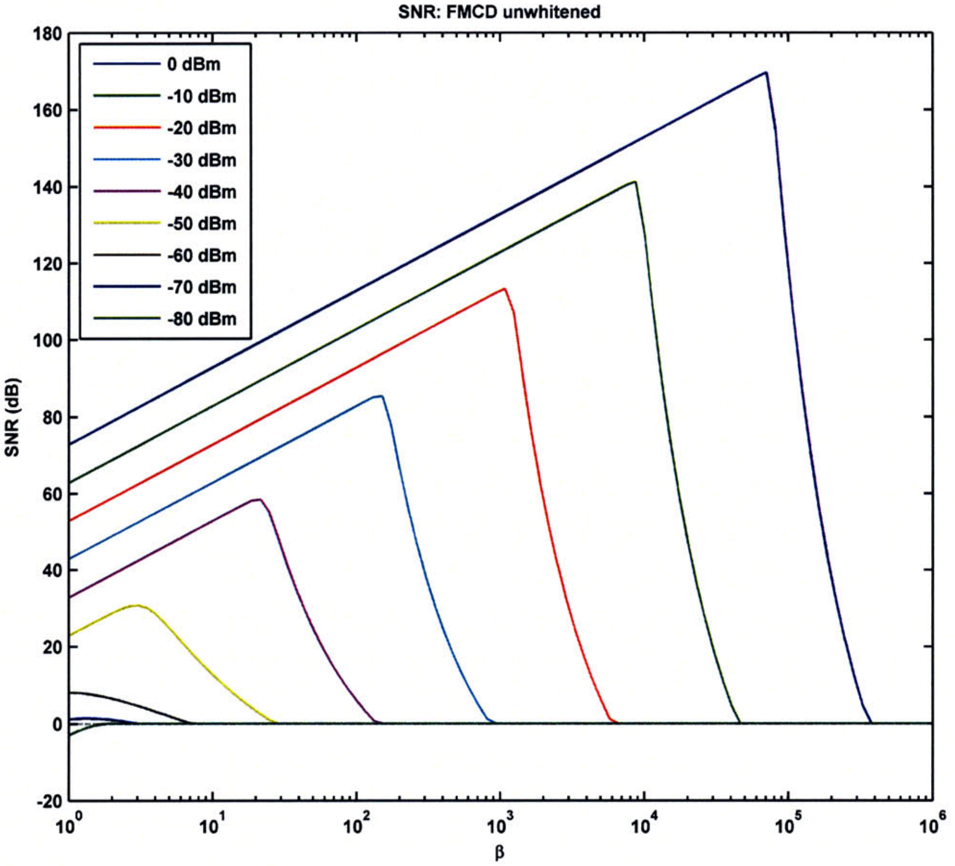

Figure A-2: SNR of FM–CD link versus β at various received optical power levels.

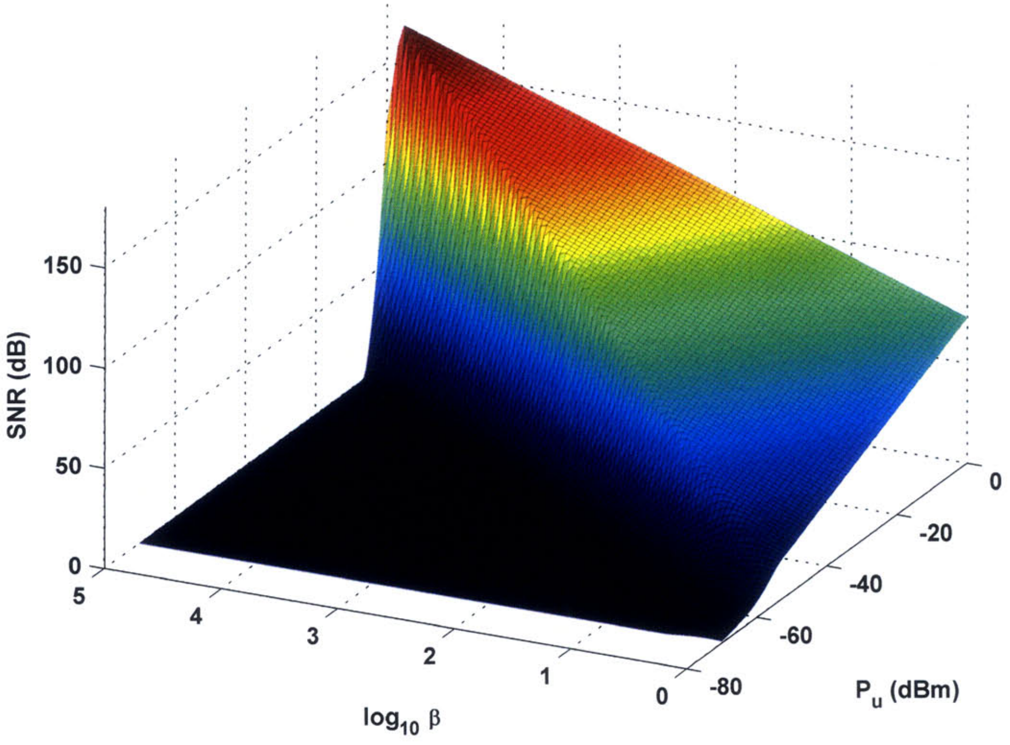

Figure A-3: SNR of FM–CD link versus received optical power and β.

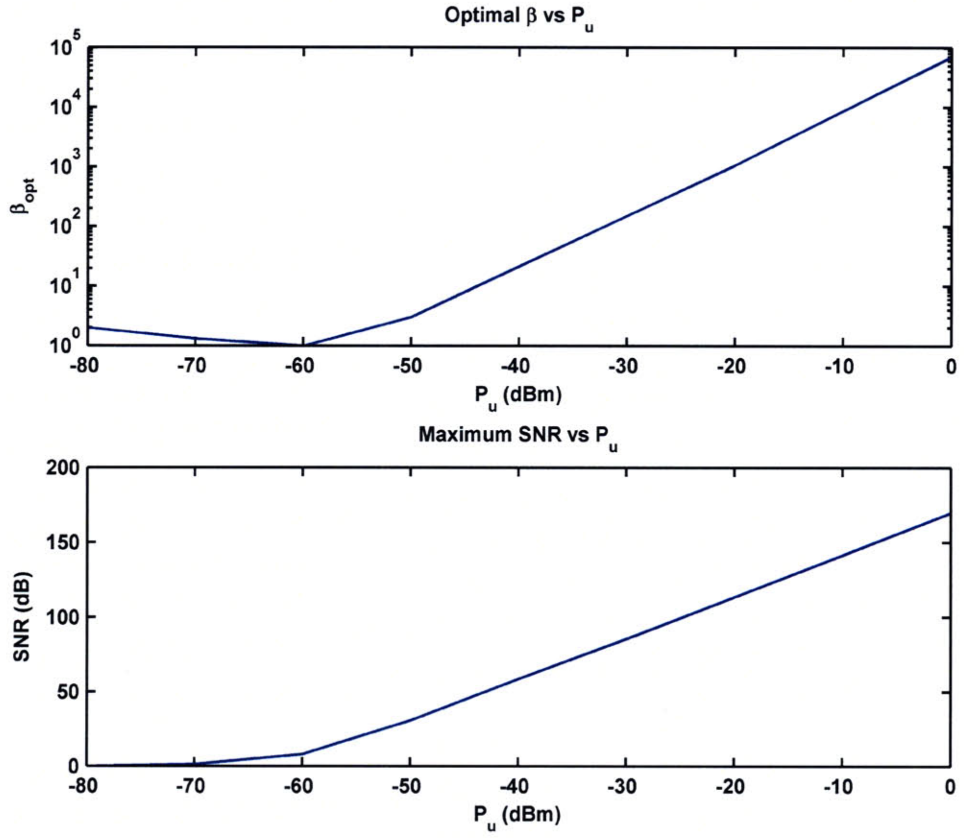

Figure A-4: Optimum β and SNR of FM–CD link versus received optical power.

THIS PAGE INTENTIONALLY LEFT BLANK

Appendix B

Example Code

The numerical calculations and charts in this thesis were generated using MATLAB. To facilitate the comparison between architectures with alternate parameters, example MATLAB code is included below. The script when run asks for the operating parameters, as in Section 4.2. It then generates a figure like Figure 4-1 comparing the bit-error probability of each architecture versus received optical power. The minimum received power for each architecture is returned, as in Table 4.1.

Two Channel Nulling Performance Comparison

```
%% 2-Channel Complete Nulling System
%  Author: James Glettler
%  Project: 2009 Masters Thesis
%  Section: Two Links, Two Users, Complete Nulling

%% Simulation Parameters (Defaults, over-ride with dialog)
%Name of .mat file to store params
param_filename = '2chan_params.mat';

h = 6.62606896e-34; % planck's constant
c = 299792458; % Speed of light
qc = 1.602e-19; %Charge of an electron
kb = 1.3806e-23; %Boltzmans Constant
Temp = 273; %Operation temperature (K)
RLoad = 50; %Optical detector load (ohms)


lambda = 1.55e-6;  %wavelength of transport laser crosslink
hv = h * (c/lambda); %Energy of photon
eta = 0.9; %Quantum efficiency of detector
```

```
K = 0.9; %Modulation Index for IMDD <=1

%% Prompt for values
prompt = {'T_b (s)','E_b/N_0 (dB) at one antenna',...
  'ISAR (linear)','Quantizer Bits','User/Interferr Angle (norm [0,1])'
      ,...
  'Digital transport P_e limit','P_e Goal'};

%Recall last used values
try
  load(param_filename)
  disp('Loaded defaults from file');
catch
  disp('Parameter file not found');
  answers = {'','','','','','',''};
end

%Prompt
dlgoptions.Resize='on'; dlgoptions.WindowStyle='modal';
dlgoptions.Interpreter='tex';
answers = inputdlg(prompt,'Parameters',1,answers,dlgoptions);

%Check values
if isempty(answers);
  h = msgbox('Dialog cancelled, defaults will be used.','Warning','warn'
      )
  uiwait(h);
else
  Tb = str2double(answers{1});
  Eb_N0_dB = str2double(answers{2});
  ISAR = str2double(answers{3});
  b = str2double(answers{4});
  u = str2double(answers{5});
  pe_dig_limit = str2double(answers{6});
  pe_goal = str2double(answers{7});

  %Check results
  if sum(isnan([Tb Eb_N0_dB ISAR b u pe_goal])) %Fail out
    delete(param_filename); %Clear this just to be sure
    msgbox('Parameters incorrect, operation aborted','Error','error');
    return;
  else %Save parameters used
    save(param_filename,'answers');
  end;

end;

%% Ranges
beta = logspace(0,5,300); %Range of Beta
Pu_dBm = linspace(-80,0,1500); %Range of received power
Pu = 10.^(Pu_dBm/10).*1e-3; %Received power (Watts)

%Setup grid of parameters for finding optimum beta
[PuZ,betaZ] = meshgrid(Pu,beta);

%% Front-End
```

```
Eb_N0 = 10^(Eb_N0_dB/10); %Linear signal to noise ratio

B = 1/Tb; %Baseband bandwidth

% AWGN normalized PSD = (N0/2)(T_b/Eb)(1/(1+ISAR)^2)
Sn_awgn = Tb/(2*Eb_N0*(1+ISAR)^2);

% Energy in normalized sig = E_b * G_FE =
Eb_norm = Tb / ( 1 + ISAR )^2;

%% Channel Performance
% rho is gain due to 2-channal nulling for close in users
rho = 2*sin(pi*u)^2;

% Quantization/ADC (common to all)
Sn_quant = 1/(3*B)*2.^(-2*b);
Rq = 2*B*b; %Rate in bits per second

% IMDD
%Sn_IMDD = (2*kb*Temp/RLoad + qc^2*eta/hv.*Pu)./(Pu.^2.*K.^2.*(qc*eta/hv
    )^2); % With Thermal noise
Sn_IMDD = (qc^2*eta/hv.*Pu)./(Pu.^2.*K.^2.*(qc*eta/hv)^2);
snr_imdd = Eb_norm./(Sn_awgn + Sn_IMDD); %Without ADC
pe_imdd = qfunc(sqrt(rho*snr_imdd));
snr_imdd_q = Eb_norm./(Sn_awgn + Sn_quant + Sn_IMDD); %With ADC
pe_imdd_q = qfunc(sqrt(rho*snr_imdd_q));

% FMCD
cnr_fmcd = eta.*PuZ./(hv.*B.*(betaZ+2)); %Carier to Noise ratio
pa_fmcd = 1/sqrt(3).*(betaZ+2).*qfunc(sqrt(cnr_fmcd)); %Prob of anomaly
pa_fmcd(pa_fmcd>1) = 1; pa_fmcd(pa_fmcd<0) = 0;  %hard limit pa_q to
    [0,1]
pr_good_fmcd = (1-pa_fmcd).^2; % Probability both channels good
  % First without quantization
a = sqrt(Sn_awgn);
g = sqrt(hv./(2.*eta.*PuZ.*B.^2.*betaZ.^2));
zeta_fmcd = 1./(2*pi*Tb*a^3).*(2*pi*Tb*a+g.*(exp(-2*pi*Tb.*a./g)-1));
pe_fmcd = qfunc(sqrt(rho*Eb_norm.*zeta_fmcd)).*pr_good_fmcd + 1/2*(1-
    pr_good_fmcd);
  % With quantization
a = sqrt(Sn_awgn + Sn_quant);
zeta_fmcd_q = 1./(2*pi*Tb*a^3).*(2*pi*Tb*a+g.*(exp(-2*pi*Tb.*a./g)-1));
pe_fmcd_q = qfunc(sqrt(rho*Eb_norm.*zeta_fmcd_q)).*pr_good_fmcd +
    1/2*(1-pr_good_fmcd);

 % Find Optimum beta for FM--CD
[pe_fmcd_opt beta_opt] = find_opt_pe(pe_fmcd,beta);
[pe_fmcd_opt_q beta_opt_q] = find_opt_pe(pe_fmcd_q,beta);

% Digital transport
Ns = Pu./(Rq*hv); %Number of signal photons per slot
pe_dig = 1/2.*exp(-Ns); %Assume low background photons
Sn_dxport = 4.*pe_dig./(3*B); %
snr_dxport = Eb_norm./(Sn_awgn + Sn_quant + Sn_dxport);
pe_dxport = qfunc(sqrt(rho*snr_dxport));
 % Drop digital link if probability of transport error is too high
```

```matlab
pe_dxport(pe_dig>pe_dig_limit) = 1/2;

% Reference performance (no transport induced losses
snr_ref = Eb_norm./(Sn_awgn).*ones(1,length(Pu)); %both
pe_ref = qfunc(sqrt(rho*snr_ref));
snr_ref_q = Eb_norm./(Sn_awgn + Sn_quant).*ones(1,length(Pu)); %both
pe_ref_q = qfunc(sqrt(rho*snr_ref_q));

%% PE goal calculation
if ( min(pe_ref) > pe_goal )
  h = warndlg('Quantized reference system cannot meet error probability goal','Reference Goal Failure','replace');
  uiwait(h);
end

if ( min(pe_imdd_q) < pe_goal )
  goal_imq_ii = find(pe_imdd_q<pe_goal,1);
  disp(sprintf(' Minimum power for IMDD-Q  %f dBm',Pu_dBm(goal_imq_ii)));
else
  goal_imq_ii = length(Pu_dBm);
end
if ( min(pe_fmcd_opt_q) < pe_goal )
  goal_fmq_ii = find(pe_fmcd_opt_q<pe_goal,1);
  disp(sprintf(' Minimum power for FMCD-Q  %f dBm with beta = %f',Pu_dBm(goal_fmq_ii),beta_opt_q(goal_fmq_ii)));
else
  goal_fmq_ii = length(Pu_dBm);
end
if ( min(pe_dxport) < pe_goal )
  goal_dig_ii = find(pe_dxport<pe_goal,1);
  disp(sprintf(' Minimum power for Digital %f dBm',Pu_dBm(goal_dig_ii)));
else
  goal_dig_ii = length(Pu_dBm);
end

%% Plot Comparison Graphs
set(gcf,'DefaultAxesColorOrder',[0 0 0;0 1 0;0 0 1;1 0 0]) %K,G,B,R

%Combine output arrays for plotting
pe_ARRAY = [pe_ref;pe_imdd;pe_fmcd_opt;pe_dxport];
pe_ARRAY_q = [pe_ref_q;pe_imdd_q;pe_fmcd_opt_q;pe_dxport];

subplot(2,1,1)
  semilogy(Pu_dBm,pe_ARRAY,'',[min(Pu_dBm),max(Pu_dBm)],[pe_goal,pe_goal],'k:')
  legend('Reference','Analog IMDD','Analog FMCD (opt. \beta)',...
    sprintf('Digital %.0f-bit',b),sprintf('Goal %.0e',pe_goal),'location','NorthEast')
  title('Without Quantizer Limit')
  axis_settings = axis;
  xlabel('Recieved Optical Power - P_u (dBm)')
  ylabel('Probability of Error')

subplot(2,1,2)
```

```
  semilogy(Pu_dBm,pe_ARRAY_q,'',[min(Pu_dBm),max(Pu_dBm)],[pe_goal,
      pe_goal],'k:')
  %legend('Reference)','Analog IMDD','Analog FMCD (Optimal)','Digital','
      location','NorthEast')
  title(sprintf('With %.0f-bit Quantizer Limit',b))
  axis(axis_settings); %Match axis with reference graph
  xlabel('Recieved Optical Power - P_u (dBm)')
  ylabel('Probability of Error')

  %Put parameters on graph
  param_text = {sprintf('T_b: %.1e s',Tb),sprintf('E_b/N_0: %.0f dB',
      Eb_N0_dB),...
                sprintf('ISAR: %.0f',ISAR),sprintf('ADC: %.0f-bits',b)
                    ,...
                sprintf('u_{sz}: %.2f',u)   };
  text(axis_settings(2)-axis_settings(1)*2/3+axis_settings(1),...
    10^(log10(axis_settings(4))-log10(axis_settings(3))*2/3+log10(
        axis_settings(3))),param_text);
```

Listing B.1: Two channel nulling comparison (MATLAB)

```
function [pe_opt, param_opt] = find_opt_pe(pe,params)
% This function takes a 2d array of error probability and finds the
    minimum
% pe and the optimum parameter value over range of

%Get size
[num_params,num_pts] = size(pe);

%Check input
if ( length(params) ~= num_params )
  error('Size of parameters does not match or out of range');
end

%Find minimum
for ii = 1:num_pts %Step through each operating point
  [pe_opt(ii) min_jj] = min(pe(:,ii)); %find Min
  if (min_jj == length(params) )
    %End of range - cannot be certain it is global peak
    param_opt(ii) = NaN;
  else
    param_opt(ii) = params(min_jj);
  end
end

return;
```

Listing B.2: Optimum parameter search (MATLAB)

THIS PAGE INTENTIONALLY LEFT BLANK

Appendix C

Notation

Abbreviations

Abbreviation	**Meaning**
ADC	Analog to Digital Converter
AM	Amplitude Modulation
AWGN	Additive White Gaussian Noise
BPSK	Binary Phase Shift Keying
bps	Bits per second
CD	Coherent Detection
CNR	Carrier to Noise Ratio
DD	Direct Detection
E/O	Electrical to Optical transducer
EHF	Extremely High Frequency
FM	Frequency Modulation
FSO	Free-Space Optical
GEO	Geosynchronous Orbit
IM	Intensity Modulation
ISAR	Interference to Signal Amplitude Ratio
ISL	Inter-Satellite Link

Abbreviation	**Meaning**
LLR	Log Likelihood Ratio
MSE	Mean Square Error
MUSIC	Multiple Signal Classification algorithm
O/E	Optical to Electrical transducer
OOK	On-Off Keying
PDF	Probability Distribution Function
PM	Phase Modulation
PSD	Power Spectral Density
RF	Radio Frequency
RIN	Receiver (Laser) Intensity Noise
SNR	Signal to Noise Ratio

Table C.1: Abbreviations

Symbols

Symbol	**Meaning**
A_{e_r},A_{e_t}	Effective area of optical apertures (receive and transmit)
A_x	Amplitude gain of function x
$\mathcal{A}$	FM anomaly event
a	Maximum dimension of an aperture
B	Bandwidth (Hz) (single sided)
b	Number of bits in uniform quantizer
c	Speed of light in a vacuum $299,792,458$ m/s
D	Diameter of reflector antenna or optical aperture (m)
d	Distance between elements of receiver array or optical telescopes
E_b	Energy per bit (Joules)
$E_{LO}(t)$	Electric field of local oscillator signal with power P_{LO}
$E_s(t)$	Electric field of transmitted optical signal with power P_s

Symbol	Meaning
$E_u(t)$	Electric field of received optical signal with power P_u
$\mathsf{E}[\alpha]$	Expected value of α
$\mathcal{F}\{\alpha\}$	Fourier Transform of α
f	Frequency (Hz)
f_{samp}	Sample Rate (Samples per second)
f_Δ	Maximum instantaneous frequency deviation (FM/PM)
G_x	Power gain of function x, $G_x = A_x^2$
$g(t)$	Signal at remote antenna to analog modulator or digitizer
$\hat{g}(t)$	Signal reconstructed at array processor after transport
$\mathfrak{g}_i(f)$	Function with Fourier transform $\mathfrak{G}_i(\mathfrak{s})$
good	Event when all transport channels are functioning
$H(f)$	Frequency domain transfer function of linear filter
$H_D(f)$	Post FM detection filter
$H_W(f)$	Whitening filter
$\mathbf{H}(f)$	Array processing filter bank
h	Planck's constant $6.6261 \cdot 10^{-34}$ $\text{m}^2\text{kg/s}$
$h(t)$	Impulse response function
I_{dk}	Photo-detector dark current
I_0	Mean photo generated current in optical detector
$I_N(t)$	Noise component of photo-current
$I_s(t)$	Information bearing component of photo-current
$\mathbf{I}$	Identity matrix
i,j,k,n	Index variables
J	Number of orthonormal basis functions
j	Imaginary number $j = \sqrt{-1}$
K	Number of separate RF signals
k	Spatial frequency (cycles/m)
k_B	Boltzmann's constant $1.3806 \cdot 10^{-23}$ J/K
$\mathbf{k}_s$	Wavenumber

Symbol	Meaning
L	Number of discrete output levels in quantizer
$m(t)$	Baseband RF signal modulated with information
$m[n]$	Symbol stream to transmit via RF link
$\hat{m}[n]$	Recovered symbol stream at receiver
N	Number of antennas in receiver array
N_0	noise power per mode
N_D	Integrated noise power after FM discriminator
N_s	Photons per slot in digital optical communication
N_e	Count of incorrect binary digits in Word_i
$\mathcal{N}(\mu, \sigma^2)$	Standard normal distribution with mean μ and variance σ^2
$\mathbb{N}^*$	Set of all natural numbers greater than zero
$n(t)$	Noise signal
$n_c(t)$,$n_s(t)$	In-phase and quadrature representation of noise
$\mathbf{n}$	Vector representation of independent noise
$\mathrm{p}_X(x)$	PDF of random variable X evaluated at x
p_ε	Probability of error in digital optical transport link
$\mathbf{p}$	Position vector of antennas in receiver array
$Q(\alpha)$	Complementary normal CDF, $\frac{1}{\sqrt{2\pi}}\int_\alpha^\infty \exp(-x^2/2)\mathrm{d}x$
q	Elementary charge $1.602 \cdot 10^{-19}$ C
R	Responsivity (A/W)
R_L	Load resistance for photo-detector
R_q	Bit rate of quantized signal (bits per second)
$\mathbf{R}$	Receiver LLR random variable
$\mathcal{R}_{xx}$	Input covariance matrix of signal $\mathbf{x}$
$r(t)$	Received RF signal
$r^\circ(t)$	Whitened received signal
$r_{\max}$	Maximum amplitude $r(t)$
$\mathbf{r}_i$	Vector representation of received $r_i(t)$
$S_x(f)$	Power spectral density (PSD) of signal x

Symbol	**Meaning**
$s(t)$	Passband user signal (plane wave approximation)
T	Temperature
T_b	Time per single bit
t	Time
u_{sz}	Normalized angle between signal and interference relative to $\frac{\lambda}{d}$
$\mathbf{u}_s$	Unit directional vector pointing to RF source
$\mathsf{Var}\left[\alpha\right]$	Variance of α
$\mathbf{v}_{\mathbf{k}}(\mathbf{k})$	Array manifold vector of wavenumber $\mathbf{k}$
W	Optical bandwidth
Word_i	Binary codeword representing quantizer output for y_i
$\mathbf{w}$	Complex array weights
x	Input to quantizer
x_i	Boundaries on quantizer levels
$x_i(t, \mathbf{p}_i)$	Complete received signal at antenna i
$\mathbf{x}(t, \mathbf{p})$	Vector representation of array signals
y	Output of quantizer
y_i	Output step of quantizer
$y(t)$	Output of array processor
Z	Distance between RF transmitter and RF receiver antennas
$z(t)$	Interfering signal
α	Arbitrary variable; white noise component
β	Frequency modulation index $\beta = \frac{f_\Delta}{B}$
Γ	A constant
γ	Quadratic noise component
Δ	Spacing of least significant digit in quantizer
ϵ	Error in communication system
ε	Error in digital optical transport
ζ	Inverse of total energy of whitened noise
η	Quantum efficiency of photo-detector

Symbol	**Meaning**
θ_x	Angle of x, see Figure 3-4
κ	Intensity modulation index
$\Lambda(\mathbf{r})$	Likelihood ratio
λ	Wavelength
μ_x	Mean of x
ν	Photon frequency (Hz)
ξ_{dig}	Mean square error of digital modulation
ξ_q	Mean square error of quantizer
ϱ	Additional margin required due to signal suppression by nulling
σ_x^2	Variance of x
τ_{si}	Time delay of signal s to antenna i
$\Phi(f)$	Fourier transform of $\varphi(t)$
$\phi(t)$	Phase noise
$\varphi(t)$	Orthonormal basis function
$\boldsymbol{\varphi}(t)$	Set of Orthonormal basis functions
χ	Distance between the user and the interferer
ω	Radian frequency $\omega = 2\pi$

Table C.2: Symbols

Bibliography

[1] G. L. Abbas, V. W. S. Chan, and T. K. Yee. Local-oscillator excess-noise suppression for homodyne and heterodyne detection. *Optics Letters*, 8(8):419–421, 1983.

[2] Govind P. Agrawal. *Fiber-optic Communication Systems.* Wiley-Interscience, 2002.

[3] Stephen B. Alexander. *Optical Communication Receiver Design.* IET, 1997.

[4] Nikolaos I. Andrikogiannopoulos. RF phase modulation of optical signals and optical/electrical signal processing. Master's thesis, Massachusetts Institute of Technology, 2006.

[5] W. R. Bennett. Spectra of quantized signals. *Bell System Technical Journal*, 27:446–472, July 1948.

[6] Delta IV Launch Vehicles. `http://www.boeing.com/defense-space/space/delta/delta4/delta4.htm`, June 2007. Retrieved 7 Feb 2009.

[7] B. Cai and A. J. Seeds. Optical frequency modulation link for microwave signal transmission. *Microwave Symposium Digest, 1994., IEEE MTT-S International*, 1:163–166, May 1994.

[8] B. Cai and A. J. Seeds. Optical frequency modulation links: Theory and experiments. *Microwave Theory and Techniques, IEEE Transactions on*, 45(4):505–511, Apr 1997.

[9] David O. Caplan. Laser communication transmitter and receiver design. *Journal of Optical and Fiber Communication Research*, 4(4–5):225–362, Sept 2007.

[10] J. R. Carson. Notes on the theory of modulation. *Proceedings of the IRE*, 10(1):57–64, Feb. 1922.

[11] V. W. S. Chan. Free space optical communication and networks. Course notes for 6.972 retrieved from `https://web.mit.edu/6.972/handouts/` 10 April 2009, October 2008.

[12] V. W. S. Chan, Lori L. Jeromin, and John E. Kaufmann. Heterodyne lasercom systems using GaAs lasers for ISL applications. In *International Conference on Communications, IEEE*, pages 1201–1207, June 1983.

[13] Vincent W. S. Chan. Optical space communication. *Selected Topics in Quantum Electronics, IEEE Journal of*, 6(6):959–975, Nov 2000.

[14] Vincent W. S. Chan. Optical satellite networks. *Journal of Lightwave Technology*, 21(11):2811, 2003.

[15] H. T. Friis. A note on a simple transmission formula. *IRE, Proceedings of the*, 34(5):254–256, 1934.

[16] Robert G. Gallager. *Principles of Digital Communication.* MIT Copytech, preprint edition, August 2007.

[17] James B. Glettler, Pablo I. Hopman, Simon Verghese, Joseph C. Aversa, Larry M. Candell, Joseph P. Donnelly, Erik K. Duerr, Jonathan P. Frechette, Joseph E. Funk, Z. L. Liau, K. A. McIntosh, Leonard J. Mahoney, Karen M. Molvar, Douglas C. Oakley, E. J. Ouellette, Gary M. Smith, and Christopher J. Vineis. Inp-based single-photon detector arrays with asynchronous readout integrated circuits. *Optical Engineering*, 47(10), 2008.

[18] R. Helkey. Relative-intensity-noise cancellation in bandpass external-modulation links. *Microwave Theory and Techniques, IEEE Transactions on*, 46(12):2083–2091, Dec 1998.

[19] P. I. Hopman, P. W. Boettcher, L. M. Candell, J. B. Glettler, R. Shoup, and G. Zogbi. An end-to-end demonstration of a receiver array based free-space photon counting communications link. *Free-Space Laser Communications VI. Proceedings of SPIE*, 2006.

[20] W. Cary Huffman and Vera Pless. *Fundamentals of Error-Correcting Codes.* Cambridge University Press, 2003.

[21] William A. Imbriale. Large antennas of the deep space network. Technical Report 02-6, Jet Propulsion Laboratory, Pasadena, CA, 2002.

[22] J. B. Johnson. Thermal agitation of electricity in conductors. *Phys. Rev.*, 32(1):97–109, Jul 1928.

[23] J. E. Kaufmann and Vincent W. S. Chan. Coherent optical intersatellite crosslink systems. *IEEE MILCOM*, 2:533–540, October 1988.

[24] J. E. Kaufmann and W. K. Hutchinson. Emitter location with LES-8/9 using differential time-of-arrival and differential doppler shift. Technical Report 698, Lincoln Laboratory, Massachusetts Institute of Technology, Lexington, MA, August 1985. Reissued 31 March 2000 for Public Release.

[25] Gunter Dirk Krebs. ETS 8 (Kiku 8). `http://www.skyrocket.de/space/doc_sdat/ets-8.htm`, March 2009. Retrieved 10 April 2009.

[26] Gregory Kriehn, Andrew Kiruluta, Paulo E. X. Silveira, Sam Weaver, Shawn Kraut, Kelvin Wagner, R. Ted Weverka, and Lloyd Griffiths. Optical BEAMTAP beam-forming and jammer-nulling system for broadband phased-array antennas. *Applied Optics*, 39(2):212–230, 2000.

[27] Milstar. `http://www.lockheedmartin.com/products/Milstar/`. Retrieved 7 April 2009.

[28] C. John Mankins. Technology readyness levels. Technical report, NASA, Office of Space Access and Technology, April 1995.

[29] D. Marco and D. L. Neuhoff. The validity of the additive noise model for uniform scalar quantizers. *Information Theory, IEEE Transactions on*, 51(5):1739–1755, May 2005.

[30] Joel Max. Quantizing for minimum distortion. *Information Theory, IRE Transactions on*, 6(1):7–12, March 1960.

[31] G. Stephen Mecherle and Michael Horstein. Comparison of radio frequency and optical architectures for deep-space communications via a relay satellite. *Free-Space Laser Communication Technologies VI, Proceedings of SPIE*, 2123:36–53, August 1994.

[32] Ronald A. Mucci. A comparison of efficient beamforming algorithms. *Acoustics, Speech and Signal Processing, IEEE Transactions on*, 32(3):548–558, Jun 1984.

[33] Alan V. Oppenheim, Ronald W. Schafer, and John R. Buck. *Discrete-Time Signal Processing.* Prentice Hall, second edition, 1999.

[34] Joseph C. Palais. *Fiber Optic Communication.* Prentice Hall, 4th edition, 1998.

[35] A. Pezeshki, B.D. Van Veen, L.L. Scharf, H. Cox, and M.L Nordenvaad. Eigenvalue beamforming using a multirank mvdr beamformer and subspace selection. *Signal Processing, IEEE Transactions on*, 56(5):1954–1967, May 2008.

[36] Poompat Saengudomlert and V. W. S. Chan. Hybrid optical and electronic signal processing for wideband RF antenna arrays. Technical Report 2640, Massachusetts Institute of Technology, Laboratory for Information Decision Systems, August 2004.

[37] Ralph O. Schmidt. Multiple emitter location and signal parameter estimation. *Antennas and Propagation, IEEE Transactions on*, 34(3):276–280, Mar 1986.

[38] A. J. Seeds. Optical transmission of microwaves. In W. R. Stone, editor, *The Review of Radio Science 1993-1996*, chapter 14, pages 335–343. Oxford University Press, 1996.

[39] C.E. Shannon. Communication in the presence of noise. *Proceedings of the IRE*, 37(1):10–21, Jan. 1949.

[40] W. Stephens and T. Joseph. System characteristics of direct modulated and externally modulated RF fiber-optic links. *Lightwave Technology, Journal of*, 5(3):380–387, Mar 1987.

[41] Jeffrey A. Stern and William H. Farr. Fabrication and characterization of superconducting NbN nanowire single photon detectors. *Applied Superconductivity, IEEE Transactions on*, 17(2):306–309, June 2007.

[42] Morio Toyoshima, Walter R. Leeb, Hiroo Kunimori, and Tadashi Takano. Comparison of microwave and light wave communication systems in space applications. *Optical Engineering*, 46(1):015003, 2007.

[43] Fawwaz T. Ulaby. *Fundamentals of Applied Electromagnetics.* Prentice Hall, 2001.

[44] Harry L. Van Trees. *Detection, Estimation and Modulation Theory, Part II.* John Wiley & Sons, New York, 1971.

[45] Harry L. Van Trees. *Detection, Estimation and Modulation Theory, Part I.* John Wiley & Sons, New York, 2001.

[46] Harry L. Van Trees. *Optimum Array Processing. Part IV of Detection, Estimation and Modulation Theory.* John Wiley & Sons, New York, 2002.

[47] R.G. Vaughan, N.L. Scott, and D.R. White. The theory of bandpass sampling. *Signal Processing, IEEE Transactions on*, 39(9):1973–1984, September 1991.

[48] Robert Alexander Wannamaker. *The Theory of Dithered Quantization.* PhD thesis, University of Waterloo, 1997.

[49] B. Widrow, I. Kollár, and Ming-Chang Liu. Statistical theory of quantization. *Instrumentation and Measurement, IEEE Transactions on*, 45(2):353–361, Apr 1996.

[50] Roger Wood. On optimum quantization. *Information Theory, IEEE Transactions on*, 15(2):248–252, Mar 1969.

[51] John M. Wozencraft and Irwin Mark Jacobs. *Principles of Communication Engineering.* Waveland Press, 1965.

[52] Horace P. Yuen and Vincent W. S. Chan. Noise in homodyne and heterodyne detection. *Optics Letters*, 8(3):177–179, 1983.